Catarina Alexandra Neto Nunes

Bachelor in Chemical and Biochemical Engineering

Application of zeolite membranes to separate fermentation products

Dissertation for obtaining the Master degree in
Chemical and Biochemical Engineering

Adviser: Izumi Kumakiri, Assistant Professor, Yamaguchi University

Co-adviser: João Paulo Crespo, Full Professor, FCT - NOVA University of Lisbon

Jury:

President: Prof. Dr. Mário Fernando José Eusébio, FCT-UNL
Examiner: Prof. Dr. Isabel Maria Rôla Coelhoso, FCT-UNL
Member: Prof. Dr. João Paulo Serejo Goulão Crespo, FCT-UNL

FACULDADE DE CIÊNCIAS E TECNOLOGIA
UNIVERSIDADE NOVA DE LISBOA

November, 2017

Catarina Alexandra Neto Nunes

Bachelor in Chemical and Biochemical Engineering

Application of zeolite membranes to separate fermentation products

Dissertation for obtaining the Master degree in
Chemical and Biochemical Engineering

Adviser: Izumi Kumakiri, Assistant Professor, Yamaguchi University

Co-adviser: João Paulo Crespo, Full Professor, FCT - NOVA University of Lisbon

Jury:

President: Prof. Dr. Mário Fernando José Eusébio, FCT-UNL
Examiner: Prof. Dr. Isabel Maria Rôla Coelhoso, FCT-UNL
Member: Prof. Dr. João Paulo Serejo Goulão Crespo, FCT-UNL

November, 2017

Application of zeolite membranes to separate fermentation products

This document was created using the (pdf)LaTeX processor, based in the "novathesis" template[1], developed at the Dep. Informática of FCT-NOVA [2].
[1] https://github.com/joaomlourenco/novathesis [2] http://www.di.fct.unl.pt

"The world is a dangerous place to live, not because of the people who are evil, but because of the people who don't do anything about it." - Albert Einstein

Acknowledgements

I would like to express my special acknowledgement to Professor Izumi Kumakiri for giving me this enormous opportunity of study in Japan, and for all the support and knowledge that she shared with me during this period.

I am particularly grateful to my co-adviser Professor João Paulo Crespo for showing me this big opportunity, and for all the help and suggestions to improve my work.

I would like to acknowledge my universities, Graduate School of Sciences and Technology for Innovation of Yamaguchi University and Faculty of Sciences and Technology of NOVA University of Lisbon.

I also express my sincere thanks to Professor Mário Eusébio for "pushing" me to this adventure, and showing me that this was the right way, and also for all the knowledge that he shared with me in these last two years of university.

A special thanks to my colleagues and friends that I met during this journey, thanks to your help, everything was easier and special.

I would like to express my love for my family, and in special to my mother. She believed in me, and encouraged me to take the risk and come to an adventure in the other side of the globe. I also express my sincere thanks to my friends in Portugal, thanks for all the help, support and skype talks at strange hours. Finally, a special thanks to my love, which was my big support in the most difficult moments of this journey.

Abstract

Due to the negative impact caused by the use of fossil fuels and their limited sources, the worldwide production of bioproducts has been increasing significantly in the last years. After converting biomass to biochemicals or biofuels, separation and purification processes are required. Although distillation is a well-established process, it is energy intensive, especially when faced with close-boiling, azeotropic or dilute mixtures. Recently, a significant energy reduction is reported by replacing azeotropic or extractive distillation with a membrane separation in alcohol dehydration process. Membrane properties are the key to achieve such separation, however, application of industrialized zeolite A membranes is limited due to their poor stability. To overcome this limitation, a new type of zeolite membranes, mordenite membranes (MOR), with higher Si/Al ratio than the commercially available zeolite A membranes were developed [24].

This study reports the pervaporation performance and stability of the mordenite membranes in synthetic aqueous alcohol solutions and in an ethanolic fermentation broth. The influence of operating conditions, such as the composition and the temperature of the feed mixture, on the performance of the mordenite membranes was studied. Also, the stability of zeolite A membranes in ethanolic fermentation broth was evaluated. The mordenite membranes exhibited water perm-selectivity and long-term stability for the dehydration of alcohol-water mixtures by pervaporation. In the dehydration of the distilled ethanolic fermentation broth, the total flux and separation factor of the membrane remained at ≈ 1.43 kg m^{-2} h^{-1} and ≈ 1127, respectively, at 75°C even after 53.4h of soaking and pervaporation experiments. On the contrary, the zeolite A membrane lost its pervaporation performance after being soaked in the distilled ethanolic fermentation broth, due to acidic conditions or the high water content of the broth.

Keywords: bioproducts; fermentation; dehydration; pervaporation; zeolite membranes

Resumo

Devido ao impacto negativo causado pela utilização de combustíveis fósseis e a sua consequente limitação, a produção mundial de bioprodutos tem vindo a aumentar nos últimos anos. Após a conversão de biomassa em bioprodutos, é necessária a execução de processos de separação e purificação. Embora a destilação seja um processo plenamente estabelecido na indústria, este apresenta elevados consumos de energia, especialmente quando utilizado para separar misturas com pontos de ebulição próximos, azeótropos ou soluções diluídas. Recentemente, foi reportada uma significativa redução de energia no processo de desidratação de álcoois, ao ser realizada uma separação por membranas em lugar de uma destilação extrativa ou azeotrópica. As propriedades das membranas são a chave para alcançar uma separação energeticamente eficiente, no entanto, a utilização de membranas industriais de zeólito A é limitada devido à sua fraca estabilidade. De forma a superar esta limitação, foi desenvolvido um novo tipo de membranas de zeólito, denominadas membranas de mordenite (MOR), que apresentam um rácio Si/Al superior ao das membranas de zeólito A comerciais [24].

Este estudo reporta o desempenho de pervaporação e a estabilidade das membranas de mordenite em soluções aquosas sintéticas de álcool e num caldo de fermentação etanólico. Foi estudada a influência das condições de operação, como a composição e a temperatura da mistura de alimentação, na performance das membranas de mordenite. Além disso, foi avaliada a estabilidade das membranas de zeólita A no caldo de fermentação etanólico. As membranas de mordenite exibiram seletividade à água e estabilidade a longo prazo na desidratação de misturas aquosas de álcool por pervaporação. Na desidratação do caldo de fermentação etanólico, o fluxo total e o factor de separação da membrana permaneceram $\approx 1{,}43$ kg m^{-2} h^{-1} e ≈ 1127, respectivamente, a 75°C, mesmo após 53,4h de experiências de imersão e pervaporação. Pelo contrário, a membrana do

zeólito A perdeu a sua performance de pervaporação após ter sido imersa no caldo de fermentação, devido às condições ácidas ou ao elevado teor em água do caldo.

Palavras-chave: bioprodutos; fermentação; desidratação; pervaporação; membranas de zeólito

Contents

List of Figures

List of Tables

Nomenclature

A (LTA)	Zeolite A.
AD	Azeotropic distillation.
ASTM	American Society for Testing and Materials.
DWC	Diving-wall column.
ED	Extractive distillation.
E-DWC	Extractive diving-wall column.
EF	Extractive fermentation.
EPMA	Electron probe microanalysis.
EtOH	Ethanol.
FGE	Fuel-grade ethanol.
GHG	Greenhouse gas.
GP	Gas permeation.
HAc	Acetic Acid.
HIAG	Holz Industrie Actien Gesellschaft.
ICP	Inductively coupled plasma.
IZA	International Zeolite Association.
LCV	Lower calorific value.
LLE	Liquid-liquid extraction.
MAS	Mass separating agent.
MD	Membrane distillation.
MetOH	Methanol.
MOR	Modernite.
NCCP	National Climate Change Plan.

NEBP	National Ethanol Blending Programme.
PDMS	poly(dimethyl siloxane).
PSA	Pressure swing adsorption.
PTMSP	poly[1-(trimethylsilyl)-1–ropyne].
PV	Pervaporation.
RFS	Renewable Fuel Standard.
SEM	Scanning electron microscope.
TEM	Transmission electron microscope.
TSA	Temperature swing adsorption.
VLE	Vapor-liquid equilibrium.
VMD	Scanning electron microscope.
VP	Vapor permeation.
XRD	X-ray diffraction.
α_{ij}	Separation factor of i over j.
$\alpha_{w/o}$	Separation factor of water over organics.
α'_{ij}	Selectivity of i over j.
Si/Al	Silica/Aluminum ratio.
J_{total}	Total permeation flux.
J_i	Permeation flux of component i.
p_i^F	Partial vapor pressure of component i at feed side.
p_i^P	Partial vapor pressure of component i at permeate side.
c_i^F	Concentration of component i at feed side.
c_i^P	Concentration of component i at permeate side.
S	Membrane effective surface area.
d	Membrane outside diameter.
l	Membrane effective lenght.
δ	Membrane thickness.
t	Test time.
m	Mass permeate collected over a known test time.
Y_i	Mass fraction of i at permeate side.

X_i	Mass fraction of i at feed side.
P_i	Membrane permeability or Permeability coefficient.
P_i/δ	Membrane permeance.
ΔP	Pressure driving force.
P	Total Pressure.
P_i^{sat}	Saturated vapor pressure of component i.
y_i	Molar fraction of the component i in the vapor phase.
x_i	Molar fraction of the component i in the liquid phase.
γ_i	Activity coefficient of the component i.
A, B, C	Component-specific constants of Antoine's equation.
T	Temperature.
$\Lambda_{12}, \Lambda_{21}$	Binary systems parameters of Wilson's equation.
v_i	Molar volume of the component i.
M_i	Molar mass of component i.
ρ_i	Specific weight of the component i.
E_p	Apparent activation energy of permeation.
E_D	Activation energy of diffusion.
E_j	Overestimated apparent activation energy.
ΔH_s	Heat of sorption.
ΔH_v	Heat of vaporization.
D_i	Diffusivity coefficient.
S_i	Solubility coefficient.
P_0	Pre-exponential factor.
R	Ideal gas constant.
$vol\,\%$	Volume percent.
$mol\,\%$	Molar percent.
$wt\,\%$	Weight percent.
$CaCl_2$	Calcium chloride.
CO_2	Carbon dioxide.
C_2H_6O	Ethanol.

$\mathbf{CH_4O}$	Methanol.
$\mathbf{N_2}$	Nitrogen.
$\mathbf{H_2SO_4}$	Sulfuric acid.
$\mathbf{H_2O}$	Water.

Chapter 1

Introduction

1.1 Context

Currently, fossil fuels - coal, petroleum and gas - make modern life possible and are the major energy sources, accounting for more than 80% of world energy demand [1, 2]. For over a century, fossil fuels have been the primary source of a wide range of products including electricity, fuels, lubricants, chemicals, waxes, synthetic rubbers, plastics, pharmaceuticals and asphalt [1, 3]. However, these fuels are nonrenewable and their reserves are not unlimited [4]. It was recently reported that the supply of coal, natural gas and petroleum will only last over 120, 60 and 45 years, respectively [4]. Furthermore, huge amounts of greenhouse gas (GHG) emissions have been released from fossil fuels consumption, raising the atmospheric carbon dioxide (CO_2) concentration to 400 ppm from the pre-industrial level of 280 ppm and inducing disastrous climate changes [4].

Due to the negative environmental impact caused by the use of fossil fuels and their limited sources, the worldwide production of bioproducts has been increasing significantly in last years [2, 3]. In particular, biofuels such as bioethanol and biodiesel are being largely produced to complement the rapidly depleting of petroleum reserves [4]. According to *Renewables 2017 Global Status Report*, in 2016, bioethanol and biodiesel world production was 98.6 and 30.8 billion liters, respectively [5].

Bioproducts, which include biochemicals and biofuels, can be produced directly from biomass and are considered to be a promising solution because they are relatively

cleaner [6, 7]. These bio-based products are not only made from renewable sources, they also frequently require less energy to produce than petroleum-based products and are biodegradable [7].

It was reported that the use of renewable fuels results in 20% reduction in GHG emissions, which can be further improved to 60% if biofuels are produced from cellulosic biomass, which are in the category of second generation biofuels [3, 6]. Thereby, diverse countries have adopted different measures to introduce biofuels, depending on their resource base [6]. The *European Commission* proposed 20% replacement of conventional fossil fuels by alternative renewable sources in the European Union's total energy needs, and at least 10% in the road transport sector by 2020 [3, 6]. In the United States, *Renewable Fuel Standard* (RFS) requires 136 billion liters of biofuels in transport fuels, of which 79 billion liters must be second generation biofuels by 2022 [3]. In 2014, China approved a *National Climate Change Plan* (NCCP) which sets a target of 130 billion liters of biofuel production by 2020 [3]. Unfortunately, the current reality is far from that target because the previous actions of the central government appear to discourage biofuels production [3]. On the contrary, in 2010, India launched a *National Ethanol Blending Programme* (NEBP), thus establishing a 5% mandatory ethanol blending in 20 states across the country [6].

The most relevant biomass sources are wood, residues from agriculture or forestry, organic components of municipal and industrial wastes, animal wastes, plants, aquatic plants and algae [8, 9]. Besides, biomass has been described as the fourth largest available energy resource of the world [10]. The effective application of these renewable resources would lead to a reduction on environmental pollution and an improvement on rural economy [10].

When biomass is heated in presence of small amounts of oxygen, carbon monoxide and hydrogen are produced [7]. This gas mixture is called biosynthesis gas and can be used to make polymers and acids [7]. Moreover, there are a number of technologies and several under development for production of biofuels such as fermentation of sugar substrates, hydrolysis of cellulose, production of biobutanol by fermentation, transesterification of natural oils and fats to produce biodiesel, among others [11].

Southeast Asian countries have huge amounts of biomass production, including sugar cane bagasse, forestry residue and agricultural waste [12, 13]. This region produces nearly 230 million tonnes of biomass feedstock annually [13].

Currently, Asia's largest biofuel producers are China, Indonesia, Malaysia, The Philippines and Thailand [14, 15]. These countries have their biofuel strategies focused on their main agricultural product [14]. Indonesia and Malaysia dominate Asia biodiesel production, while China, India and Thailand focus largely on the production of bioethanol [15]. On the other hand, The Philippines is promoting both ethanol and biodiesel production [15].

China and Thailand have relatively more advanced level of biofuel development compared to other countries in the region [15]. In fact, China is now the third largest bioethanol producer in the world, after the United States and Brazil [15]. Thailand has an important role in biomass feedstock supply, production, domestic consumption and export of bioethanol [16]. Moreover, Indonesia and Malaysia are the top two largest producers of palm oil in the world, these countries also being expected to play a major role in the global biodiesel market [15].

Like other countries, Southeast Asian countries also have specific policy targets for biofuels production and consumption. Thailand established a target of 44% replacement of petroleum import by biofuels until 2021 [16]. Furthermore, Thailand also supports the sale of gasoline blended with ethanol, this fuel mixture is named gasohol and contains 10%, 15% or 20% of bioethanol [15, 16]. Indonesia sets a policy target of 5% of biodiesel blending with diesel fuel by 2025 [15, 16]. Malaysia has a policy target to displace 5% of diesel in road transport sector with biodiesel by 2030 [16]. The Philippines intends to displace 15% of diesel and 20% of gasoline with biofuels by 2030 [15, 16].

Biofuels production in Southeast Asia is often associated with farmers in rural and poor areas [15]. In addition, these regions have a tropical climate which sometimes makes the cooling system difficult and increases the costs of a fermentation process [17]. The industries that use fermentation processes stop their production for about 2 months during the hot seasons [17]. Therefore, a type of fermentation to produce bioproducts that have numerous benefits for rural and tropical areas is being researched and developed [17–19]. In this fermentation are used thermotolerant microbes, which can ferment a wide range of sugars at temperatures around 40°C [17, 19]. Moreover, this high-temperature fermentation has several advantages including high product conversion, more-efficient simultaneous scarification and fermentation, reduced need for utilities, reduced risk of contamination, and reduction of cooling and operating costs [17–19]. Besides, this type of fermentation is able to achieve a significant reduction in total running cost of the process

as well as a stable fermentation [17, 19]. It is expected to be one of the next generation fermentation technologies [17, 19]. The arising of this new technology demonstrates potential to generate new incomes for farmers, new jobs and business to alleviate poverty in developing countries [15].

Similar to the requirement to reduce the costs of fermentation processes, and regarding the production of biochemicals and liquid biofuels, it was reported the need for advances in the energy-efficient separation of chemicals from fermentation broths [20], specifically, the need for alternatives to distillation [20, 21]. Using distillation to separate and recover alcohols or other products from dilute solutions is not very attractive from an energy standpoint [20]. Although, there are many advantages in using distillation, including high alcohol recovery, high concentration factor, easy to simulate the process with simulation programs and simple scale-up [20]. Unfortunately, concerning dilute solutions (>96 wt % of water) the distillation presents major disadvantages, such as azeotropes formation and higher energy requirement [20, 21].

1.2 Motivation

In the chemical industries, it is estimated that about 40% of the total energy consumption is expended in separation processes [21]. More than 90% of this energy is used in distillation, a reduction in distillation energy demand will have a great positive impact in existing and future processes [21].

An interesting alternative to distillation may be a membrane technology [21]. Membrane separations offer great opportunities to significantly reduce energy consumption in separation processes [20, 21].

Comparing both separation processes, if distillation was completely replaced with a membrane separation process, such as pervaporation (PV) or vapor permeation (VP), with a high performance dehydration membrane, highly selective and permeable, a reduction of about 85% in energy demand could be achieved [21]. However, the complete substitution of distillation with membrane separation requires significantly high performance of the membrane and large investment cost, which may block its large-scale application [21]. Although, this previous analysis suggests that just installing a membrane separation unit after the distillation is efficient enough to widely reduce the energy demand for the separation [21].

Considering all the inputs of energy and a low performance membrane, the installation of a membrane process in the late part of the distillation tower enables a reduction of around 70% of the energy consumption for the separation [21]. The energy efficiency of this distillation–membrane hybrid separation technology highly depends on the separation factor (α) of the membrane [21]. According to this, the performance of this hybrid separation process can be increased by replacing membranes as the membranes properties are improved [20, 21].

Membrane separation processes are capable of dealing with mixtures whit close boiling points and azeotropes formation, in contrast to azeotropic and extractive distillation, where entrainers or extra components are used to eradicate the azeotrope [20–23]. Furthermore, these membrane technologies are a simple and continuous operation, with the potential to save energy and they are also considered a clean and environmentally friendly technology [22, 23].

Membrane properties are the key to achieve such energy-efficient separation, however, conventional polymeric membranes do not have sufficient selectivity and permeation properties, and the commercial inorganic membranes, such as zeolite A membranes, show poor stability in aqueous and acidic solutions, which limits their application [21]. However, thermal and chemical stability of zeolite membranes can be improve by increasing the silica/aluminum (Si/Al) ratio of the zeolite framework [21].

It was recent developed a simple synthesis method to shape mordenite (MOR) zeolites, having higher Si/Al ratio than zeolite A, as membranes [24, 25]. These mordenite membranes showed higher thermal, acid and aqueous stability compared to the commercial zeolite A membranes [24, 25].

Dehydration of an aqueous solution is an essential step in the biorefinery industries, since the major compound of a fermentation broth is water [20, 26]. Mordenite membranes seem appropriate for dehydration of organic compounds from fermentation broths, however, they are still not commercialized [21].

The main focus of this study was to understand the potential of zeolite membranes to dehydrate aqueous mixtures of organic compounds from fermentation processes. Initially, it was evaluated the pervaporation performance and the stability of mordenite membranes in synthetic aqueous alcohol mixtures. Moreover, it was studied the influence of operating conditions on mordenite membranes performance. Regarding biofuels

production, it was evaluated the pervaporation performance and the stability of mordenite membranes in the dehydration of an ethanolic fermentation broth. Finally, the stability of zeolite A membranes in ethanolic fermentation broth was also evaluated.

1.3 Objectives

The main goal of this study was to understand the potential of the application of zeolite membranes to separate fermentation products. In particular, this study is focused on the pervaporation performance and stability of mordenite membranes in fermentation broths.

In order to reach this goal the tasks were divided into the following objectives:

- Evaluate the pervaporation performance and stability of mordenite membranes in synthetic aqueous alcohol solutions:
  - Methanol/water (MetOH/H_2O);
  - Ethanol/water (EtOH/H_2O).
- Study the influence of operating conditions, such as feed composition and temperature, on the pervaporation performance of mordenite membranes;
- Examine the pervaporation performance and stability of mordenite membranes in an ethanolic fermentation broth;
- Compare the stability in fermentation broth conditions of mordenite membranes and zeolite A membranes;
- Estimate the size of a mordenite membrane unit for the continuous dehydration of a distilled ethanolic fermentation broth.

It is important to highlight that using synthetic binary mixtures it is possible to characterize the pervaporation performance without the influence of impurities.

Chapter 2

State of the Art

2.1 Separation Technologies for Fermentation Broths

Similar to the modern petroleum refineries, biorefineries process renewable resources such as agriculture or forest biomass to produce energy and a wide diversity of precursor chemicals and bio-based materials [27]. Using wood and other lignocellulosic biomass as feedstock it is possible to produce industrial platform chemicals such as acetic acid, liquid fuels such as bioethanol and biodegradable plastics such as polyhydroxyalkanoates [27].

Unlike in refinery operations, several challenges related with the separation processes, including product recovery and purification, emerge in a biorefinery [28]. Although separation processes are relatively mature and in most cases well established in industries, they are typically energy intensive, contributing significantly to overall cost and CO_2 emissions [28, 29]. Therefore, improvements in these operations are essential to increase energy efficiency and economics of the entire process [29]. These include improvements to current separation processes, energy integration and development of energy-efficient processes such as membrane separation technology [20, 29].

Among the range of possible products from the biorefinery, liquid transportation fuels is rapidly gaining importance [27, 29]. Bioethanol is likely to be a prominent product in current and future biorefineries [27, 29]. Hence, this chapter will focus on the post-fermentation separation process, specifically and giving as an example, bioethanol recovery from the fermentation broth and further dehydration to fuel-grade ethanol

(FGE).

Downstream from the fermenter, the so-called beer, is usually a dilute aqueous solution containing about 4-12 wt % ethanol [27, 29]. The low content of ethanol in the broth is due to the toxic effect of ethanol on microorganisms and depends on the type of feedstock used and fermentation conditions [20, 29]. Regarding the bioethanol production from lignocellulosic biomass (second generation feedstock), the ethanol concentration in the beer is likely to be ≈ 5 wt % ethanol [29]. Despite the low content of ethanol in the fermentation broth, it contains several components that have higher relative volatility than ethanol in the mixture as seen in table 2.1 [30].

Table 2.1: Chemical composition of an industrial fermentation broth from an ethanolic fermentation; Results of gas chromatography analyses [30, 31].

Component	Mass fraction	Component	Mass fraction
Water	0.94	1-Pentanol	1.00×10^{-6}
Ethanol	5.75×10^{-2}	1-Hexanol	1.00×10^{-6}
Methanol	1.63×10^{-5}	Methyl acetate	1.00×10^{-6}
Isopropanol	1.00×10^{-6}	Ethyl acetate	1.88×10^{-5}
Propanol	5.74×10^{-5}	Acetaldehyde	1.09×10^{-5}
Isobutanol	4.75×10^{-5}	Acetone	1.00×10^{-6}
N-butanol	1.00×10^{-6}	Acetic acid	2.34×10^{-4}
2-Butanol	1.85×10^{-5}	Propionic acid	5.04×10^{-5}
Isoamyl alcohol	1.71×10^{-4}	CO_2	1.00×10^{-3}
2-Methyl-1-butanol	4.90×10^{-5}		

A significant amount of energy and high production costs are required to reach a concentration of ethanol equal to 99.7 wt % as specified for the European Union standards (EN 15376) or 98.7 wt % for the *American Society for Testing and Materials* (ASTM) standards [20, 32–34]. Energy-intensive separation is required to reach the purity target, mainly due to the presence of ethanol-water azeotrope at 95.6 wt % ethanol (78.15°C and 1 atm) and to the low ethanol concentration in the broth [27, 29, 34]. The major energy requirement is for ethanol recovery from 4-12 wt % ethanol to 92.4-94 wt % ethanol [27, 29, 34, 35]. This preconcentration step accounts for 60-80% of global separation cost of bioethanol from water [29]. Ethanol dehydration from near azeotropic mixture composition to fuel-grade ethanol specification is complex and has been of significant research interest [29].

In current biorefineries, distillation continues to be dominant in industries for the recovery section [29, 30]. For the dehydration section, azeotropic distillation with cyclohexane, extractive distillation with ethylene glycol and adsorption with molecular

sieves are used [27, 29, 30]. In order to achieve fuel-grade ethanol of high purity, the industry commonly use pressure swing adsorption (PSA) with molecular sieves after distillation [29, 30].

2.1.1 Distillation

Distillation is a commonly used process for separation of two or more components in a solution based on their relative volatilities or the difference in their boiling temperatures [20, 27, 30]. The ethanol–water azeotrope can be overcome to produce fuel-grade ethanol by varying the pressure of the distillation column [27, 30]. However, operating distillation columns at elevated pressure is usually avoided since it increases energy requirement, and operating a vacuum distillation column is complex and increases operating costs [27, 30]. Therefore, a conventional distillation column is often used in the preconcentration step, as mentioned above [27, 34, 35].

Other alternative methods for overcoming the azeotropic point of a liquid mixture are azeotropic distillation (AD) and extractive distillation (ED) [27, 30]. Usually, azeotropic distillation and extractive distillation systems are performed in a sequence of two columns, the first column is used to separate ethanol coming from the simple distillation while the other one is used to split water from the recovered mass separating agent (MSA) that is recycled back [27, 34, 35].

Azeotropic distillation involves adding a third volatile component, usually called entrainer, which forms a ternary azeotrope with the two components of the original mixture, and, thus, changes their relative volatilities and finally modifies their separation factor [27, 36]. Therefore, azeotropic distillation can be used to separate mixtures of components having similar boiling points and to break azeotropes [27, 36].

In biorefinery, azeotropic distillation is commonly used for dehydration of concentrated ethanol solution coming from the conventional distillation column [27, 29, 36]. The typically used entrainers to eliminate the ethanol-water azeotrope by azeotropic distillation are cyclohexane, benzene and toluene [20, 27, 29, 36].

The azeotropic distillation system mentioned above has several disadvantages including high energy requirement, large capital cost, and safety and health concerns with the storage of either highly flammable (cyclohexane) or carcinogenic (benzene) entrainers [27, 35, 36].

Similar to azeotropic distillation, extractive distillation is a vapor–liquid separation process with the addition of a third component to enhance the relative volatility of the

components to be separated [27, 37]. This added component is used to modify the activity coefficients and hence increase the separation factor [27]. In contrast to azeotropic distillation, extractive distillation performs the separation in the presence of a miscible, high boiling point, relatively non-volatile component that does not form any azeotrope with the other components of the mixture [27, 34].

The third component added as separating agent can be a non-volatile liquid solvent, a dissolved salt, a mixture of non-volatile liquid solvent and dissolved salt, an ionic liquid, or a hyperbranched polymer [27]. For the extractive distillation of ethanol-water, ethylene glycol remains the most commonly used entrainer [27, 34, 37].

Extractive distillation using ethylene glycol has propitious advantages such as high product quality, suitability for large scale production and relatively low volatilization amount [30]. However, a large amount of solvent is required to reach the purity target of fuel-grade ethanol and has to be recovered and recycled within the process, which results in high energy requirement [27, 30, 35].

Instead of a liquid solvent, a dissolved salt could be used as the separating agent [30]. The relative volatility of the ethanol-water mixture can be widely increased at relatively low concentrations of salt [27, 30]. This is known as "salt effect", which is the preferential solvation of ions formed when the salt dissociates in the mixture [27, 28, 30].

Compared to extractive distillation with a liquid solvent, the advantages of using a soluble salt are: high energy savings due to the absence of additional vaporization-condensation cycle of a liquid solvent inside the column, production of a distillate completely free of the added component, and lower toxicity level of certain salts in comparison to liquid solvents [27, 30]. However, special and more expensive construction materials for the equipment involved will be required to prevent corrosion problems [27, 30].

A well-known example of extractive distillation with soluble salts is the *Holz Industrie Acetien Geselleschaft* (HIAG) process, which employs a 70/30 molten mixture of potassium and sodium acetate as the separating agent to produce more than 99.8 wt % ethanol, with lower capital and operating costs compared to conventional azeotropic distillation with benzene or extractive distillation with ethylene glycol [27, 30].

It has been shown that extractive distillation using calcium chloride ($CaCl_2$), the salt that provides the best salting out effect on ethanol, as the separating agent has lower energy requirement than that using ethylene glycol as well as azeotropic distillation using benzene [27, 30]. It was also reported that extractive distillation with $CaCl_2$ consumes

almost the same energy as membrane pervaporation [27, 30].

Briefly, extractive distillation with ionic liquids or hyperbranched polymers represent two promising novel separations and has excellent selectivity and separation efficiency without polluting the distillate by separating agents, thus requires less energy consumption compared to extractive distillation using liquid solvent, dissolved salt or the mixture of both [27].

Dividing-wall column (DWC) has been suggested as a novel distillation technology, which has been asserted to be more energy-efficient compared to conventional 2-column sequence for dehydration after preconcentration [30]. This type of column can be used in the extractive distillation and azeotropic distillation of near azeotropic ethanol–water feed [30, 35].

In the case of a dividing-wall column used for ethanol dehydration, part of a single column shell is split into two sections by the insertion of a vertical wall in the column at a suitable position [30, 35]. Accordingly, high savings in equipment cost can be achieved as only one column is required for the separation [30, 35]. Moreover, the operating cost can be reduced by the use of less utility in reboilers and condensers [30, 35]. It has been reported that use of dividing-wall column can result in up to 30% saving in capital cost and up to 40% saving in operating cost [30, 35].

Kiss and Suszwalak [35] proposed a conventional extractive dividing-wall column (E-DWC) for ethanol–water–ethylene glycol system. Extractive dividing-wall column is a split-shell column with divided overhead sections and a common bottoms section as seen on figure 2.1 for concentrated ethanol feed [30].

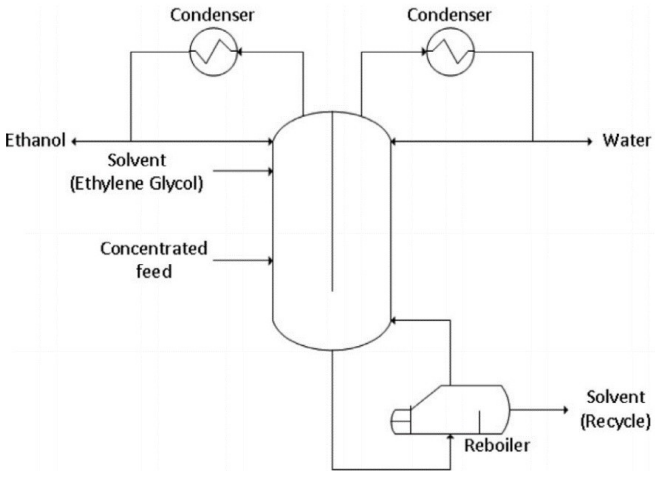

Figure 2.1: Conventional E-DWC proposed by Kiss and Suszwalak [35] for concentrated ethanol–water feed [30].

Compared to the optimized conventional extractive distillation system, around 10% energy saving is possible by using extractive dividing-wall column for ethanol dehydration [30, 35].

Kiss and Ignat [38] proposed a novel configuration that integrates all three columns of the conventional process, recovery and dehydration columns, into a single dividing-wall column, hence reducing capital cost and footprint significantly [30]. In order to reduce the significant energy requirement in evaporating water, in this design, water is removed as a liquid side stream at the feed side or the preconcentration section towards the lower part of the dividing wall [30, 38]. However, an additional side reboiler is required in order to return sufficient amount of water vapour to the extractive dividing-wall column [30, 38]. Figure 2.2 shows the novel configuration of extractive dividing-wall column proposed by Kiss and Ignat [38].

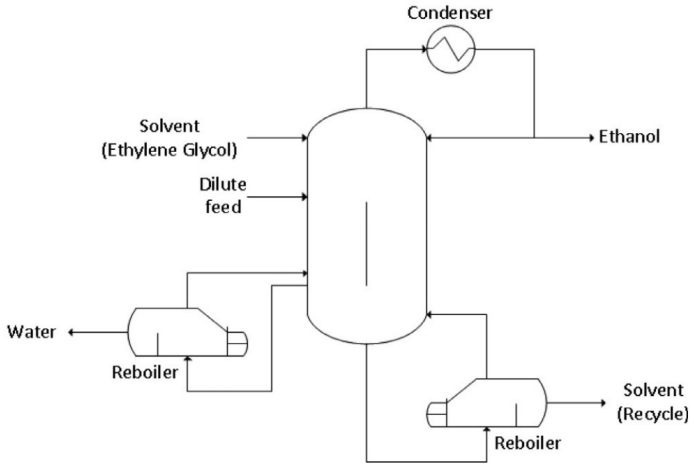

Figure 2.2: Novel configuration of E-DWC proposed by Kiss and Ignat [38] for dilute ethanol–water feed [30].

The innovative extractive dividing-wall column results in total energy savings of 17%, and a similar reduction of total investment and total annual cost as compared to the conventional extractive dividing-wall column proposed by Kiss and Suszwalak [30, 35, 38].

2.1.2 Adsorption

Adsorption is a separation technology that works on the molecular level [30]. This process involves the entrapment of target molecules in pores by the formation of temporary bonds so that they can be separated from other molecules [30, 39]. For removing small quantities of specified components from a mixture, adsorption using molecular sieves is a popular method because of its selectivity and ease of maintenance [30].

A molecular sieve is a material containing precise and uniform pores of molecular dimensions [39]. Making use of this advantage, the pore size is made such that molecules larger than the target molecules cannot enter [30, 39]. For instance, 3A zeolite molecular sieves, which has a nominal pore size of 3 Å, are used for dehydration process since water molecules are roughly 2.6 Å in diameter [20, 27, 30, 39]. Thus, molecules larger than 3 Å cannot enter in the pores and pass right over the molecular sieves [20, 27, 30, 39].

Strength of adsorption of target molecules in molecular sieves depends strongly on pressure and temperature, thus giving rise to two types of adsorption processes: pressure swing adsorption (PSA) and temperature swing adsorption (TSA), respectively [30]. The molecules are strongly adsorbed on molecular sieves at high pressures and low temperatures and the molecular sieves are regenerated at low pressures and high temperatures [27, 30, 39]. Both methods are fairly effective, but pressure swing adsorption is usually preferred than temperature swing adsorption due to lower operating cost [39]. The existence of heat of adsorption increases temperature during adsorption and decreases temperature during desorption, making temperature swing adsorption disadvantageous because a large amount of energy has to be supplied and removed in every cycle, creating difficulties in maintaining temperature of the temperature swing adsorption column [30].

The pressure swing adsorption system involves at least 2 columns/beds, between which adsorption and desorption processes are alternated [30]. As seen in the figure 2.3, in a 2-column configuration, the first column is used for adsorption under pressure while the other is regenerated under vacuum conditions [30].

To guarantee a better regenerative process, some of the pure product exiting column 1 is channelled through column 2 for purging, by opening valves 5 and 6 [30]. Once column 1 is exhausted, column 2 is re-pressurized to adsorption conditions and the processes are switched [30]. While column 2 is now used for adsorption, column 1 is depressurized to vacuum conditions to be regenerated [30].

A comparison of different pressure swing adsorption system configurations found that 2-column configuration is capable of producing high purity ethanol, although multi-tube and 3-column processes tend to be more stable and energy efficient [30].

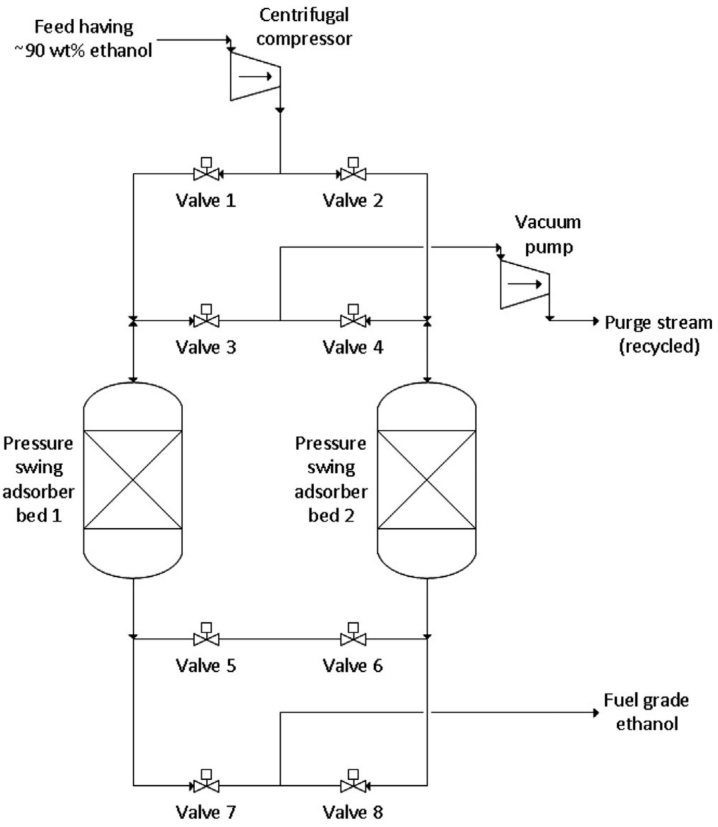

Figure 2.3: Conventional PSA system of 2-column configuration [30].

Comparing different molecular sieves, zeolite molecular sieves are highly selective, but water is very strongly adsorbed, thus low pressures and/or high temperatures are required to regenerate them [27]. Although, bio-based adsorbents have lower separation capacity than zeolite molecular sieves, but their regeneration temperature is much lower comparing to the previous one [27]. In addition, zeolite molecular sieves are more expensive than bio-based adsorbents [27].

2.1.3 Liquid-liquid Extraction

In liquid-liquid extraction (LLE), the fermentation broth is placed in mass-transfer contact with a liquid extractant and compounds are transferred from the broth to the extractant [20]. Liquid-liquid extraction is a particularly promising method for the recovery of ethanol from dilute aqueous solution with low energy requirement [27]. However, this method alone is unable to produce the purity levels required to reach fuel-grade ethanol [37].

Usually, liquid-liquid extraction is combined with fermentation, called extractive fermentation (EF), where *in situ* extraction is carried out to remove the bioproduct and other

inhibitory compounds, hence inhibitions caused by the bioproduct and other inhibitors are eliminated, increasing the fermentation yield [27].

In extractive fermentation, the selection of a high efficient solvent is a very important step [27]. The solvent can not be toxic to microorganisms and expensive; it must present high distribution coefficient, high stability, high selectivity for the product, low solubility in the aqueous phase, different density from that of the broth to ensure separation by gravity, low viscosity, large interfacial tension and low tendency to emulsify in the broth [27].

Oleyl alcohol, n-dodecanol, n-dodecane, isoamyl acetate, isooctyl alcohol, and nonanoic acid are some examples of potential biocompatible solvents for extraction of bioethanol from the broth [27, 29, 33].

Gyamerah and Glover [40] developed a pilot-scale extractive fermentation with n-dodecanol as extractant to remove the ethanol and with recycle of the treated fermentation broth [27]. It was found a reduction of 78% on the fresh water consumption, due to the successful recycle of the fermentation water [27, 40].

In short, extractive fermentation results show an increase in bioethanol yield and a decrease in fresh water consumption, resulting in an obvious reduction of overall ethanol production cost [27].

2.1.4 Membrane Separation

Membrane processes are mass transfer unit operations utilized to separate liquid and gas streams [39]. Membrane is an ultra thin semipermeable barrier which, under a certain driving force, permits preferential transport of one or more selected species of a mixture through the barrier [39, 41, 42]. The driving force for permeation can be a concentration gradient, a pressure gradient, an electrical potential gradient, among others [41]. The capacity to permeate gives to the membrane its utility and potential to separate a diversity of process streams [39].

Membranes can be classified according to their morphology, for instance, dense, porous or composite [41, 43]. They can also be categorized in terms of structure, which can be symmetric or asymmetric [41, 43]. Moreover, in terms of membrane materials, membranes can be classified in two different categories: organic (polymeric) or inorganic (ceramic and metallic) [27, 41, 43].

In comparison to polymeric membranes, inorganic membranes have excellent thermal, chemical and mechanical stability and exhibit higher antifouling property due to the

hydrophilic nature of inorganic material [27, 41, 43]. Although, polymeric membranes have easy preparation, low capital cost, small size, lower energy requirement, flexibility in membrane configuration, and relatively low operating temperature which is also related with less rigorous demands for the materials need in the construction of module [43].

Moreover, according to the type of separation applied, they can be categorized in microfiltration, ultrafiltration, reverse osmosis, gas separation, pervaporation and vapor permeation membranes [41]. In all membrane methods, the membrane separates the fluid passing through it into: a permeate, that which passes through the membrane, and a retentate, that which is left behind [39].

Pervaporation (PV), vapor permeation (VP) and gas permeation (GP) are closely related processes [44]. These three methods are described by the "solution-diffusion" mechanism and the driving force for the transport of components through the membrane is a chemical potential gradient that can best be described by a gradient in partial vapor pressure of the components [20, 27, 41, 44]. Their main differences are determined by the phase state and the thermodynamic conditions of the feed mixture and the condensability of the permeate [44].

Pervaporation enables the separation of some mixtures that are energy-intensive and difficult to separate by distillation, extraction, and adsorption [27, 45]. Pervaporation presents advantages in the separation of azeotropes, close-boiling mixtures, and thermally sensitive compounds, and in the removal of species present in low concentrations [27, 41, 45]. During pervaporation, only a fraction of a mixture is vaporized, thus lower temperatures than those required in distillation are usually used [45]. Furthermore, membranes operate continuously without requiring sorbent regeneration, and they are modular, which allows design flexibility [45]. All these advantages make pervaporation processes economically attractive in many industrial applications [27, 45].

In pervaporation a feed liquid mixture, such as a fermentation broth, contacts one side of a non-porous or molecularly porous membrane and the permeate is removed as a vapor from the other side [20, 46, 47]. A vacuum or, less common, a gas purge is applied to the permeate side of the membrane creating the permeate vapor stream [20, 27]. In the laboratory, the vapor pressure difference can be maintained by a vacuum pump, used to draw vacuum on the permeate side [20, 27, 46]. Industrially, the permeate vacuum is most economically generated by cooling the permeate vapor, causing it to condense and spontaneously creating a partial vacuum [46].

A simplified scheme of a pervaporation process is shown in figure 2.4 [20, 46]. Certain compounds can be enriched in the permeate relative to the feed, due to the different sorption and diffusion behaviours with the selective membrane material of compounds in the feed liquid [20]. As liquid moves through the membrane, the concentration of the preferentially permeating compound is reduced and the liquid leaving the membrane system, referred to as the retentate, is depleted in that compound [20].

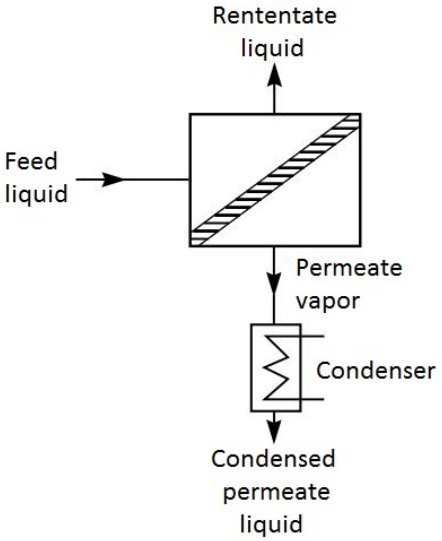

Figure 2.4: Simplified schematic diagram of a PV process [46].

The flux of a component i through a pervaporation membrane can be expressed in terms of the partial vapor pressures on either side of the membrane by the following equation [46].

$$J_i = \frac{P_i}{\delta}(p_i^F - p_i^P) \tag{2.1}$$

where J_i is the flux, P_i is the permeability coefficient, δ is the membrane thickness, p_i^F and p_i^P are the partial vapor pressures of component i at the feed and permeate side, respectively [46]. Equation 2.1 is used to describe membrane performance and it separates the two contributions to the membrane flux: the membrane contribution (P_i/δ) and the driving force contribution ($p_i^F - p_i^P$) [46].

The pervaporation performance is reported in terms of total flux, J_{total}, through the membrane and separation factor, α_{ij}, defined for a binary mixture as the ratio of the two components on the permeate side of the membrane divided by the ratio of the two components on the feed side of the membrane [46].

$$\alpha_{ij} = \frac{c_i^P / c_j^P}{c_i^F / c_j^F} = \frac{p_i^P / p_j^P}{p_i^F / p_j^F} \tag{2.2}$$

where c_i and c_j are the concentrations and p_i and p_j are the partial vapor pressures of the two components i and j at feed (F) and permeate (P) side [46].

Generally, most membranes are hydrophilic or water perm-selective due to the small size of water molecules, while few membranes are hydrophobic or alcohol perm-selective [20, 27].

In the case of alcohol recovery from fermentation broths by pervaporation, the use of hydrophobic alcohol-selective membranes will result in a permeate enriched in alcohol [20, 47]. Although, the permeate must be purified further in order to meet fuel-grade ethanol specifications or to even match the output from a conventional distillation [20]. Fortunately, to meet the purity produced in distillation, efficient fractional condensation schemes have been developed which allow a combined pervaporation-condensation system [20, 48].

Many membrane materials have been studied for the recover of organic compounds from water by pervaporation [27, 48]. The most potential hydrophobic polymeric membranes are poly(dimethyl siloxane) (PDMS or "silicone rubber") and poly[1-(trimethylsilyl)-1-propyne] (PTMSP) membranes [27, 47, 48]. It has been reported that PDMS membranes present a ethanol-water separation factor ranging from 4.4 to 10.8 and a butanol-water separation factor ranging from 40 to 60 [27, 48]. PTMSP is a high free volume polymer displaying a permeability greater than that of PDMS and also presents a higher ethanol–water separation factor, ranging from 9 to 26 [27, 48]. The butanol–water separation factor for PTMSP is approximately equal to 70 [48]. Unfortunately, PTMSP membranes deliver unstable performance, with flux and selectivity declining with time [48]. The most studied hydrophobic zeolite membrane for this application is silicalite-1 membrane and has been reported that this membrane presents an ethanol–water separation factor ranging from 12 to 106 with a typical value around 40, four to five times higher than of PDMS [27, 48]. In addition, fluxes observed with silicalite-1 membranes meet or exceed those of the thinnest PDMS films reported [48]. Like with all inorganic membranes in other applications, silicalite-1 membranes are expected to be more expensive per unit area than polymeric membranes [27, 48]. Although, silicalite-1 membranes may be cost effective per unit of ethanol recovered owing to the higher separation factor and flux

afforded [27, 48]. Due to the difficulty and cost of manufacturing silicalite-1 membranes, it has been investigated the potential of silicalite-PDMS mixed matrix membranes [48]. This mixed matrix membranes present a range of ethanol–water separation factors of 7 to 59 [48]. The performance of these mixed matrix membranes strongly depends on the source and loading of silicalite-1, size of the particles, and membrane casting conditions [48]. The increased performance properties with small cost increase has led to the interest in mixed matrix membrane materials [29, 48].

Another membrane process, membrane distillation (MD), is often mentioned for the recovery of organic compounds, such as alcohols from water [20, 47, 48]. In membrane distillation, a porous membrane separates the feed liquid from the gas or vacuum purge applied on the permeate side of the membrane [20]. In the case of a vacuum purge, the process is referred to as vacuum membrane distillation (VMD) [20, 27, 48]. Actually, vacuum membrane distillation is quite similar to pervaporation, the only difference being that the separation factor here is established by vapor–liquid equilibrium (VLE) of the feed solution which is not affected by the type of membrane used [27]. Since a vacuum membrane distillation system requires similar equipment to a pervaporation system, but does not offer any improvement in the purity of the permeate, it is not a very attractive alternative [20].

In the case of alcohol dehydration from concentrated alcohol aqueous solutions, the use of hydrophilic water-selective membranes will result in a rententate enriched in alcohol [20, 28].

The most significant competition to molecular sieve adsorption for alcohol dehydration has come from the membrane technologies of pervaporation and vapor permeation [20, 48]. Unlike the cyclic nature of molecular sieve adsorption, pervaporation and vapor permeation can be operated continuously [20]. In addition, in most cases, the membrane processes were reported to require less energy than a molecular sieve adsorption system [20].

The potential of pervaporation and vapor permeation for dehydration is owing to the ability of the hydrophilic membranes to selectively remove water from alcohols even when the vapor–liquid equilibrium behaviour is unfavorable and in a continuous manner [20, 27]. Furthermore, water-ethanol separation factors achieved with pervaporation and vapor permeation dehydration membranes range from 10 to 10 000 [20]. Butanol-water separation factors for the same materials are typically even higher [20].

A range of membrane materials can be considered, depending on the particular conditions of the separation [20]. The most common hydrophilic polymeric membrane material for this application is poly(vinyl alcohol) (PVA) [20]. In case of inorganic membranes, the most common membranes for dehydration of alcohols are zeolite A membranes [20, 27]. Unfortunately, within a given class of materials, a trade-off is observed between selectivity and permeability, thus, materials that present higher water selectivity also present lower fluxes [20].

In summary, developing membranes that can provide high permeance, selectivity, operating life, and sustain higher temperatures would reduce the capital cost and operating cost of the current membrane separation processes to the point that the technology is even more competitive than other conventional and implemented technologies [20, 29].

2.1.5 Hybrid Processes

Azeotrope formation and the large range of concentrations involved in producing anhydrous alcohol from a dilute aqueous solution all make it difficult for one process to efficiently perform this separation [20]. Thence, hybrid processes are considered to be the most energy efficient and cost effective alternatives [20, 29].

As mentioned previously, the usual ethanol-water separation process, in current biorefineries, is a hybrid process of distillation and molecular sieve adsorption [20, 29, 30]. In this hybrid process, the distillation is used to recover the alcohol from the fermentation broth, and the molecular sieve adsorption is used to dehydrate the solution that results from the previous distillation.

Recently, the pervaporation and vapor permeation performance of several zeolite membranes has been discussed regarding the energy savings of its use in a distillation-membrane hybrid system [21].

It was reported that a distillation-pervaporation hybrid would require an equivalent of 5.02 MJ_{fuel}/kg_{EtOH} to produce 99.8 wt % ethanol from 8.8 wt % ethanol [20, 49]. However, a heat-integrated distillation-adsorption hybrid system would require about 4.6-5.6 MJ_{fuel}/kg_{EtOH}, approximately the same as the previous alternative hybrid [20].

A hybrid distillation-vapor permeation system, which used distillation to produce an 80 wt % ethanol concentrate from a 10 wt % ethanol feed stream followed by a vapor permeation membrane to produce 99.5 wt % ethanol, was proposed [20, 50]. Heat integration was considered, the latent heat from the vapor permeation retentate was recovered in the distillation reboiler [20, 50]. Although, an equivalent of 5.17 MJ_{fuel}/kg_{EtOH} of

steam was required and, again, it is in the range of what would be expected for a heat-integrated distillation-adsorption hybrid system (4.4-5.4 MJ_{fuel}/kg_{EtOH} for a 10 wt % ethanol feed) [20, 50].

A similar study was made, comparing energy demand and energy cost for the recovery and dehydration of a 10 wt % ethanol stream using a two-column distillation unit connected with either a molecular sieve unit or a vapor permeation unit [20, 51]. The results showed that the distillation-vapor permeation combination required 3.6% less energy than the distillation-molecular sieve hybrid and a 3.8% reduction in the energy cost [20, 51]. It is notable that both studies reached the same conclusion, the hybrid distillation-vapor permeation system presents a small reduction in energy consumption comparing with the current hybrid distillation-molecular sieve process. Even though, distillation-vapor permeation hybrid processes are likely near-term alternatives to distillation-molecular sieves systems for alcohol recovery and dehydration [20].

Most of the energy used for the separation is in the form of steam and can be obtained, for instance, by burning solid waste of bioethanol plants [29]. In summary, energy for bioethanol separation using efficient technologies is expected to be 19% to 24% of the lower calorific value (LCV) of ethanol (26.7 MJ_{fuel}/kg_{EtOH}) [29]. Thus, it is expected that an energy-efficient process does not consume more than 6.4 MJ_{fuel}/kg_{EtOH} [29].

Often, complexity is introduced in order to improve the quality of the separation, because no process is totally efficient, however, each added step frequently leads to additional costs [20]. Combination of different technologies can be an exception to this rule [20].

2.2 Zeolites

A zeolite is a hydrated crystalline aluminosilicate material with a three-dimensional framework structure that forms uniformly sized pores of molecular dimensions [52, 53]. These materials occur in nature, but can be synthetically manufactured and are composed of tetrahedra building units of TO_4 (T = Si, Al or P) with oxygen atoms connecting neighboring tetrahedra [53–56].

When the zeolite is composed exclusively of $Si^{4+}O_4^{2-}$ tetrahedra, the framework is neutral, since an oxygen atom connects with two silicon atoms [54, 56]. In this case, the zeolite exhibits hydrophobic properties [54, 56]. Upon incorporation of aluminum into the silica framework, the structure becomes negatively charged, since the valency of

aluminum is +3 [54, 56]. In this scenario it is required the presence of extra-framework cations within the structure to preserve the electroneutrality of the zeolite [52, 54, 56]. These extra-framework cations are ion exchangeable and give rise to the ion-exchange capacity of these materials [52, 54]. The presence of aluminum in the zeolite framework has several effects, the zeolite becomes hydrophilic and acidic, and the presence of the extra-framework cations can render the zeolite catalytically active and sometimes might obstruct the pores thus reducing the pore size of the structure [56]. Therefore, decreasing the Si/Al ratio increases the number of cations that are required to balance the charge and the hydrophilicity of the zeolite [56].

Zeolites are microporous structures and the size of their pores is determined by the number of oxygen atoms that form the pore aperture (usually 6, 8, 10 or 12 atoms) and the possible obstruction of the pores by the extra-framework cations [54, 56]. The diameter of the zeolite pores typically ranges between 0.3 to 1.0 nm and can have ellipsoidal and spherical shapes [53, 55, 56]. The framework projections for commonly studied zeolite frameworks are given in figure 2.5 [54, 56].

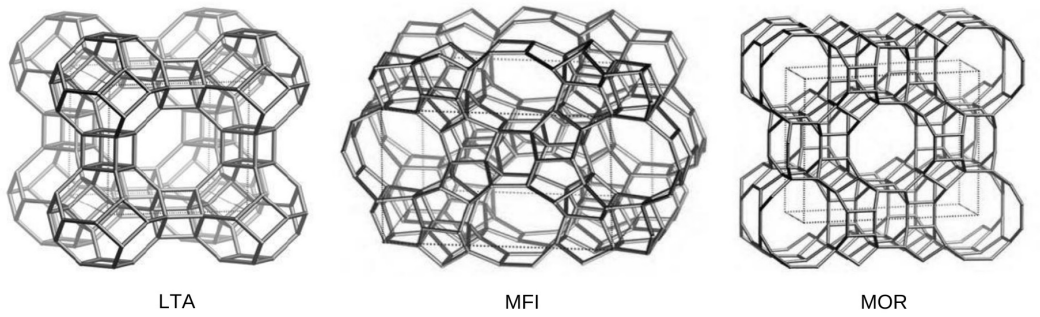

Figure 2.5: Zeolite framework projections: LTA (8-ring), MFI (10-ring) and MOR (12-ring and 8-ring between 12-ring channels) [57, 58].

The crystalline nature of the framework ensures that the pore openings are uniform throughout the crystal and can easily exclude molecules based on their molecular size, giving rise to the name molecular sieves [54, 56].

The exploitable properties of zeolitic materials, including ion-exchange properties, sorption capacity, shape selectivity, catalytic activity, and role as hosts in advanced materials, are primarily determined by their structures [52, 54]. For instance, the ion-exchange selectivity depends on the number and nature of the cation sites and their accessibility; the sorption capacity depends on the size of the pore openings and the void volume; the catalytic behaviour depends on the pore openings, the dimensionality of the channel

system, the cation sites, and the space available for reaction intermediates [52].

Generally, most zeolites are synthesized by dissolving an amount of silica and an amount of alumina in a strongly basic aqueous solution [52]. Ultimately, the structure that is formed highly depends on the solubility, the Si/Al ratio, the nature of the cation, and the synthesis temperature of the resultant gel [52].

The use of zeolites is well established in several areas such as laundry detergents, oil refining and petrochemical industries, gas separations, agriculture and horticulture, pigments, and jewelry [52, 54, 56]. These materials are extensively used as ion-exchangers, catalysts, and adsorbents in the above mentioned industries [54].

In laundry detergents, the major ion-exchange market for zeolites, the cation exchange capacity determines how well the zeolite can replace the calcium and magnesium cations ("hard cations") in the wash water with sodium cations ("soft cations") [52, 56]. As an adsorbent, maximum extra-framework cation density increases the extent to which the molecular sieves are able to hold onto polar adsorbates [52]. Moreover, in catalytic applications it is desirable to have a high silica content in the framework because the structure becomes resistant to the high temperatures of the catalytic and regeneration cycles [52].

Figure 2.6 summarizes the characteristics of several zeolite frameworks that have been applied in zeolite membranes, in terms of Si/Al ratio and pore dimensions together with the kinetic diameter of several molecules [21, 56].

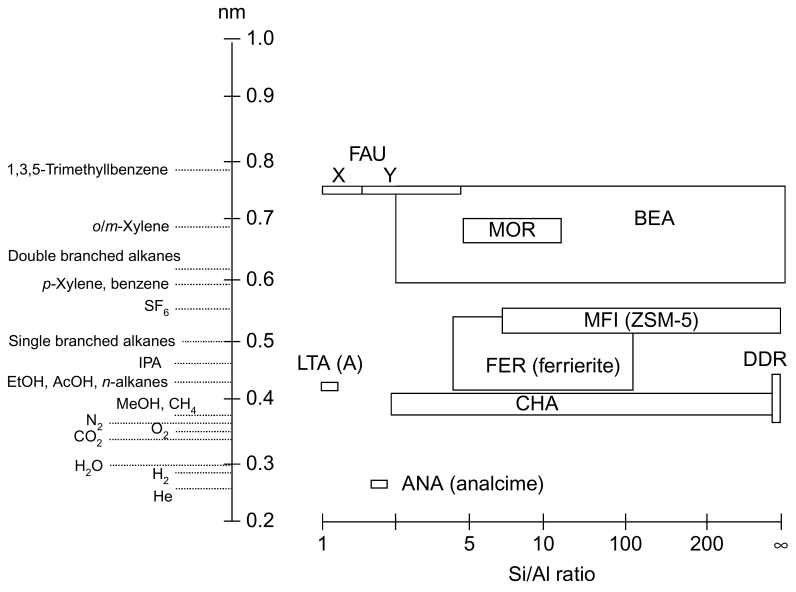

Figure 2.6: Pore dimensions of zeolites in relation to the kinetic diameter of several molecules and the respective Si/Al ration of zeolite framework [21, 56].

2.3 Zeolite Membranes

As mentioned in the chapter 2.1, membrane separation technology is attractive from the stand point of both energy consumption and separation selectivity and efficiency [59, 60]. In particular, inorganic membranes such as zeolite membranes are especially interesting because of their high thermal, mechanical, and chemical stability [59, 60].

Zeolites are an ideal membrane material because they have uniform, molecular-sized pores, allowing an efficient separation based on differences in molecular size and adsorption strength [21, 45, 61]. The hydrophilic/hydrophobic nature and stability of zeolites can be adjusted by changing the Si/Al ratio in the zeolite framework [21]. Nevertheless, the crystallographic structure and chemical composition of a given zeolite determine their separation properties and allow the rational design of membranes [59].

Although zeolite membranes have shown remarkable progress at laboratory scale and promising results in industrial applications such as alcohol dehydration, butane isomer separation, xylene isomer separation and natural gas purification, only hydrophilic membranes used in the dehydration of industrial solvents and fuels have been commercialized to date [45, 59, 60].

Zeolite membranes are polycrystalline zeolite layers deposited on porous inorganic supports [45]. These membranes offer several advantages over polymeric membranes, including high thermal and chemical stability, and do not swell [45]. The chemical stability allow these membranes to separate strong solvents and low pH mixtures [45].

Since the first zeolite membrane was reported [62], significant progress has been made to improve zeolite membranes quality and extend their range of applications [45, 63]. Although more than 232 zeolite frameworks have been indexed by the *International Zeolite Association* (IZA) [58], only about 20 structure types were prepared as membranes [45, 63].

Although hydrophilic zeolite A membranes have been commercialized since 1997 for alcohol dehydration, the MFI structure (figure 2.5) is most largely studied in zeolite membranes, due to their large attractive industrial properties, such as suitable pore sizes, high thermal and chemical stability, easy synthesis and possible modification of their chemical composition [45, 63]. This type of structure includes silicalite-1, that is made up of pure silica, and ZSM-5, with Al atoms substituting some of the Si atoms [45].

2.3.1 Synthesis

Since the mechanical strength of self-supporting, thin zeolite membranes is insufficient for practical use, zeolites are usually directly grown on a porous ceramic or metal support [21, 59, 64]. The most common support materials are alumina and stainless steel [21, 45, 59]. Typically, alumina supports have pore diameters between 5 nm (γ-Al_2O_3) and 200 nm (α-Al_2O_3), and stainless steel support pore diameters are between 0.5 and 4.0 μm [45, 65].

One of the challenges of the preparation of zeolite membrane is preparing them with high flux whilst maintaining high separation selectivity [65]. In order to achieve this goal, zeolite membranes should be preferably made of pure zeolite crystals with uniform and small particle size [65]. During the formation of zeolite membranes, two critical steps occurred, namely nucleation on the support followed by crystal growth, to form a continuous zeolite layer covering the support [65, 66].

The most common method used for zeolite membrane synthesis is the conventional hydrothermal synthesis [45, 65]. In this procedure, the porous support is completely immersed into the synthesis solution [45, 65]. This solution is usually composed of water, amorphous silica, a source of tetrahedral framework atoms other than Si such as alumina, a structure directing agent (SDA), and sometimes a mineralizing agent [45]. A zeolite film is formed on the surface of the support by direct crystallization [45, 65]. The hydrothermal synthesis method is easier to operate, but the characteristics of the support surface have significant influence on the synthesized membrane properties [65]. In addition, due to the low heating rate and the heterogeneous heating, zeolite crystals formed are not uniform in size because the zeolite nuclei do not form on the support surface simultaneously [65].

Secondary growth method is an effective method to synthesize high quality zeolite membranes [45, 64, 65]. In this method, zeolite seeds are used to coat the support surface, before hydrothermal synthesis, in order to provide sites for zeolites growth and improve control of crystal growth [45, 64, 65]. The secondary growth technique presents advantages such as higher reproducibility and better control over membrane microstructure (thickness and orientation) [64, 65]. This method has been used to prepare thin and oriented zeolite membranes, which have increased fluxes by aligning pores in a desired direction [45]. Seeding is also an effective technique to obtain zeolite membranes free or with lesser amounts of structure directing agents [21]. Organic structure directing

agents are corrosive and expensive, therefore, synthesis of zeolite membranes without these agents is important for the environment and for the membrane cost [21, 64]. Although the secondary growth method allows improved control of nucleation site location and density, by rendering the nature of support less importance for membrane growth, with growth proceeding from a layer of seed crystals covering the support [21, 66], this preparation method is complicated being involved in multi-step synthesis [65].

An alternative technique for synthesis of inner-side zeolite membranes is the continuous flow synthesis method [65]. Growing a zeolite layer in the inner side of the support is a difficult task due to the low accessibility of the interior of tubular supports [65]. In the continuous flow synthesis method, the synthesis solution is continuously supplied to the inner surface of the support [65]. This synthesis method has several advantages, it is energy efficient by eliminating the high energy consumption that is required for repeated heat-up and cool down in batch crystallizers, it produces a more uniform product because of the readily controlled operating conditions, and it requires smaller equipment and possibly lower capital costs as compared to a batch process at the same production rate [65].

Lately, the microwave synthesis has been reported for the preparation of zeolite membranes [25, 65]. This synthesis method has the advantages of short synthesis time, broad synthesis composition, small zeolite particle size, narrow particle size distribution and high purity, comparing with the conventional hydrothermal synthesis [65]. Microwave method is more efficient in transferring thermal energy to a volume of material because the energy is supplied by electromagnetic field directly to the material, while in the conventional thermal processing the transport of heat through the surface of the material is supplied by convection, conduction and radiation [65].

However, the synthesis reproducibility is still, since the first zeolite membrane was reported, the main drawback [59]. This lack of reproducibility is notable when the performance of membranes of the same zeolitic phase, but prepared in different laboratories, are compared [59]. This difference in the performance can be related to the thickness of the membrane, the presence of different concentrations of intercrystalline defects, and also the distribution of the zeolite material in the support [59].

2.3.2 Characterization

Zeolite membrane characterization is essential to evaluate the quality of the synthesized membrane [45, 65].

Scanning electron microscope (SEM) can be used to determine the microstructure, crystal size and membrane thickness [45, 65]. This characterization method can also give a qualitative idea of zeolite layer continuity and uniformity [45, 65]. In addition, surface morphology and crystallinity can also be determined by transmission electron microscope (TEM). X-ray diffraction (XRD) is typically used to determine zeolite phase, framework structure and orientation, and relative crystallinity [45, 65]. Zeolite composition is measured using electron probe microanalysis (EPMA) or inductively coupled plasma (ICP) [45, 65]. Electron probe microanalysis can also be used to determine the distance that the zeolite layer penetrates into the pores of the support [45]. The possible presence of large non-zeolite pores can be evaluated with single gas permeation such as nitrogen permeation [45, 65]. Lastly, nitrogen adsorption is used to examine the BET surface area, pore size distribution, micropore and mesopore volume and isotherm [65].

2.3.3 Dehydration Technology

As mentioned above, zeolite A membranes are the only one type of zeolite membranes that has been commercialized [21, 64]. These membranes are used in the dehydration of different alcohols because of their strong hydrophilicity and suitable small pore size, which enable the obtention of a high-purity product [21, 64].

A pioneering role in the development of zeolite NaA membranes for the dehydration of bioethanol was played by *Bussan Nanotech Research Institute Inc.* (BNRI), Japan, a member of the *Mitsui Holding* [64, 67, 68]. The zeolite NaA membrane from BNRI has been tested in a pilot plant combined with a distillation column placed before the zeolite membrane vapor permeation process to produce fuel-grade ethanol from sugar-cane fermentation broth [68].

Hitachi Zosen Corporation commercializes zeolite A membranes, to incorporate in hybrid distillation systems, that are suitable for the dehydration of ethanol and isopropyl alcohol [59, 65]. This company reported the performance of zeolite A membranes with extremely high water flux (>50 kg m^{-2} h^{-1}) and high water perm-selectivity (>1000) for a ethanol-water mixture of 90/10 wt % at 130°C [21].

Zeolite A membranes show excellent alcohol dehydration performance and, therefore, have been commercialized at an early stage in the development of zeolite membranes [21].

Regarding the production of acetic acid, the development of membranes for dehydration of organic acids are highly desired due to their significant impact on energy saving [21]. Although hydrophilic zeolite A membranes have been applied industrially

for the dehydration of alcohols, these membranes are not stable at high temperatures and low pH systems, such as organic acid systems [21, 59]. As mentioned before, it is possible to enhance the thermal and acid stability of zeolite membranes by increasing the Si/Al ratio of the zeolite framework, however there is a trade-off with hydrophilicity [21]. Therefore, zeolite membranes with medium Si/Al ratio, such as MOR and ZSM-5 membranes, seem appropriate for dehydration of organic acids [21]. For this reason, attention has been given to the development of these zeolite membranes for potential applications where zeolite A membranes cannot be applied [21, 59].

There are many challenges to be overcomed for the large-scale application of zeolite membranes in future industries, including improvement of membrane performance, development of a membrane synthesis method suitable to be scaled-up, and design of optimum process flow schemes [21].

2.4 Mordenite Membranes

Acetic acid (HAc) is one of the most important organic intermediates used in chemical industry [69, 70]. However, like ethanol case, separation of acetic acid-water mixtures by traditional distillation is an energy-intensive procedure due to the small differences in volatility between water and acetic acid [69, 70]. In recent years, pervaporation using zeolite membranes has been recognized as a promising candidate for the dehydration of organic acid aqueous solution [69, 70].

Most of the separation processes and chemical reactions, such as the dehydration of acetic acid and the esterification reaction, involve carboxylic acids or inorganic acids [25]. Therefore, the development of long-term acid-stable and durable zeolite membranes is essential for energy savings in chemical or biochemical engineering processes [25].

Mordenite membranes are an alternative and promising membranes for the dehydration of organic mixtures in industry, especially for the harsh acidic aqueous mixtures because they show a great resistance in acidic medium and high hydrophilicity [24, 25, 71, 72]. These type of zeolite membranes present medium Si/Al ratio (3-10) and two types of regular channels (0.65x0.70 nm parallel to the c-axis and 0.26x0.57 nm parallel to the b-axis) [24, 25]. Figure 2.7 shows the mordenite framework and its channels size.

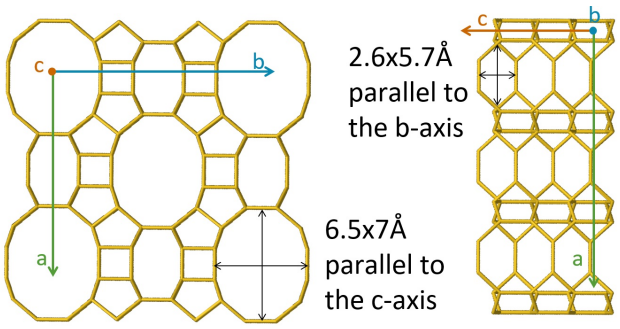

Figure 2.7: Mordenite framework projections and channels size [58].

The literature contains many publications on the preparation of acid-stable mordenite membranes and also the optimization of synthesis parameters [24, 25, 70–73]. However, few publications study in depth the pervaporation performance and the influence of pervaporation operating conditions in the performance of these membranes.

Zhou et al. prepared mordenite membranes in fluoride media on porous tubular mullite supports by a direct hydrothermal synthesis [73]. These thin mordenite membranes showed high average flux of 1.6 kg m^{-2} h^{-1} and high average separation factor of 1300 for 90/10 wt % ethanol-water mixture at 75°C by pervaporation [73].

When mordenite membranes are prepared by conventional hydrothermal synthesis, the synthesis time ranges from 8 to 96h [25]. Shortening the synthesis time is an important factor for the industrial preparation of mordenite membranes [25].

Zhu et al. reported, for the first time, the rapidly preparation of acid-stable mordenite membranes by microwave-assisted synthesis [25]. These acid stable mordenite membranes, synthesized in 3h, exhibited fluxes of 1.10 and 0.44 kg m^{-2} h^{-1} and high selectivities of 7500 and 2300 for ethanol-water and acetic acid-water (90/10 wt %) mixtures at 75°C by pervaporation, respectively [25].

After two years, Zhu et al. applied a mordenite membrane as a "membrane extractor reactor" for the esterification of acetic acid and alcohol with the sulfuric acid (H_2SO_4) as catalyst [71]. These mordenite membrane reactors were placed into the reaction mixtures and continuously remove water from the esterification mixture by pervaporation, which greatly improved the alcohol conversions of esterification [71]. Moreover, theses mordenite membranes showed long-term stability for the pervaporation-esterification with H_2SO_4 as catalyst [71].

Li et al. synthesized high performance mordenite membranes in a short synthesis time

from fluoride-containing dilute solution without structure directing agent by microwave-assisted synthesis [70]. These mordenite membranes exhibited high fluxes of 0.87 ± 0.06 kg m^{-2} h^{-1} and excellent selectivities, that is only pure water was detected in the permeate side for dehydration of 90 wt % acetic acid aqueous mixtures at 75°C [70].

Well acid-resistant mordenite membranes were successfully and rapidly prepared by microwave-assisted synthesis in previous studies [25, 70]. However, regarding the scale up of membrane preparation, the mordenite membranes should be prepared by the conventional secondary hydrothermal synthesis [24].

In the end of 2016, Zhu et al. reported the preparation of acid-resistant mordenite membranes on porous mullite supports by secondary hydrothermal synthesis [24]. It was studied in detail the influence of the synthesis parameters (synthesis time, the fluoride content and type, Si/Al ratio, and alkalinity) on the growth of the mordenite crystals and on the pervaporation performance of the synthesized membranes [24]. These long-term acid-resistant mordenite membranes showed high average flux of 0.81 kg m^{-2} h^{-1} and average separation factor of 736 for 90/10 wt % acetic acid-water mixture at 75°C by pervaporation [24]. Furthermore, the mordenite membranes synthesized kept their integrity after immersion in a 95 wt % HAc/H_2O mixture at 90 or 100°C for 48h [24].

Mordenite membrane can be considered a promising separation membrane for the production of biofuels and biochemicals by continuous dehydration of fermentation broths, and also for the production of esters by continuous removal of water from esterification reactions [25]. Table 2.2 summarizes the pervaporation performance of mordenite membranes prepared by different research groups.

Table 2.2: Pervaporation performances of mordenite membranes for organics/water mixtures [73].

Support	Synthesis conditions		Feed			Pervaporation performance		Ref.
	Temperature (°C)	Time (h)	Temperature (°C)	Solution	Composition (wt %)	Flux ($kgm^{-2}h^{-1}$)	$\alpha_{w/o}$ (-)	
Mullite	170	5	75	HAc/H_2O	90/10	0,81	736	[24]
α-Al_2O_3	170	3	75	EtOH/H_2O	90/10	1.10	7500	[25]
				IPA/H_2O	90/10	1.45	12800	[25]
				HAc/H_2O	80/20	1.00	>39996	[25]
				HAc/H_2O	90/10	0.44	2300	[25]
α-Al_2O_3	165	4	75	HAc/H_2O	90/10	0.87 ± 0.06	>11400	[70]
Mullite	170	16	75	EtOH/H_2O	90/10	1.60	1300	[73]
				IPA/H_2O	90/10	1.85	3300	[73]
α-Al_2O_3	180	8	150	EtOH/H_2O	90/10	0.20	150	[74]
	After post-treatment with NaOH solution		150	EtOH/H_2O	90/10	0.91	203	[75]
α-Al_2O_3	180	18		EtOH/H_2O	90/10	0.08	32	[76]
	After post-treatment with oxalic acid solution			EtOH/H_2O	90/10	0.12	10000	[76]
Mullite	170	96		EtOH/H_2O	90/10	0.39	1000	[77]
	165	12		EtOH/H_2O	90/10	0.11	>10000	[77]

[a]IPA: isopropanol

Chapter 3

Materials and Methods

3.1 Materials

3.1.1 Zeolite membranes and modules

To elaborate this study, it was used two mordenite membranes previously synthesized by master student Yoshihiro Kajimura and one zeolite A membrane synthesized by bachelor student Naoyuki Aso were used.

The mordenite membranes were prepared on the outer surface of tubular porous mullite supports (Nikkato Corporation, outer diameter = 12 mm, inner diameter = 9 mm, pore size = 1.33 μm, length = 100 mm, porosity = 43%) by secondary hydrothermal synthesis, based on the reference [24]. The zeolite A membrane was also synthesized by secondary hydrothermal synthesis on the outer surface of a tubular porous mullite support.

In order to use the membranes in pervaporation experiments it was necessary to seal them in membrane modules. Tubular membranes have open ends on each side of the porous support, thus, one of the ends is completely sealed and the other end is connected to a glass tube with the same inner diameter of the porous support. To close one of the ends a compact small glass cylinder and a polymeric tube are used. This polymeric tube connects the membrane and the glass cylinder. After this step, a shrinkable polymeric tube is placed in the connection and heated to completely seal that end. The same procedure is made in the other end, but using a glass tube and not a

compact cylinder. To a better understanding, the figure 3.1 shows a membrane module and also all the materials used to prepare it.

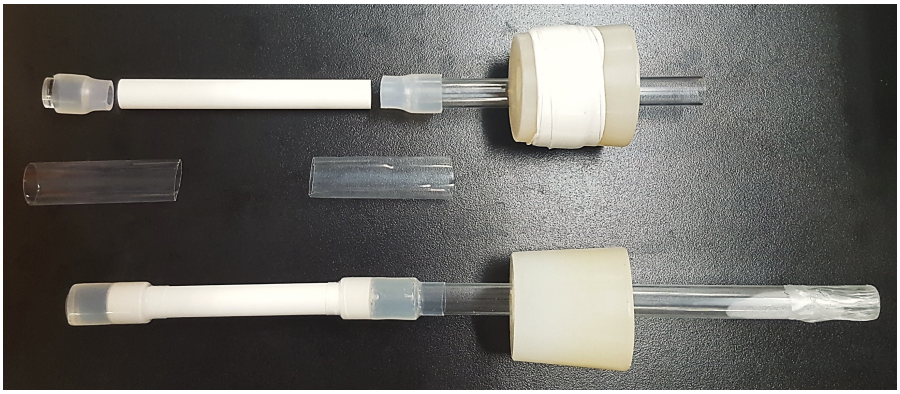

Figure 3.1: Membrane module and all the materials used to prepare it.

After the preparation of the membrane module, the effective length of the membrane is measured with a ruler. Due to irregularities in the membrane module preparation, the membrane length is measured in 3 different points, and, thus, the effective length of the membrane is the average of the 3 results obtained. In table 3.1 are presented the effective length, the effective surface area and the number of pervaporation experiments performed with each membrane.

Table 3.1: Effective length, effective surface area and number of pervaporation experiments of each membrane.

Membrane identification	**Effective length (cm)**	**Effective Surface Area (cm^2)**	**Number of PV experiments**
MOR-72	6.23 ± 0.05	23.50 ± 0.18	25
MOR-73	6.57 ± 0.05	24.76 ± 0.18	44
A-7	6.83 ± 0.05	25.76 ± 0.18	6

In Appendix A are presented the steady state performance results of all pervaporation experiments for each membrane.

3.1.2 Synthetic Mixtures

Initially, in the first pervaporation experiments were used synthetic aqueous solutions with different alcohol compositions as feed liquid. In table 3.2 are summarized the binary mixtures and the range of compositions used in the pervaporation experiments. These solutions were prepared based on weight and using a weighing balance (A&D Company, Ltd., GX-1000, ± 0.001 g), and, thus, it is accepted an error of ± 2 wt % of alcohol in the final composition of the mixtures.

Table 3.2: Range of compositions used as feed in pervaporation experiments.

Systems	Range of Compositions	
EtOH/H_2O	10-90 wt % EtOH	4 - 78 mol % EtOH
MetOH/H_2O	10-90 wt % MetOH	6 - 84 mol % MetOH

Besides binary mixtures, it was also used, in some pervaporation experiments, distilled water as feed liquid. In table 3.3 are summarized the pure components used to prepare the synthetic binary mixtures for the pervaporation experiments.

Table 3.3: Pure components used to prepare the synthetic binary mixtures for the pervaporation experiments.

Pure Components	Chemical formula	Purity (vol %)	Molecular weight (g/mol)	Boiling Temperature (°C)
Water	H_2O	100.0	18.02	100.0
EtOH[a]	C_2H_6O	> 99.5	46.07	78.2
MetOH[b]	CH_4O	> 99.8	32.04	64.6

[a]Mitsubishi Chemical Corporation [78]; [b]Wako Pure Chemical Industries, Ltd. [79].

3.1.3 Distilled fermentation broth

Furthermore, it was used a real fermentation broth, kindly provided by the Agriculture Department of Yamaguchi University, as feed liquid in pervaporation and soaking experiments with zeolite membranes. This fermentation broth was the result of an ethanolic high-temperature fermentation [17], and it was previously treated with a simple laboratory distillation.

The distilled fermentation broth had a composition of about 41 wt % EtOH and an impurity that appears in the gas chromatograms with a retention time around 10 minutes, which it was not possible to characterize. The pH value of the distilled fermentation broth was measured using pH test paper (Advantec, Univ test paper, pH 1-11); the paper colour showed a pH around 5.

3.2 Methods

3.2.1 Scanning Electron Microscopy

Scanning electron microscopy was used to determine the zeolite mordenite crystals shape, and the mordenite membrane thickness on top of the mullite support. These membrane images were obtained by master student Yoshihiro Kajimura and presented in this study for a better understanding of the membrane morphology. It is important to note that the SEM images obtained are from a mordenite membrane synthesized in the

same way as those used in the pervaporation experiments, which does not mean that the thickness is exactly the same.

The surface and cross section of the mordenite membranes were observed by JEOL JSM 6335F field emission scanning electron microscope, operated with an electron beam intensity of 5 kV. The samples were cut and then were coated with a thin layer of platinum particles to facilitate the conduction of the electron beam.

3.2.2 X-ray Diffraction

In this work, X-ray diffraction was used to identify structure changes in zeolite A-7 membrane after immersion in the fermentation broth for 13.5 hours.

A Rigaku Smartlab X-ray diffractometer with Cu Kα radiation was used, which operates at 45 kV and 200 mA. The diffractograms were obtained in the range of $2\theta = 5 - 45°$ at a scanning rate of 4° min^{-1}.

3.2.3 Gas Chromatography

During pervaporation experiments, the composition of the feed mixture and the permeate samples was analyzed by gas chromatography. It was used a Shimadzu GC-8AIT gas chromatograph equipped with a thermal conductivity detector (TCD) and a stainless steel column (outer diameter = 5 mm, inner diameter = 4 mm, length = 6 m) [80]. The column is packed with an inert high purity carbon support (ShinCarbon A, particle size = 60 ~ 80 mesh), and the support particles are coated with TSG-1 liquid stationary phase, with a liquid phase amount of 15%. Moreover, the threshold detection level of this type of equipment is below 0.01 wt %.

In table 3.4 are summarized the operating conditions of the gas chromatography measurements.

Table 3.4: Operating conditions of the gas chromatography measurements.

Carrier gas	Helium
Injection volume	1 μl
Injection port temperature	250°C
Detector temperature	250°C
Column oven temperature	90°C
Current	100 mA

3.2.4 Pervaporation

The mordenite membranes were used to separate binary aqueous alcohol mixtures with different compositions, as well as the distilled fermentation broth by pervaporation

at different temperatures (40°C, 60°C and 75°C). The zeolite A membrane was used in pervaporation experiments with the synthetic standard mixture of 90 wt % EtOH after soaking experiments in the distilled ethanolic fermentation broth in order to study the membrane stability in those conditions. The pervaporation experimental apparatus is illustrated in the figure 3.2.

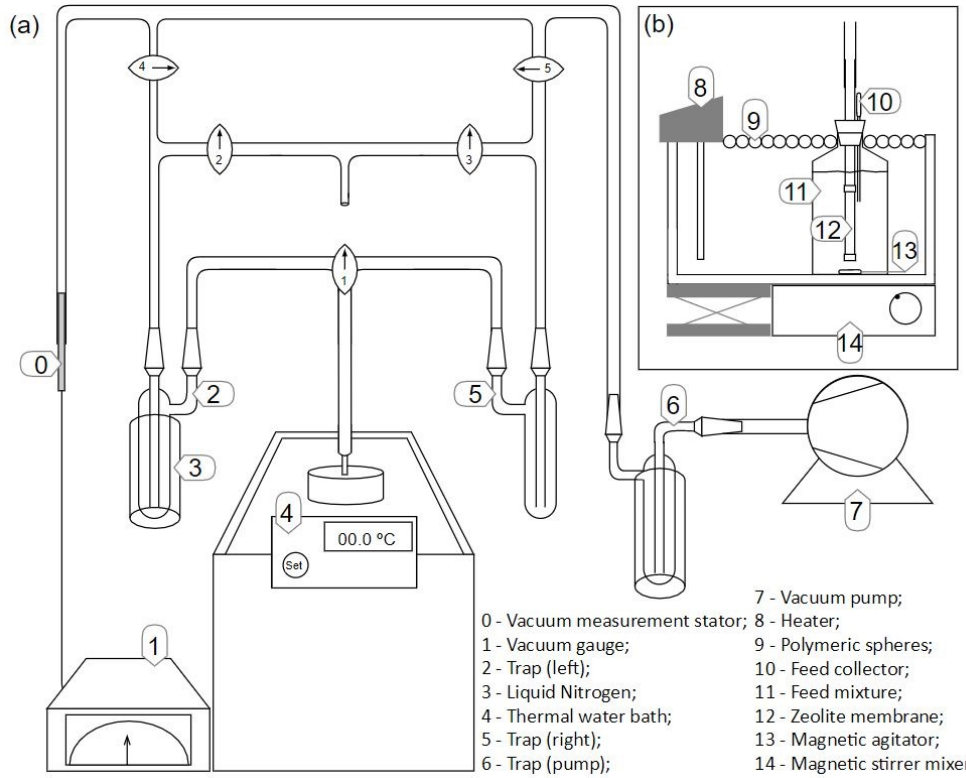

Figure 3.2: Schematic representation of the pervaporation experimental apparatus; (a) outside front view, (b) inside lateral view.

The vacuum gauge (Ulvac Japan, Ltd., Pirani Vacuum Gauge Control GP-2A) measures and displays the permeate side pressure, but, unfortunately, this pressure is neither controlled nor programmed. On the contrary, the temperature of the thermal water bath (Tokyo Rikakikai Co., Ltd., Eyela NTT-2400) can be controlled and programmed up to 180°C. Notably, the vacuum pump (Ulvac Sinku Kiko, GLD-136) is used to apply vacuum on the permeate side and, in this study, the permeate pressures were maintained below $\approx$ 50 Pa. Moreover, the magnetic stirrer mixer (Ikeda Scientific Co., Ltd., IS-3C) is used to keep the homogeneity of the feed mixture.

The feed liquid mixture is placed in the thermal water bath and heated to the set temperature. After this first step, the zeolite membrane module is directly immersed into the feed liquid mixture. The permeates, in vapor phase, are collected and solidified in

the cold trap by liquid nitrogen (N_2). As mentioned above, the composition of the feed mixture and the permeate samples was analyzed using a gas chromatograph (Shimadzu Corporation, GC-8AIT) at certain times. To maintain the amount and the composition of the feed mixture, the feed and permeate samples collected are recycled during the pervaporation experiment.

Initially, the pervaporation experiment starts with the opening to the left of valve 1 and the opening of valve 4. The first permeate is collected in the left trap for 1 hour. After the first hour, the bottle of liquid nitrogen is placed in the right side, the valve 4 is closed, the valve 1 is turned right and the valve 5 is opened, the permeate is collected in the right trap during a certain amount of time, enough to collect at least $\approx$ 1 gram of permeate. When the objective of the experiment is to reach the steady state, the permeate side is alternated successively until it reaches approximately constant values of total flux and permeate composition. Valves 2 and 3 are used to remove the trap with the solid permeate from the installation by eliminating the vacuum in that side. After this step, the trap is immersed in water at room temperature for about 10 - 15 minutes, to melt the solid permeate. Posteriorly, the liquid permeate mass is measured using a weighing balance (A&D Company, Ltd., GH-252, $\pm$ 0.1 mg).

Zeolite membranes can adsorb impurities during pervaporation and also from the atmosphere during storage, and these impurities can significantly affect the membrane performance [45]. To avoid this situation, after each pervaporation experiment, the zeolite membranes were kept in empty recipients, covered with paper at room temperature. Figure 3.3 shows the membrane module storage.

Figure 3.3: Membrane module storage.

3.2.5 Calculation Methods

3.2.5.1 Pervaporation performance

The pervaporation performance of the zeolite membranes was evaluated by the total flux (J_{total}), the component flux (J_i), and the separation factor of water over organics ($\alpha_{w/o}$). The effective surface area (S) and the total flux of the membrane were determined with the following equations [24, 25].

$$S = \pi d l \quad [m^2] \tag{3.1}$$

$$J_{total} = \frac{m}{St} \quad [kg\, m^{-2}\, h^{-1}] \tag{3.2}$$

where d is the outside diameter, l is the effective length of the membrane, t is the test time, and m is the mass of permeate collected in the liquid N_2 trap over a known test time. Accounting the equipments uncertainties, the error propagation in the total flux calculation, during a pervaporation experiment, yields a relative standard deviation of 8×10^{-3}. In the steady state, the flux is the average of the last three results of a pervaporation experiment after reach the steady state. In appendix A is presented the standard deviation of the steady state results.

The flux of the component i is calculated using the equation 3.3.

$$J_i = \frac{m_i}{St} \quad [kg\, m^{-2}\, h^{-1}] \tag{3.3}$$

where m_i is the mass of component i in the permeate collected by the liquid N_2 trap over a known test time.

The separation factor of water over organics is experimentally determined using the equation 3.4 [24, 25].

$$\alpha_{w/o} = \frac{Y_w/Y_o}{X_w/X_o} \quad [-] \tag{3.4}$$

where Y_w, Y_o, X_w and X_o denote the mass fractions of the water (w) and organic (o) components at the permeate (Y) and feed (X) sides, respectively. It is important to highlight that the separation factor is a ratio of ratios, and small changes in the composition can lead to large changes in the separation factors, especially at low feed concentrations and high permeate concentrations [45].

The flux and the separation factor are not only a function of the intrinsic properties of the membrane used, but also depend on the operating conditions of the experiment, such as feed concentration, permeate pressure and feed temperature [81]. Hence, it becomes difficult to compare pervaporation performance results of experiments

with different operating conditions [81]. A more useful way to report pervaporation performance is presenting membrane permeabilities (P_i), permeances (P_i/δ) and selectivities (α'_{ij}), which are related to the intrinsic properties of the separation membranes [81]. These intrinsic and driving force normalized properties do not depend on operating conditions [81]. However, a majority of the pervaporation papers report results as fluxes and separation factors, avoiding the direct comparison of the results [81].

Membrane permeability is a component flux normalized for membrane thickness and driving force, while membrane permeance is a component flux just normalized for driving force [81]. Membrane permeability and permeance can be calculated using the equations 3.5 and 3.6, respectively [81].

$$P_i = J_i \frac{\delta}{\Delta P} \quad [mol\, m^{-1}\, s^{-1}\, Pa^{-1}] \tag{3.5}$$

$$\frac{P_i}{\delta} = \frac{J_i}{\Delta P} \quad [mol\, m^{-2}\, s^{-1}\, Pa^{-1}] \tag{3.6}$$

where δ is the membrane thickness and ΔP is the pressure difference across the membrane, also called driving force. However, it was decided to present the results in terms of membrane permeance, because the real thickness of the mordenite membranes used are not known [81].

Membrane selectivity can be determined by the equation 3.7 and it is defined as the ratio of permeabilities or permeances of the components i and j through the membrane [81].

$$\alpha'_{ij} = \frac{P_i}{P_j} = \frac{P_i/\delta}{P_j/\delta} \quad [-] \tag{3.7}$$

In the calculation of permeance, it was assumed that the boundary layer deposited on the surface of the membrane is in equilibrium with the permeate vapor (vapor-liquid equilibrium) and the partial pressure of the components in the permeate side (p_i^P) is ≈ 0 Pa, because it is considered total vacuum.

To calculate the permeance of the component i, it is necessary to calculate the driving force, which is $\Delta P = p_i^F - p_i^P$. Since it was assumed that $p_i^P \approx 0$, the previous equation becomes $\Delta P \approx p_i^F$. To calculate the partial pressure of the component i in the feed side (p_i^F) it was used the Modified Raoult's Law (equation 3.8) [82].

$$p_i^F = y_i P = x_i \gamma_i P_i^{sat} \tag{3.8}$$

where P is the total pressure, y_i and x_i is the molar fraction of the component i in the vapor and liquid phase, respectively, P_i^{sat} is the saturated vapor pressure of the component i, and γ_i is the activity coefficient of the component i.

Moreover, the Antoine equation (equation 3.9) was used to calculate the saturated vapor pressure (P_i^{sat}) of each component of the mixtures [83].

$$\log_{10} P_i^{sat}[kPa] = A - \frac{B}{C + T[^\circ C]} \tag{3.9}$$

where T is the temperature and A, B and C are the component-specific constants. In table 3.5 are presented the component-specific constants for the components used in this work.

Table 3.5: Component-specific constants of Raoult's Law [83].

Component	A	B	C	Temperature range (°C)
Water	7.07	1657.46	227.02	[10;168]
EtOH	7.34	1652.05	231.48	[-3;97]
MetOH	7.20	1574.99	238.86	[-16;91]

To calculate the activity coefficient (γ_i) of each component it was used the Wilson's Equation (equation 3.10). The Wilson's Equation contains two adjustable parameters for binary systems, Λ_{12} and Λ_{21} [84].

$$\begin{aligned}
\ln \gamma_1 &= -\ln(x_1 + \Lambda_{12} x_2) + x_2 \left(\frac{\Lambda_{12}}{x_1 + \Lambda_{12} x_2} - \frac{\Lambda_{21}}{\Lambda_{21} x_1 + x_2} \right) \\
\ln \gamma_2 &= -\ln(x_2 + \Lambda_{21} x_1) - x_1 \left(\frac{\Lambda_{12}}{x_1 + \Lambda_{12} x_2} - \frac{\Lambda_{21}}{\Lambda_{21} x_1 + x_2} \right) \\
\Lambda_{12} &= \frac{v_2}{v_1} e^{-\frac{\gamma_{12} - \gamma_{11}}{RT}} \\
\Lambda_{21} &= \frac{v_1}{v_2} e^{-\frac{\gamma_{12} - \gamma_{22}}{RT}}
\end{aligned} \tag{3.10}$$

where x_i is the molar fraction of the component i in the liquid phase, v_i is the molar volume of the component i ($cm^3\ mol^{-1}$) and T is the temperature (K). In the table 3.6 are presented the constants of the binary mixtures used in this work.

Table 3.6: Constants of Wilson's Equation for binary systems [84].

Binary system		$\frac{\gamma_{12} - \gamma_{11}}{R}$	$\frac{\gamma_{12} - \gamma_{22}}{R}$
(1)	(2)		
EtOH	Water	112.10	503.66
MetOH	Water	41.76	262.00

The molar volume (v_i) is the volume occupied by one mole of a substance at a given temperature and pressure. To calculate the molar volumes it was used the equation 3.11.

$$v_i = \frac{M_i}{\rho_i} \tag{3.11}$$

where M_i is the molar mass of the component i and ρ_i is the specific weight of the component i at a given temperature and pressure. In table 3.7 are presented the calculated molar volumes of the components used at different temperatures.

Table 3.7: Calculated molar volumes of the components used at a pressure of 101325 Pa (1 atm) [85, 86].

Component	**Temperature (ºC)**		
	75ºC	**60ºC**	**40ºC**
Water	18.48	18.32	18.16
EtOH	62.33	61.10	59.67
MetOH	43.47	42.56	41.50

3.2.5.2 Apparent Activation Energy

In pervaporation processes, both membrane permeability and driving force for mass transport are influenced by temperature [87]. The permeability of the compound i (P_i) depends in the partition and diffusion through the membrane [87], resulting in equation 3.12.

$$P_i = D_i S_i \tag{3.12}$$

where D_i and S_i are the diffusivity and solubility coefficients of the component i, respectively. The temperature dependence of both coefficients can normally be expressed by Arrhenius's Equation, resulting in the following equations [87].

$$D_i = D_0 exp\left(\frac{-E_D}{RT}\right) \tag{3.13}$$

$$S_i = S_0 exp\left(\frac{-\Delta H}{RT}\right) \tag{3.14}$$

Thus, it results the equation 3.15, which relates the temperature with the membrane permeability [87].

$$P_i = P_0 exp\left(\frac{-E_p}{RT}\right) \tag{3.15}$$

where E_p ($= E_D + \Delta H$) is the activation energy of permeation, which is a combination of the activation energy of diffusion (E_D) and the heat of sorption (ΔH_s) of the permeant in the membrane [87]. In addition, P_0 ($= D_0 S_0$) is a pre-exponential factor [87].

As a practical matter, the used of membrane permeance (P_i/δ) is often more convenient, especially in the case of asymmetric and composite membranes where an accurate determination of effective membrane thickness is difficult [87]. Thus, rearranging the equation 3.15, it is possible to correlate the temperature with the membrane permeance yielding the equation 3.16.

$$\frac{P_i}{\delta} = \frac{P_0}{\delta} exp\left(\frac{-E_p}{RT}\right) \tag{3.16}$$

Thus, the apparent activation energy of permeation (E_p) should be evaluated from the slope of $\ln(P_i/\delta)$ vs. $1/T$, instead of $\ln(J_i)$ vs. $1/T$, which is the most common way reported in the literature, however this linearization leads to an overestimated activation energy (E_J), which normally is a positive value and can be related with the apparent activation energy (E_p) by the equation 3.17 [87].

$$E_p = E_J - \Delta H_v \tag{3.17}$$

where ΔH_v is the heat of vaporization.

In this study, the apparent activation energy for the permeation of ethanol and water was calculated by the temperature dependence of ethanol and water permeances, using the following linearizations, respectively.

$$ln\left(\frac{P_{EtOH}}{\delta}\right) = \frac{-E_p^{EtOH}}{R}\left(\frac{1}{T}\right) + ln\left(\frac{P_0}{\delta}\right) \tag{3.18}$$

$$ln\left(\frac{P_{Water}}{\delta}\right) = \frac{-E_p^{Water}}{R}\left(\frac{1}{T}\right) + ln\left(\frac{P_0}{\delta}\right) \tag{3.19}$$

where E_p^{EtOH} is the apparent activation energy of ethanol permeation, E_p^{Water} is the apparent activation energy of water permeation, R is the ideal gas constant (8.314 J K^{-1} mol^{-1}) and T is the temperature (K).

CHAPTER 4

RESULTS AND DISCUSSION

4.1 Scanning Electron Microscopy

A mordenite membrane was analyzed by scanning electron microscopy (SEM) in order to study the morphology of the crystals and to determine the zeolite membrane thickness on top of the support. The surface and the cross sectional SEM images of the mordenite membrane are displayed in figure 4.1a and b, respectively. It is important to note that the membrane observed is neither the mordenite membrane MOR-73 nor the mordenite membrane MOR-72.

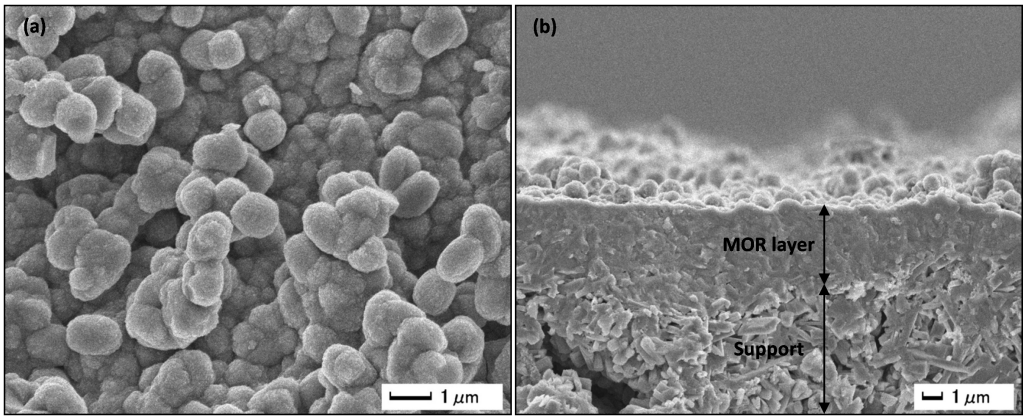

Figure 4.1: (a) Surface and (b) cross-sectional SEM images of a mordenite membrane.

As shown in figure 4.1a, highly intergrown and aggregated spherical mordenite crystals fully covered the mullite support surface. The crystal morphology observed in figure 4.1a is similar to that reported in the literature for the mordenite membranes [24, 25].

In figure 4.1b it is possible to observe a clear boundary between the zeolite layer and the support. The thickness of the mordenite zeolite layer was approximately 4 μm. The mordenite layer thickness was calculated to give an idea of the order of magnitude of the membrane thickness, however it is not used in further calculations because it could not correspond to the real thickness of the mordenite membranes MOR-73 and MOR-72.

4.2 Pervaporation

4.2.1 Synthetic Feed Mixtures

Synthetic binary aqueous mixtures of methanol and ethanol were used to study the pervaporation performance and the influence of operating conditions on the performance of the mordenite membranes. The objective of most experiments performed in this section is to characterize the pervaporation performance of the mordenite membranes at the steady state.

4.2.1.1 Influence of feed composition

It was studied the influence of the feed composition on the pervaporation performance of the mordenite membranes. The feed temperature must be constant and below the boiling temperature of the feed mixture, therefore the experiments were carried out at temperatures below the boiling point of the pure components. In methanol-water systems the feed temperature was kept constant at 60°C and in ethanol-water systems the feed temperature was kept at 75°C. The feed composition was gradually increased from 0 to 90 wt % of alcohol in order to understand its influence on the mordenite membrane pervaporation performance.

In methanol-water experiments, it was used as standard composition the mixture with 10 wt % MetOH. The standard composition is used to check the membrane stability after a certain number of experiments. Table 4.1 shows the steady state pervaporation performance results of the mordenite membrane MOR-73 for methanol-water feed mixtures at 60°C with the variation of the methanol concentration in the feed side from 0 to 90 wt %.

Table 4.1: PV performance of MOR-73 for different compositions of MetOH/H_2O mixtures at 60°C (333 K).

Run No.	Feed (wt % MetOH)	Permeate (wt % MetOH)	J_{MetOH} (kg m^{-2} h^{-1})	J_{H_2O} (kg m^{-2} h^{-1})	$\alpha_{w/m}$ (-)
29	0	0.00	-	0.88	-
19	10	0.04	2.87×10^{-4}	0.67	265
20	20	0.06	3.61×10^{-4}	0.58	401
21	50	0.19	6.73×10^{-4}	0.35	505
22	80	0.65	8.48×10^{-4}	0.13	607
23	90	1.18	6.71×10^{-4}	0.06	728

As shown in table 4.1, both methanol and water fluxes were influenced by the increase of feed methanol composition. The water flux clearly decreased with the increase of feed methanol composition. In addition, the mordenite membrane MOR-73 showed water perm-selectivity with separation factors above 260 for the whole methanol concentration range studied. The separation factor increases with the alcohol concentration, since the ratio of water to alcohol molecules in the feed side decreases faster than in the permeate side [88].

For a general understanding, figure 4.2 shows the influence of feed composition on the total flux (figure 4.2a) and on the permeate composition (figure 4.2b) of the mordenite membrane MOR-73 for methanol-water mixtures at 60°C.

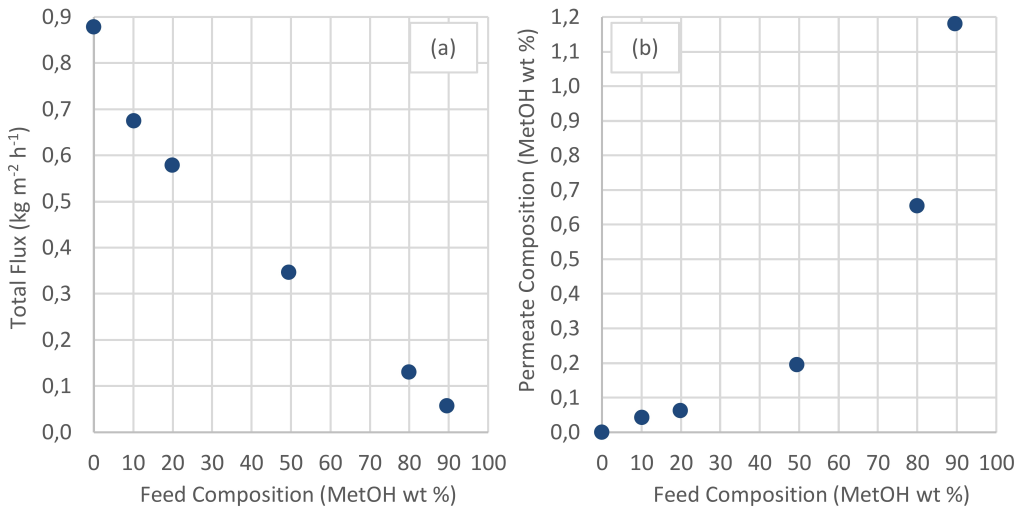

Figure 4.2: Influence of feed composition on (a) total flux and (b) permeate composition of MOR-73 for MetOH/H_2O mixtures at 60°C (333 K).

As shown in figure 4.2a, the total flux of the mordenite membrane MOR-73 decreased with the increase of the methanol content in the feed mixture. On the other hand, the

methanol content in the permeate side increased with the increase of the methanol content in the feed side. Therefore, due to the hydrophilic nature of the mordenite membranes, the feed composition highly influenced the total flux and the permeate composition, once the effective number of water molecules in the feed side gradually decreased with the increase of methanol concentration, which affects the driving force for water permeation.

Zhang et. al also studied the influence of feed methanol composition on the pervaporation performance of small crystals mordenite membranes at 20°C, and also reported a decrease in the total flux when the methanol concentration increases in the feed side [89].

Even for a different system of acetic acid-water, Zhu et al. reported, for mordenite membranes, a decrease in the total flux and an increase in the permeate acid composition when the number of active water molecules, around the membrane, gradually decreases [25].

In ethanol-water experiments, it was used as standard composition the mixture with 90 wt % EtOH. In table 4.2 are presented the steady state pervaporation performance results of the mordenite membrane MOR-73 for ethanol-water feed mixtures at 75°C with the variation of the ethanol concentration in the feed side from 0 to 90 wt %.

Table 4.2: PV performance of MOR-73 for different compositions of EtOH/H_2O mixtures at 75°C (348 K).

Run No.	Feed (wt % EtOH)	Permeate (wt % EtOH)	J_{EtOH} (kg m^{-2} h^{-1})	J_{H_2O} (kg m^{-2} h^{-1})	$\alpha_{w/e}$ (-)
16	0	0.04	-	1.51	-
32	10	0.05	6.76×10^{-4}	1.46	239
33	20	0.05	5.65×10^{-4}	1.15	515
34	50	0.06	6.53×10^{-4}	1.11	1830
35	81	0.14	1.25×10^{-3}	0.89	3012
36	90	0.17	1.11×10^{-3}	0.64	5051

As shown in table 4.2, the ethanol flux remained practically constant in the composition range of 10 to 50 wt % EtOH, increasing significantly in pervaporation experiments with higher ethanol content. The water flux decreased with the increase of feed ethanol composition. Moreover, the mordenite membrane MOR-73 also showed water permselectivity with separation factors above 230 for the whole ethanol concentration range studied.

For a general understanding of the experimental results, figure 4.3 shows the influence of feed composition on the total flux (figure 4.3a) and on the permeate composition

(figure 4.3b) of the mordenite membrane MOR-73 for ethanol-water mixtures at 75°C.

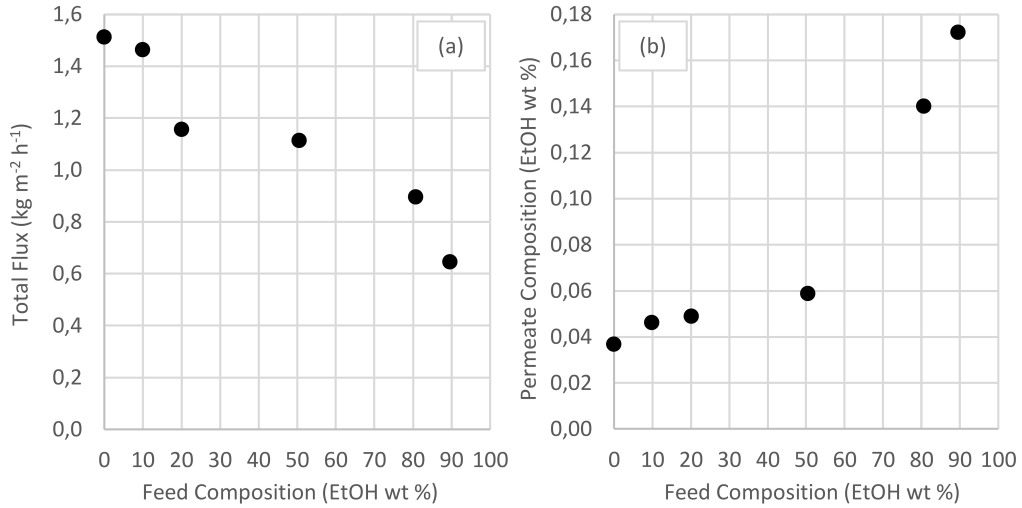

Figure 4.3: Influence of feed composition on (a) total flux and (b) permeate composition of MOR-73 for EtOH/H_2O mixtures at 75°C (348 K).

As seen in figure 4.3a, the total flux of the mordenite membrane MOR-73 gradually decreased with the increase of the ethanol content in the feed mixture. However, in the composition range of 20 to 50 wt % EtOH, the total flux remained approximately constant. Regarding the permeate composition, the ethanol content in the permeate side increased with the increase of the ethanol content in the feed side, creating an almost constant value between the composition range of 10 to 50 wt % EtOH (figure 4.3b). An explanation for this phenomenon may be related with the water concentration close to the membrane surface, possibly this concentration is practically constant in the bulk concentration range, above mentioned, due to the high hydrophilic nature of the mordenite membranes.

Casado et al. studied the influence of the ethanol concentration in the feed side on the pervaporation performance of mordenite membranes. In this study, the feed composition was varied from 25 to 85 wt % EtOH. The results reported a practically linear decrease in water flux and an increase in the ethanol flux with the increase of ethanol content in the feed liquid. Casado et al. interpreted the influence of the feed composition on the pervaporation performance as a result of an adsorption-controlled permeation process [88]. An increase in the ethanol concentration at the feed side certainly increase the driving force for ethanol permeation, and, thus, increase the ethanol flux through the membrane and the ethanol content in the permeate side [88]. However, the simultaneous decrease of water flux can be interpreted as a consequence of an adsorption equilibrium

displacement at the rententate side [88].Therefore, high ethanol concentration in the feed side makes it possible the replacement of water molecules in some adsorption sites, and some channels previously blocked by water become available for ethanol permeation [88].

Shah et al. studied the influence of the ethanol concentration in the feed (0 to 100 wt % EtOH) on the total flux of zeolite NaA membranes [90]. They reported that the total flux decreased with the increase of ethanol concentration in the feed side, but it did not vary significantly in the range of 30 to 50 wt % EtOH in the feed mixture at 70°C [90]. This behaviour is due to the fact that zeolite NaA has a high affinity for water and is very hydrophilic in nature [90]. Thus, the active layer of the membrane selectively sorbs water over ethanol and as a result, the total flux through the membrane remains stable over a wide range of ethanol concentrations [90].

To eliminate the effect of driving force in the study of the influence of the feed composition on the pervaporation performance of the mordenite membrane MOR-73, it was analyzed the influence of the feed composition on the alcohol and water permeances. Figure 4.4 shows the influence of feed composition on the methanol permeance (figure 4.4a) and on the water permeance (figure 4.4b) of the mordenite membrane MOR-73 for methanol-water mixtures at 60°C.

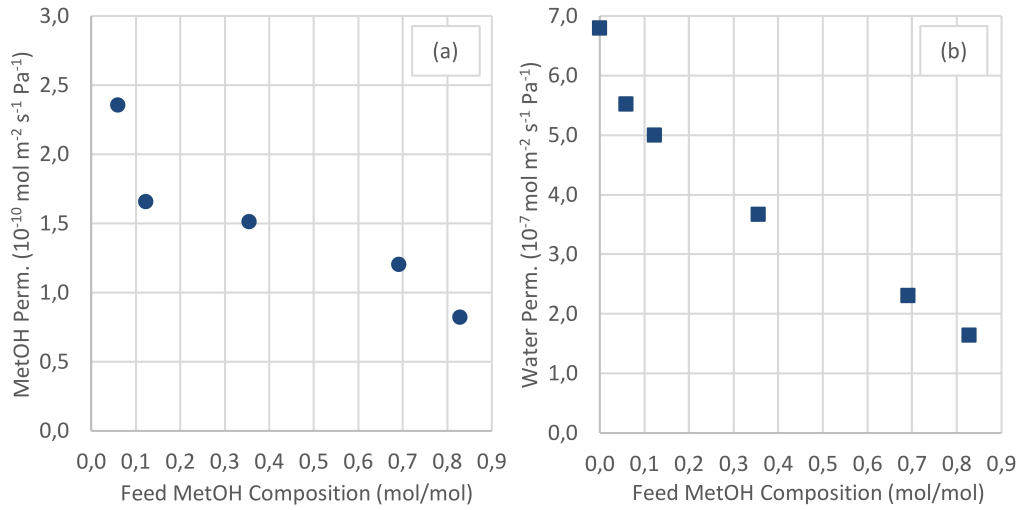

Figure 4.4: Influence of feed composition on (a) methanol permeance and (b) water permeance of MOR-73 for MetOH/H_2O mixtures at 60°C (333 K).

As shown in figure 4.4, when the driving force effect is removed, both methanol and water permeances decreased with the increase of methanol concentration in the feed side. It is notorious that the influence of the feed composition is greater in the decrease of the

water permeance than in the decrease of methanol permeance. Thus, it can be assumed that changes in water adsorption are influenced by the feed methanol composition. Therefore, when the methanol content in the feed side increase, the competitive adsorption between methanol and water molecules increase.

In table 4.3 is presented the selectivity of the mordenite membrane MOR-73 for methanol-water feed mixtures at 60°C with the variation of the methanol concentration in the feed side from 0 to 90 wt %.

Table 4.3: Permeance and selectivity of MOR-73 for different compositions of MetOH/H_2O mixtures at 60°C (333 K).

Run No.	Feed (wt % MetOH)	P_{MetOH}/δ (mol m^{-2} s^{-1} Pa^{-1})	P_{H_2O}/δ (mol m^{-2} s^{-1} Pa^{-1})	$\alpha'_{w/m}$ (-)
29	0	-	6.79×10^{-7}	-
19	10	2.35×10^{-10}	5.52×10^{-7}	2349
20	20	1.66×10^{-10}	5.00×10^{-7}	3012
21	50	1.51×10^{-10}	3.67×10^{-7}	2430
22	80	1.20×10^{-10}	2.30×10^{-7}	1917
23	90	0.82×10^{-10}	1.64×10^{-7}	2002

As shown in table 4.3, the membrane selectivity was above 1900 for the whole methanol concentration range studied. For this reason, it can be concluded that the mordenite membrane MOR-73 is highly selective to water in methanol-water systems.

Figure 4.5 shows the influence of feed composition on the ethanol permeance (figure 4.5a) and on the water permeance (figure 4.5b) of the mordenite membrane MOR-73 for ethanol-water mixtures at 75°C (348 K).

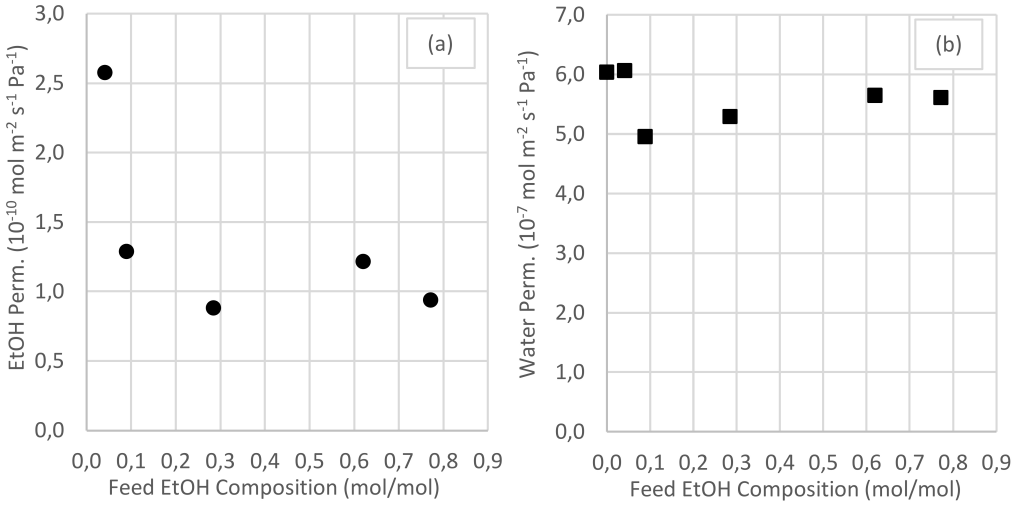

Figure 4.5: Influence of feed composition on (a) ethanol permeance and (b) water permeance of MOR-73 for EtOH/H_2O mixtures at 75°C (348 K).

As shown in figure 4.5a, the ethanol permeance decreased from the first experimental point to the second experimental point and, after this drop, the ethanol permeance remained practically constant with the increase of ethanol concentration in the feed side. The average value of ethanol permeance for the range of practically constant results is 1.1×10^{-10} mol m^{-2} s^{-1} Pa^{-1}. As shown in figure 4.5b, the water permeance remained practically constant with the increase of ethanol content in the feed side. The average value of water permeance is 5.6×10^{-7} mol m^{-2} s^{-1} Pa^{-1}.

By normalizing for driving force, it becomes clear that the feed composition dependence of total flux in figure 4.5a is mostly due to changes in ethanol and water vapor pressure (driving force) with the feed composition [91]. When the effect of driving force is removed, the water and ethanol permeances of mordenite membrane MOR-73 are practically constant. Therefore, it can be assume that the adsorption and diffusivity of the molecules through the membrane is practically stable with the increase of ethanol concentration in the feed mixture. Moreover, the water permeance in the pervaporation experiment with distilled water (0 wt % EtOH) is 6.0×10^{-7} mol m^{-2} s^{-1} Pa^{-1}, when the content of ethanol increase in the feed side similar water permeance is obtained (6.1×10^{-7} mol m^{-2} s^{-1} Pa^{-1} for 10 wt % EtOH in the feed), which indicates that the adsorption of water did not change with the presence of ethanol molecules in the feed mixture.

In table 4.4 is presented the selectivity of the mordenite membrane MOR-73 for ethanol-water feed mixtures at 75°C with the variation of the ethanol concentration in the feed side from 0 to 90 wt %.

Table 4.4: Permeance and selectivity of MOR-73 for different compositions of EtOH/H_2O mixtures at 75°C (348 K).

Run No.	Feed (wt % EtOH)	P_{EtOH}/δ (mol m^{-2} s^{-1} Pa^{-1})	P_{H_2O}/δ (mol m^{-2} s^{-1} Pa^{-1})	$\alpha'_{w/e}$ (-)
16	0	-	6.04×10^{-7}	-
32	10	2.57×10^{-10}	6.06×10^{-7}	2358
33	20	1.29×10^{-10}	4.95×10^{-7}	3837
34	50	0.88×10^{-10}	5.30×10^{-7}	6023
35	81	1.21×10^{-10}	5.64×10^{-7}	4661
36	90	0.94×10^{-10}	5.61×10^{-7}	5987

As shown in table 4.4, the membrane selectivity, for ethanol-water mixtures, was above 2350 for the whole ethanol concentration range studied. Thus, it can be concluded that the mordenite membrane MOR-73 is extremely selective to water in ethanol-water systems.

Comparing the different tested systems, the water permeance linearly decreased with the increase of methanol concentration in the feed side. On the contrary, water permeance remained almost stable in ethanol-water separations, which indicates that the presence of methanol molecules in the feed side affected the water adsorption, although the presence of ethanol molecules did not affect the water adsorption. Therefore, the competitive adsorption between methanol and water molecules needs to be taken into account when separating methanol solutions, but it can be negligible for the separation of ethanol solutions.

In general, the mordenite membrane MOR-73 showed better pervaporation performance for ethanol-water systems. An explanation for this phenomenon may be related to the preferential adsorption between methanol and ethanol molecules and/or the difference in the molecular size.

The mordenite membranes studied have a Si/Al ratio of 5 and for this reason are considered hydrophilic membranes. Water is a small molecule, which adsorbs very strongly on hydrophilic membranes [63]. The preferential adsorption between methanol and ethanol molecules in the pores of the mordenite membrane can explain the difference in the pervaporation performance. The adsorption in zeolite crystals under pervaporation conditions is an example of physical adsorption, and therefore it is a non-activated, exothermic and competitive phenomena that is reversible [45]. Normally, physical adsorption includes both van der Waals forces and electrostatic forces [90]. However, since the zeolites have an ionic structure, the electrostatic forces have larger contribution in the adsorption of polar molecules, such as water molecules [90]. This effect is manifested in the fact that the heat of adsorption of water on hydrophilic zeolites is unusually high (25-30 kcal/mol) [90]. The heat of adsorption is a direct measure of the bonding strength between the adsorbate and the adsorbent, thus proving that there is a very strong interaction between water and the adsorption sites in the zeolite pores [90]. It was reported that the contribution of electrostatic forces to the heat of adsorption for water, methanol and ethanol, in the zeolite NaX, were 80, 72 and 63%, respectively [90]. It can be concluded that the phenomenon of physical adsorption in hydrophilic zeolites is more spontaneous for methanol molecules than for ethanol molecules due to the contribution of electrostatic forces.

As shown previously in figure 2.7, mordenite membranes are considered a large-pore zeolite membrane with two different types of channels (6.5×7Å parallel to the c-axis

and 2.6×5.7Å parallel to the b-axis) [21, 24]. The kinetic molecular diameter of water, methanol and ethanol molecules is 2.6Å, 3.6Å and 4.5Å, respectively [92]. Regarding molecular sieving, the three molecules studied are smaller than the channels parallel to the c-axis, which indicates that they can enter in the big pores of the mordenite crystals. In the channels parallel to the b-axis, it is notorious that water molecules can enter easily, however and because of molecular size and shape, it can be assumed that is easier to methanol molecules enter in the small pores than to ethanol molecules, which can be also one reason why mordenite membrane MOR-73 showed more selectivity in ethanol-water mixtures than in methanol-water mixtures.

In summary, the adsorption differences and the molecular size of methanol and ethanol molecules justify the difference in pervaporation performance of the mordenite membrane MOR-73 in the different alcohol-water systems.

4.2.1.2 Influence of feed temperature

It was studied the influence of the feed temperature on the pervaporation performance of the mordenite membranes. Table 4.5 shows the steady state pervaporation performance results of the mordenite membrane MOR-73 for methanol-water feed mixtures at different temperatures (40°C, 60°C, 75°C) with the variation of the methanol concentration in the feed side. As mentioned above, in this group of experiments it was used as standard composition the mixture with 10 wt % EtOH.

Table 4.5: PV performance of MOR-73 for different compositions of MetOH/H_2O mixtures at different temperatures.

Run No.	Temperature[a] (°C)	Feed (wt % MetOH)	Permeate (wt % MetOH)	J_{MetOH} (kg m^{-2} h^{-1})	J_{H_2O} (kg m^{-2} h^{-1})	$\alpha_{w/m}$ (-)
30	40	0	0.00	-	0.37	-
27		10	0.04	1.20×10^{-4}	0.30	282
28		20	0.06	1.44×10^{-4}	0.24	415
29	60	0	0.00	-	0.88	-
19		10	0.04	2.87×10^{-4}	0.67	265
20		20	0.06	3.61×10^{-4}	0.58	401
21		50	0.19	6.73×10^{-4}	0.35	505
22		80	0.65	8.48×10^{-4}	0.13	607
23		90	1.18	6.71×10^{-4}	0.06	728
25	75	0	0.00	-	1.52	-
17		10	0.04	4.38×10^{-4}	1.19	310
18		20	0.08	7.73×10^{-4}	1.01	326

[a] 40°C=313 K; 60°C=333 K; 75°C=348 K.

As shown in table 4.5, both methanol and water flux increased with the increase of feed temperature. The mordenite membrane MOR-73 showed water perm-selectivity

with separation factors above 260 for the different feed temperatures and methanol-water mixtures. In addition, the permeate water composition ranged from 98.82 to 99.96 wt % H_2O for all the pervaporation experiments with methanol-water mixtures at different temperatures, which prove that the mordenite membrane MOR-73 is highly water perm-selective. Moreover, the increase of operating temperature showed no influence on the permeate composition and on the separation factor.

For a general understanding of the experimental data, figure 4.6 shows the influence of feed temperature on the total flux (figure 4.6a) and on the permeate composition (figure 4.6b) of the mordenite membrane MOR-73 for methanol-water mixtures with different compositions.

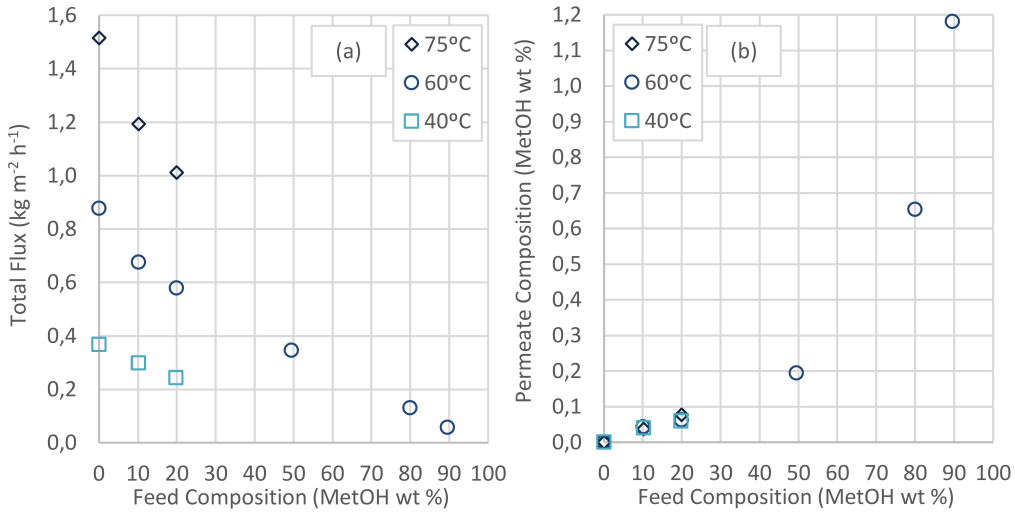

Figure 4.6: Influence of feed temperature on (a) total flux and (b) permeate composition of MOR-73 for MetOH/H_2O mixtures with different compositions. [Note: 40°C=313 K; 60°C=333 K; 75°C=348 K].

As shown in figure 4.6a, the total flux gradually increased with the increase of the operating temperature. An explanation for this trend is based on the fact that the vapor pressures of permeations at the feed side increase with the increase of the operating temperature, but the vapor pressures of them at the permeate side are not affected by temperature changes [69]. Therefore, increasing the operating temperature increases the driving force, which is the gradient in partial vapor pressure of the components, which promotes high total fluxes through the membrane.

The permeate composition was not affected by increasing the operating temperature as seen in figure 4.6b. Wei et al. indicated that the influence of the feed temperature on the separation factor, which is directly related with the permeate composition, is not

clear [47]. However, studies with mordenite membranes reported that increasing the operating temperature increase the separation factor and decrease the permeate alcohol composition [88, 89, 93].

Table 4.6 shows the steady state pervaporation performance results of the mordenite membrane MOR-72 for ethanol-water feed mixtures at different temperatures (40°C, 60°C, 75°C) with the variation of the ethanol concentration in the feed side. To check the stability of mordenite membrane MOR-72, in this group of experiments it was used as standard composition the mixture with 10 wt % EtOH.

Table 4.6: PV performance of MOR-72 for different compositions of EtOH/H_2O mixtures at different temperatures.

Run No.	Temperature[a] (°C)	Feed (wt % EtOH)	Permeate (wt % EtOH)	J_{EtOH} (kg m^{-2} h^{-1})	J_{H_2O} (kg m^{-2} h^{-1})	$\alpha_{w/e}$ (-)
44	40	20	0.04	1.81×10^{-4}	0.44	623
47		50	0.06	2.55×10^{-4}	0.44	1757
50		80	0.13	4.70×10^{-4}	0.35	3104
43	60	20	0.03	2.81×10^{-4}	1.00	876
46		51	0.05	4.61×10^{-4}	1.01	2245
49		80	0.12	1.01×10^{-3}	0.83	3392
41	75	10	0.01	2.46×10^{-4}	2.46	1105
42		20	0.02	3.86×10^{-4}	1.67	1067
45		51	0.03	5.97×10^{-4}	1.71	2942
48		80	0.07	9.91×10^{-4}	1.42	5908
51		90	0.13	1.34×10^{-4}	0.99	6920

[a] 40°C=313 K; 60°C=333 K; 75°C=348 K.

As shown in table 4.6, both ethanol and water flux increased with the increase of feed temperature. The mordenite membrane MOR-72 showed water perm-selectivity with separation factors above 620 for the different feed temperatures and ethanol-water mixtures. Again, the permeate was mostly composed by water, ranging from 99.87 to 99.99 wt % H_2O for all the pervaporation experiments with ethanol-water mixtures at different temperatures, which prove that the mordenite membrane MOR-72 is also highly water perm-selective. Moreover, the increase of operating temperature showed influence on the permeate composition and on the separation factor.

For a general understanding of the experimental results, figure 4.7 shows the influence of feed temperature on the total flux (figure 4.7a) and on the permeate composition (figure 4.7b) of the mordenite membrane MOR-72 for ethanol-water mixtures with different compositions.

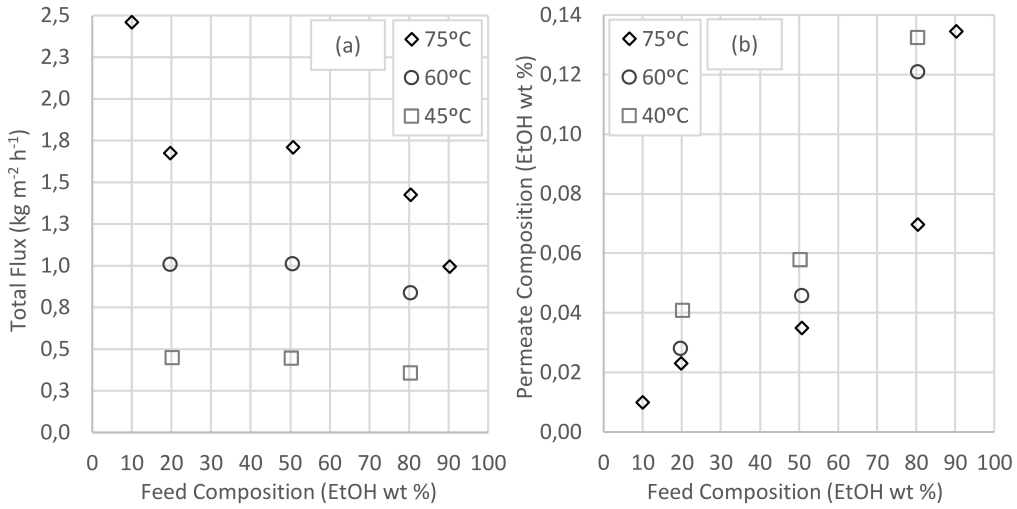

Figure 4.7: Influence of feed temperature on (a) total flux and (b) permeate composition of MOR-72 for EtOH/H_2O mixtures with different compositions. [Note: 40°C=313 K; 60°C=333 K; 75°C=348 K].

As expected, the total flux gradually increased with the increase of the operating temperature as seen in figure 4.7a. As shown in figure 4.7b, the results are different from the results obtained in methanol-water experiments, and, in this case, the operating temperature had a clear influence in the permeate composition. The permeate composition decreased with the increase of the feed temperature. An explanation for this trend can rely on the fact that the diffusivity is promoted with the increase of feed temperature [93]. As a result, the water selectivity of the membrane is enhanced by increasing feed temperature.

As mentioned above, many researchers have studied the influence of feed temperature on the pervaporation performance of mordenite membranes in ethanol-water systems, and all concluded that increasing the operating temperature, both the total flux and the separation factor increase significantly [88, 89, 93]. Thus, the pervaporation performance of the mordenite membranes improve at higher feed temperatures.

To eliminate the driving force effect in the study of the influence of the feed temperature on the pervaporation performance of the mordenite membranes, it was studied the influence of the operating temperature on the alcohol and water permeances. But firstly, it was analyzed in more detail the influence of the feed temperature on the alcohol and water permeation fluxes. In figure 4.8 is presented the influence of feed temperature on the methanol flux (figure 4.8a) and on the water flux (figure 4.8b) of the mordenite membrane MOR-73 for methanol-water mixtures with different compositions.

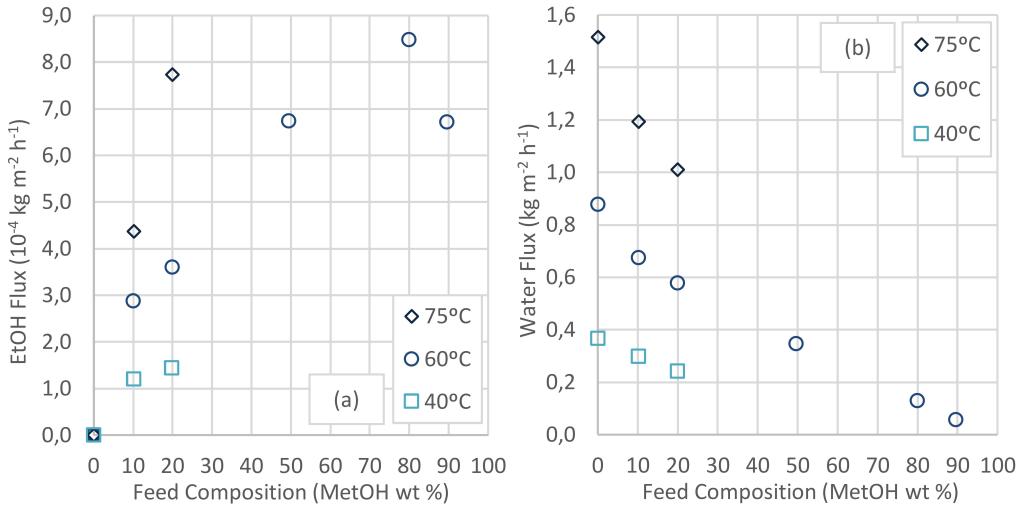

Figure 4.8: Influence of feed temperature on (a) methanol flux and (b) water flux of MOR-73 for MetOH/H_2O mixtures with different compositions. [Note: 40°C=313 K; 60°C=333 K; 75°C=348 K].

As shown in figure 4.8, the methanol flux and the water flux increased with the increase of feed temperature. This behaviour is probably due to following reasons, the increase of feed temperature leads to higher vapor pressure of the components in feed side, which is directly related with the increase of driving force for permeation, and, also, leads to the increase of mobility of adsorbed species [88].

Figure 4.9 shows the influence of feed temperature on the methanol permeance (figure 4.9a) and on the water permeance (figure 4.9b) of mordenite membrane MOR-73 for methanol-water mixtures with different compositions.

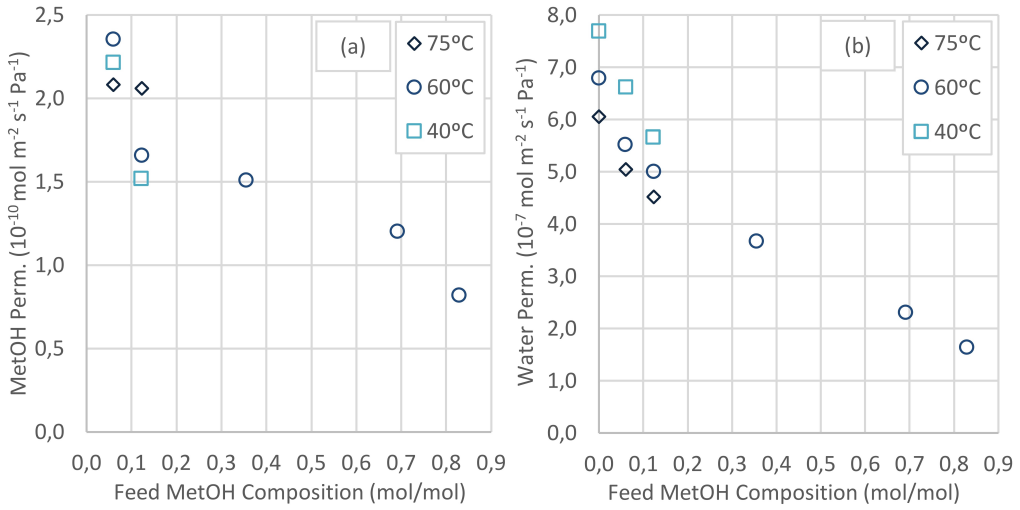

Figure 4.9: Influence of feed temperature on (a) methanol permeance and (b) water permeance of MOR-73 for MetOH/H_2O mixtures with different compositions. [Note: 40°C=313 K; 60°C=333 K; 75°C=348 K].

As shown in the figure 4.9a, the methanol permeance remained practically constant with the increase of operating temperature, which indicates that the temperature only influenced the methanol vapor pressure in the feed side. As shown in figure 4.9b, the water permeance slightly decreased with the increase of the operating temperature. In addition, diffusivity almost always increases with the increase of the temperature, on the contrary, adsorption usually decreases with the increase of the temperature [91]. Therefore, this trend indicates that in the mordenite membrane MOR-73, the change in the water adsorption outweighs the change in the diffusivity [91].

In figure 4.10 is presented the influence of feed temperature on the ethanol flux (figure 4.10a) and on the water flux (figure 4.10b) of the mordenite membrane MOR-72 for ethanol-water mixtures with different compositions.

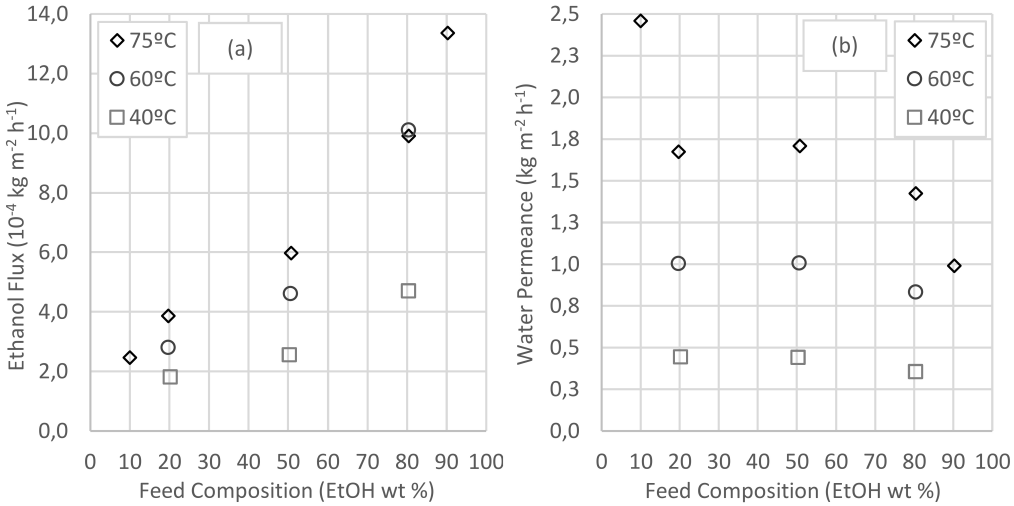

Figure 4.10: Influence of feed temperature on (a) ethanol flux and (b) water flux of MOR-72 for EtOH/H_2O mixtures with different compositions. [Note: 40°C=313 K; 60°C=333 K; 75°C=348 K].

As shown in figure 4.10, also the ethanol flux and the water flux increased with the increase of feed temperature, which is probably due to both, the higher vapor pressure of the components and the increased mobility of adsorbed species.

Figure 4.11 shows the influence of feed temperature on the ethanol permeance (figure 4.11a) and on the water permeance (figure 4.11b) of the mordenite membrane MOR-72 for ethanol-water mixtures with different compositions.

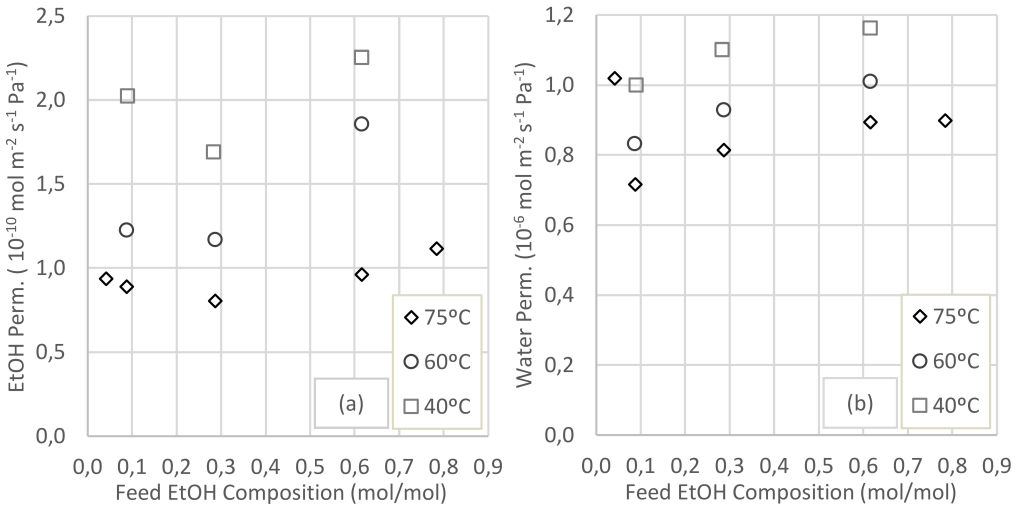

Figure 4.11: Influence of feed temperature on (a) ethanol permeance and (b) water permeance of MOR-72 for EtOH/H_2O mixtures with different compositions. [Note: 40°C=313 K; 60°C=333 K; 75°C=348 K].

As shown in figure 4.11a, the ethanol permeance gradually decreased with the increase of the feed temperature. Again, it can be assumed that the change in the ethanol adsorption with the increase of the temperature overcome the change in the diffusivity [91]. However, this result was not expected, an explanation for the observed trend can be related with the calculation of the ethanol vapor pressure in the feed side. For the permeance calculation, it was assumed that the vapor pressure of the components in the bulk is equal to the vapor pressure close to the membrane surface, this assumption helps in the permeance calculation, but also can affect the final results, changing the operating conditions.

As shown in figure 4.11b, the water permeance slightly decreased with the increase in the operating temperature, which indicates that in the mordenite membrane MOR-72, the change in the water adsorption outweighs the change in the diffusivity [91]. Therefore, it can be assumed that the feed temperature not only influenced the water vapor pressure but also change the adsorption of water molecules.

Furthermore, the membrane selectivity increased with the increase of feed temperature, which means that the water perm-selectivity is enhanced by increasing the operating temperature.

4.2.1.3 Apparent Activation Energy

For the ethanol-water case, it was estimated the apparent activation energy for permeation of ethanol-water mixtures with different compositions. By the ethanol and water

permeances of the mordenite membrane MOR-72, and the respective operating temperatures it was possible to estimate the apparent activation energy for permeation of ethanol and water using the linearizations 3.18 and 3.19, respectively. Figure 4.12 shows the Arrhenius's linearization for the temperature dependence of ethanol permeance (figure 4.12a) and water permeance (figure 4.12b).

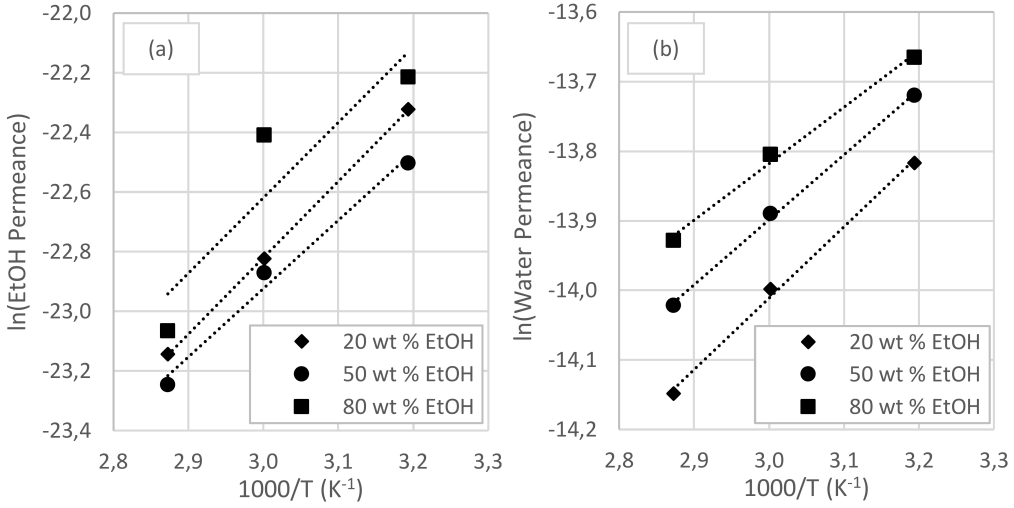

Figure 4.12: Arrhenius plots for (a) ethanol permeance and (b) water permeance. [Note: 40°C=313 K; 60°C=333 K; 75°C=348 K].

The linear trend obtained in figure 4.12 is the proof that the diffusion through mordenite crystals, and, in general, in zeolite crystals, is an activated phenomenon.

By the slope of the linearizations shown in figure 4.12 it was possible to estimate the apparent activation energy of ethanol and water permeation. In table 4.7 are presented the calculated values for the apparent activation energy of ethanol and water permeation, for ethanol-water mixtures with different compositions.

Table 4.7: Apparent activation energies of ethanol and water permeation for mixtures with different compositions.

	Feed Composition (wt % EtOH)		
Apparent Activation Energy (kJ mol^{-1})	**20**	**50**	**80**
E_p^{EtOH}	-21.3	-19.0	-21.0
E_p^{Water}	-8.5	-7.8	-6.7

As shown in table 4.7, the apparent activation energies obtained for ethanol and water permeation are negative. It is worth to remember that the apparent activation energy of permeation (E_P) is the sum of the activation energy of diffusion (E_D) and the heat of

sorption (ΔH_s). While the activation energy of diffusion is generally a positive value, the heat of sorption is usually negative for the exothermic sorption process. When the negative heat of sorption overcome the positive activation energy of diffusion, negative value of apparent activation energy of permeation occurs, which indicates that the permeance of the mordenite membrane MOR-72 decreases with the increase of operating temperature [87]. However, the permeation flux increases with the increase of feed temperature because the effect of temperature on the saturated vapor pressure is more significant [87].

4.2.1.4 Order of Experiments and Results Reproducibility

The order of the experiments showed influence on the pervaporation performance of the mordenite membranes. In order to understand this effect, it was made some pervaporation experiments with the standard composition after pervaporation experiments with different compositions.

Table 4.8 shows the steady state pervaporation results of the mordenite membrane MOR-73 for the experiments with the standard composition of 10 wt % MetOH at 60°C.

Table 4.8: PV performance of MOR-73 for the standard composition (10 wt % MetOH) at 60°C.

Run No.	Previous Run (wt % MetOH)	Feed (wt % MetOH)	Permeate (wt % MetOH)	J_{MetOH} (kg m^{-2} h^{-1})	J_{H_2O} (kg m^{-2} h^{-1})	$\alpha_{w/m}$ (-)
19	20	10	0.04	2.87×10^{-4}	0.67	265
24	90	10	0.06	4.13×10^{-4}	0.68	186
26	0	10	0.04	2.99×10^{-4}	0.71	267
31	0	10	0.04	3.03×10^{-4}	0.70	260

As shown in table 4.8, the order of the experiments influenced the pervaporation performance of the mordenite membrane MOR-73. The run no. 24 showed a permeate composition of 0.06 wt % MetOH and higher methanol flux, because the previous experiment was carried out with a high methanol content mixture (90 wt % MetOH). However, it is important to note that the mordenite membrane MOR-73 returned to the initial values of permeate composition and methanol flux, after a pervaporation experiment with distilled water (run no. 26). It can be assumed that a pervaporation experiment with water can regenerate the pervaporation performance of the mordenite membrane MOR-73.

Figure 4.13 shows the results reproducibility for the pervaporation experiments with the standard composition of 10 wt % MetOH, in terms of total flux (figure 4.13a) and permeate composition (figure 4.13b).

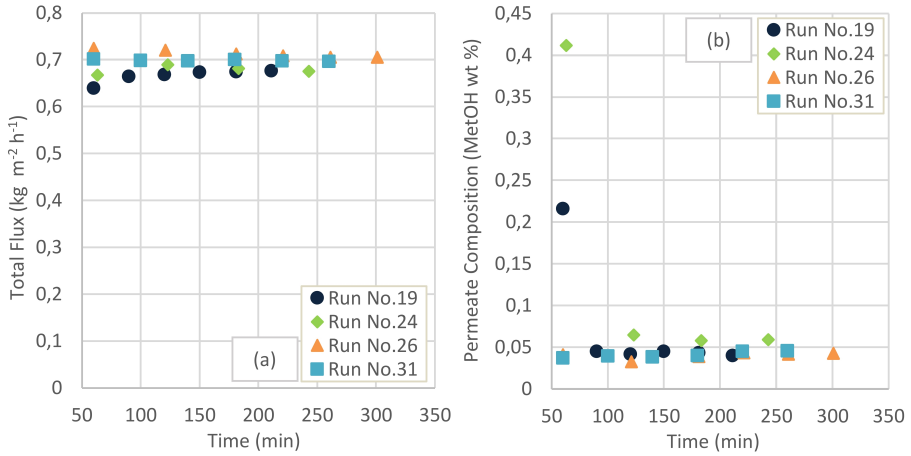

Figure 4.13: PV experiments of MOR-73 for the standard composition (10 wt % MetOH) at 60°C. (a) total flux and (b) permeate composition in function of test time.

Although the pervaporation experiments with the standard composition had different duration, in all them it was achieved a similar well defined steady state as seen in figure 4.13. Thus, can be considered that the reproducibility of the results was high.

Table 4.9 shows the steady state pervaporation results of the mordenite membrane MOR-72 for the experiments with the standard composition of 90 wt % EtOH at 75°C.

Table 4.9: PV performance of MOR-72 for the standard composition (90 wt % EtOH) at 75°C.

Run No.	Previous Run (wt % EtOH)	Feed (wt % EtOH)	Permeate (wt % EtOH)	J_{EtOH} (kg m^{-2} h^{-1})	J_{H_2O} (kg m^{-2} h^{-1})	$\alpha_{w/e}$ (-)
51	80	90	0.13	1.34×10^{-3}	0.99	6920
52	**Pervaporation experiment with distilled water**					
54	10	89	0.10	9.90×10^{-4}	0.99	8439

As shown in table 4.9, also in mordenite membrane MOR-72, the order of the experiments influenced the pervaporation performance. The run no. 51 showed a permeate composition of 0.13 wt % EtOH and higher ethanol flux, because the previous experiment was carried out with a high ethanol content mixture (80 wt % EtOH). However, with a pervaporation experiment with water (run no.52) was possible to regenerate the pervaporation performance of the mordenite membrane MOR-72.

Figure 4.14 shows the results reproducibility for the pervaporation experiments with the standard composition of 90 wt % EtOH, in terms of total flux (figure 4.14a) and permeate composition (figure 4.14b).

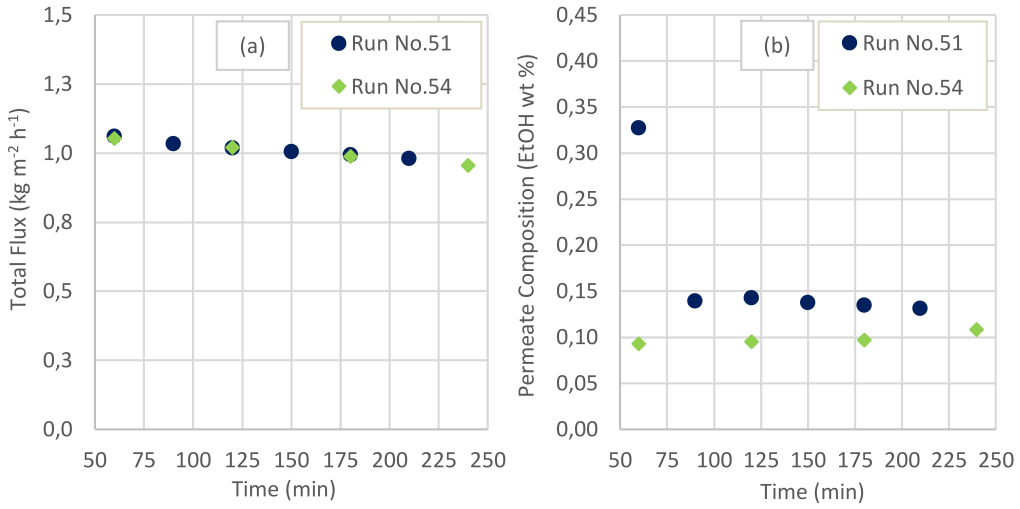

Figure 4.14: PV experiments of MOR-72 for the standard composition (90 wt % EtOH) at 75°C. (a) total flux and (b) permeate composition in function of test time.

Although the pervaporation experiments with the standard composition had different durations, in all them it was achieved a well defined steady state as seen in figure 4.14. Thus, can be considered that the reproducibility of the results was high.

4.2.1.5 Membrane Stability

The mordenite membranes stability was studied in the course of the experiments by checking and comparing the pervaporation performance of the membranes in pervaporation experiments with the standard composition. If the membrane show similar pervaporation performance it means that the membrane kept its stability during a certain number of experiments between two experiments with the standard composition.

Table 4.10 shows the steady state pervaporation results of mordenite membrane MOR-73 for the experiments with the standard composition of 90 wt % EtOH at 75°C.

Table 4.10: PV performance of MOR-73 for the standard composition (90 wt % EtOH) at 75°C.

Run No.	Previous Run (wt % EtOH)	Feed (wt % EtOH)	Permeate (wt % EtOH)	J_{EtOH} (kg m^{-2} h^{-1})	J_{H_2O} (kg m^{-2} h^{-1})	$\alpha_{w/e}$ (-)
15	10	91	0.10	6.45×10^{-4}	0.65	9978
36	80	90	0.17	1.11×10^{-3}	0.64	5051

As shown in the table 4.10, throughout the experiments with binary aqueous alcohol mixtures, the mordenite membrane MOR-73 showed similar water flux for the experiments with the standard composition of 90 wt % EtOH. On the contrary, the ethanol flux slightly increased, possibly due to the influence of the previous experiment. However, it can be assumed that the mordenite membrane MOR-73 kept its stability during 22

pervaporation experiments, which is equivalent to about 92 hours of experiments with binary aqueous alcohol mixtures.

After some experiments, the mordenite membrane MOR-73 lost its stability and for that reason the experiments continued with the mordenite membrane MOR-72.

In the table 4.11 are presented the steady state pervaporation results of the mordenite membrane MOR-72 for the experiments with the standard composition of 10 wt % EtOH at 75°C.

Table 4.11: PV performance of MOR-72 for the standard composition (10 wt % EtOH) at 75°C.

Run No.	Previous Run (wt % EtOH)	Feed (wt % EtOH)	Permeate (wt % EtOH)	J_{EtOH} (kg m^{-2} h^{-1})	J_{H_2O} (kg m^{-2} h^{-1})	$\alpha_{w/e}$ (-)
41	-	10	0.01	2.46×10^{-4}	2.46	1105
53	0	10	0.02	3.33×10^{-4}	2.01	667

As shown in the table 4.11, throughout the experiments with binary aqueous ethanol mixtures, the mordenite membrane MOR-72 did not maintained its full stability showing a reduction of 18% in the water flux, despite showing a similar ethanol flux for the experiments with the standard composition of 10 wt % EtOH. Thus, it can be concluded that the mordenite membrane MOR-72 did not keep its full stability during 13 pervaporation experiments with synthetic binary aqueous mixtures of ethanol.

Although the reduction in the water flux, the mordenite membrane MOR-72 remained highly selective to water, and with high total permeation flux, and for this reason, a "new" pervaporation performance was characterized, using now as standard composition the mixture with 90 wt % EtOH. In table 4.12 is presented the "new" pervaporation performance of the mordenite membrane MOR-72 for two experiments with the standard composition of 90 wt % EtOH at 75°C.

Table 4.12: "New" PV performance of MOR-72 for the standard composition (90 wt % EtOH) at 75°C.

Run No.	Previous Run. (wt % EtOH)	Feed (wt % EtOH)	Permeate (wt % EtOH)	J_{EtOH} (kg m^{-2} h^{-1})	J_{H_2O} (kg m^{-2} h^{-1})	$\alpha_{w/e}$ (-)
51	80	90	0.13	1.34×10^{-3}	0.99	6920
54	10	89	0.10	9.90×10^{-4}	0.99	8439

4.2.2 Distilled Fermentation Broth

After the pervaporation experiments with synthetic mixtures, the mordenite membrane MOR-72 was used in pervaporation experiments with a distilled ethanolic fermentation broth. As mentioned in the previous chapter, this fermentation broth had a composition of about 41 wt % EtOH and an impurity that appears in the gas chromatograms with a retention time around 10 minutes, which it was not possible to characterize.

4.2.2.1 Pervaporation Performance

In this section it was studied the steady state pervaporation performance of the mordenite membrane MOR-72 in a pervaporation experiment of 8h with the distilled fermentation broth at 75°C. Figure 4.15 shows the pervaporation performance as a function of operating time, in terms of total flux (figure 4.15a) and permeate composition (figure 4.17b). It is important to note that before to the fermentation broth experiment, the mordenite membrane MOR-72 was "washed" in a short pervaporation experiment with water at 75°C (run no. 55).

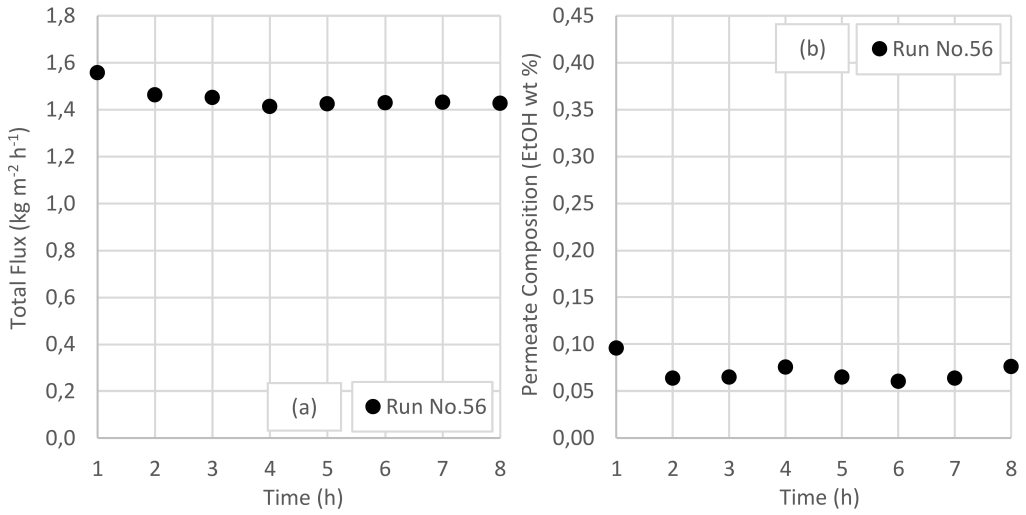

Figure 4.15: PV performance of MOR-72 for the distilled fermentation broth at 75°C. (a) total flux and (b) permeate composition in function of operating time.

As shown in the figure 4.15, in the first pervaporation experiment with the distilled fermentation broth (run no. 56), the mordenite membrane MOR-72 reached a well defined steady state. The values of total flux, permeate composition and separation factor at steady state were 1.43 kg m^{-2} h^{-1}, 0.07 wt % EtOH and 1127, respectively.

It was interesting to note that the impurity that was in the distilled fermentation broth was not detected in the gas chromatograms of the permeate, which can indicate

that the impurity has a molecular size larger than the pores of mordenite crystals, or it is a non-polar molecule, and, therefore, has no affinity for highly hydrophilic surfaces, such as mordenite membrane MOR-72. In Appendix B is presented the gas chromatograms of the first and last feed and permeate samples of the run no. 56.

Considering the reduction of the stability of the mordenite membrane MOR-72, it was estimated the steady state pervaporation performance for a pervaporation experiment with a synthetic binary mixture with the same composition of the fermentation broth. For these calculations were used the pervaporation experiments results of the mordenite membrane MOR-72 with synthetic ethanol-water mixtures of 20 and 51 wt % EtOH at 75°C (table 4.7). Table 4.13 shows the steady-state pervaporation performance estimate for a experiment with a synthetic aqueous mixture of 41 wt % EtOH at 75°C, considering that the membrane showed a reduction in the pervaporation performance.

Table 4.13: PV performance estimate of MOR-72 for a mixture with 41 wt % EtOH at 75°C.

Feed (wt % EtOH)	**Permeate (wt % EtOH)**	**J_{total} (kg m^{-2} h^{-1})**
41	0.05	1.39

Comparing the estimate with the result obtained for the pervaporation experiment with the distilled fermentation broth, it is worth to note small differences in the permeate composition and in the total flux, however it can be considered that the experiment with the distilled fermentation broth was successful. In addition, it can be concluded that the presence of the unknown impurity did not affect the pervaporation performance of the mordenite membrane MOR-72.

Regarding bioethanol recovery, some studies have reported successful separations of ethanol from fermentation broths using silicalite-1 membranes with similar separation factors to the separations of the corresponding binary mixtures [94–97]. However, most laboratory pervaporation studies with hydrophilic zeolite membranes have investigated the membrane performance just with synthetic binary mixtures. Although, in a real fermentation broth, even at low concentrations, other components in the feed can significantly affect the pervaporation performance by blocking membrane pores [45]. Regarding the bioethanol dehydration process, researchers must consider realistic feed after the recovery step rather than the simplified binary mixture [29].

4.2.2.2 Batch Concentration Process

The distilled fermentation broth was concentrated in a pervaporation experiment. In the initial part of this experiment it was achieved the steady state, and, after this step, the recycling of the collected permeate samples was stopped and the ethanol composition in the fermentation broth increased. Figure 4.16 shows the feed composition (figure 4.16a) and the pervaporation performance (figure 4.16b) in function of the operating time for the pervaporation experiment to concentrate the distilled fermentation broth at 75°C (run no. 62).

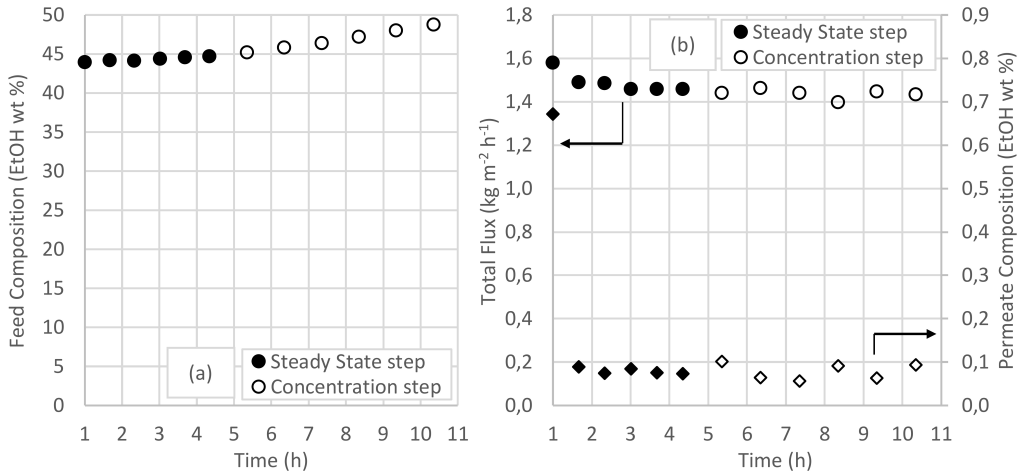

Figure 4.16: (a) Feed composition and (b) pervaporation performance in function of operating time for the PV experiment to concentrate the distilled fermentation broth at 75°C with MOR-72.

As depicted in figure 4.16, in the first 5h of experiment, the feed composition was kept practically constant and the mordenite membrane MOR-72 reached a well defined steady state. The steady state values of total flux, permeate composition and separation factor were 1.46 kg m^{-2} h^{-1}, 0.08 wt % EtOH and 1034, respectively.

After the membrane achieved the steady state performance, the feed composition started to increase, however the total flux and the permeate composition remained almost constant with average values of 1.44 kg m^{-2} h^{-1} and 0.08 wt % EtOH, respectively. This result was expected because in the pervaporation experiments with synthetic binary mixtures of ethanol-water it was prove that, in the range of compositions from 20 to 50 wt % EtOH, the influence of the feed composition on the total flux and on the permeate composition is negligible.

Again, the impurity that was in the distilled fermentation broth was not detected in the gas chromatograms of the permeate, and in the concentration step, the peak of this

impurity in the gas chromatograms of the feed started to increase. In Appendix B are presented the gas chromatograms of the first and last feed and permeate samples of the run no. 62.

In summary, the mordenite membrane MOR-72 was capable of concentrate the distilled fermentation broth from ≈ 44 to 49 wt % EtOH during 5h, keeping a stable pervaporation performance and confirming the potential of these type of zeolite membranes to selective remove water from a fermentation broth with intermediate concentration.

4.2.2.3 Membrane Stability

The long-term stability in the fermentation broth was studied by soaking the membrane in the distilled fermentation broth between pervaporation experiments. Figure 4.17 shows the long-term pervaporation performance of the mordenite membrane MOR-72 in the distilled fermentation broth at 75°C, in terms of total flux and permeate composition in function of operating time.

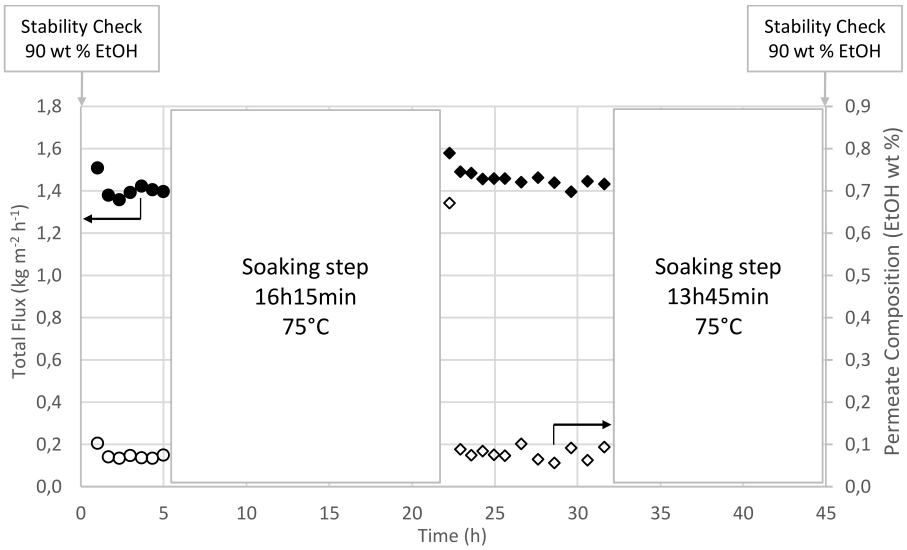

Figure 4.17: Long-term PV performance of MOR-72 in the distilled fermentation broth at 75°C, in terms of total flux and permeate composition in function of operating time (Run No.61 and Run No.62).

As shown in figure 4.17, the pervaporation performance of the mordenite membrane MOR-72 remained practically stable after soaking the membrane in the distilled fermentation broth during 16h15min at 75°C.

In order to fully understand the membrane long-term stability, it was made pervaporation experiments with the synthetic standard mixture of ≈ 90 wt % EtOH between pervaporation experiments with the distilled fermentation broth. Table 4.14 shows the steady state pervaporation performance results of the mordenite membrane MOR-72 for

all the experiments related with the distilled fermentation broth.

Table 4.14: Steady state PV performance results of MOR-72 at 75°C

Run No.	System	Feed (wt % EtOH)	Permeate (wt % EtOH)	J_{EtOH} (kg m^{-2} h^{-1})	J_{H_2O} (kg m^{-2} h^{-1})	$\alpha_{w/e}$ (-)
54	EtOH/H_2O	89	0.10	9.90×10^{-4}	0.99	8439
55	H_2O	0	Membrane regeneration (2h PV)			
56	Ferm. Broth	43	0.07	9.43×10^{-4}	1.43	1127
57	EtOH/H_2O	92	0.16	1.28×10^{-3}	0.82	6988
58	H_2O	0	Membrane regeneration (2h PV)			
59	EtOH/H_2O	91	0.17	1.43×10^{-3}	0.86	5906
60	H_2O	0	Membrane regeneration (2h PV)			
61	Ferm. Broth	44	0.07	9.83×10^{-4}	1.41	1110
Soaking the membrane in the Ferm. Broth: 44 wt % EtOH; 16h15min; 75°C.						
62	Ferm. Broth	45	0.08	1.14×10^{-3}	1.46	1034
		After concentration step: 49 wt % EtOH				
Soaking the membrane in the Ferm. Broth: 49 wt % EtOH; 13h45min; 75°C.						
63	EtOH/H_2O	91	0.16	1.33×10^{-3}	0.83	6203
64	H_2O	0	Membrane regeneration (2h PV)			
65	EtOH/H_2O	91	0.16	1.27×10^{-3}	0.80	6328

As shown in table 4.14, after the first pervaporation experiment with the distilled fermentation broth (run no. 56), the experiments with the standard composition of ≈ 90 wt % EtOH indicated that the mordenite membrane MOR-72 lost its pervaporation performance, with a reduction of 17% in the water flux and an increase of about 30% in the ethanol flux. However, after this drop in the performance, the mordenite membrane MOR-72 kept its stability in the course of soaking and pervaporation experiments with the fermentation broth, showing similar pervaporation performance in the experiments with the standard composition (runs no. 57, 59, 63 and 60). For this reason, it can be assumed that maybe the initial drop in the membrane performance was caused by external factors or by the slight difference of feed ethanol composition between run no. 54 and run no. 57, and not by the pervaporation experiment with the fermentation broth (run no. 56).

In summary, the mordenite membrane MOR-72 kept a similar pervaporation performance during 53.4h of experiments with the distilled fermentation broth, which indicates the high stability and the potential of mordenite membranes in the dehydration of fermentation broths.

4.2.3 Zeolite A Membrane

Due to the poor acidic and aqueous stability of the zeolite A membrane [25], it was studied the stability of these type of zeolite membranes in fresh distilled fermentation broth conditions (≈ 41 wt % EtOH) at 75°C.

4.2.3.1 Membrane Stability

Zeolite A-7 membrane was soaked in the fresh fermentation broth at 75°C. Between soaking experiments, it was made pervaporation experiments with the standard composition of ≈ 90 wt % EtOH at 75°C. Moreover, comparing the results obtained, it was evaluated the membrane stability in the fermentation broth conditions.

Table 4.15 shows the steady state pervaporation performance results of zeolite A-7 membrane for all the experiments related with the membrane stability in the distilled fermentation broth.

Table 4.15: PV performance of zeolite A-7 membrane for the standard composition of ≈ 90 wt % EtOH at 75°C.

Run No.	System	Feed (wt % EtOH)	Permeate (wt % EtOH)	J_{EtOH} (kg m^{-2} h^{-1})	J_{H_2O} (kg m^{-2} h^{-1})	$\alpha_{w/e}$ (-)
66	EtOH/H_2O	92	0.12	2.51×10^{-3}	2.12	9767
Soaking the membrane in distilled water: 5min; 25°C (room temperature).						
Soaking the membrane in the Ferm. Broth: 41 wt % EtOH; 13h30min; 75°C.						
67	EtOH/H_2O	91	2.20	4.37×10^{-2}	1.94	454
X-ray diffraction analysis (XRD)						
Soaking the membrane in the Ferm. Broth: 41 wt % EtOH; 44h55min; 75°C.						
68	EtOH/H_2O	90	2.39	4.77×10^{-2}	1.95	387
Soaking the membrane in the Ferm. Broth: 41 wt % EtOH; 63h45min; 75°C.						
69	EtOH/H_2O	92	1.00	1.69×10^{-2}	1.67	1158
70	H_2O	0	0.02	8.69×10^{-4}	3.79	-
71	EtOH/H_2O	92	1.35	2.22×10^{-2}	1.62	820

As shown in table 4.15, zeolite A-7 membrane showed a significant increase in the ethanol flux, after being immersed in the fermentation broth for 13.5h. However, the water flux of zeolite A-7 membrane did not decrease significantly. After ≈ 55 hours of immersion in the fermentation broth, zeolite A-7 membrane showed similar pervaporation performance to the previous experiment, but it was possible to observe a small increase in the ethanol flux. Finally, after ≈ 64 hours of immersion in the fermentation broth, it was interesting to note that the ethanol flux decreased 65% and the water flux decreased 14%, in comparison with the previous result. An explanation for this opposite behaviour can be related to the adsorption of some impurities in the non-zeolite domains of the

membrane. These impurities possibly blocked the flux through the non selective pores, and for this reason water perm-selectivity was enhanced, but the water flux decreased.

Richter et al. reported the continuous dehydration of two typical samples of distilled ethanol from different fermentation processes by pervaporation up to 99.5 wt % EtOH in feed, using a zeolite NaA membrane [98]. One sample came from drinking wine production a second from grain fermentation [98]. In both cases, high total flux of 10 kg m^{-2} h^{-1} (90 wt % EtOH in feed, 120°C, 3 m s^{-1}) was found and the permeate water concentration was >95 wt % H_2O [98]. However, for a zeolite NaA membrane to achieve this good results the samples were previously neutralised by adding sodium hydroxide (NaOH) [98].

Vane et al. reported that the typical pH of an ethanolic fermentation broth range from 3 to 6, depending on the portion and type of organic acids present in the fermentation broth [48]. The feed solution pH appears to be a critical parameter for assessing the impact of organic acids on the membranes pervaporation performance, however the pH of the feed solution is rarely controlled or even reported in the literature [48]. On the other hand, Cannilla et. al reported that the zeolite NaA membranes suffer dealumination under strong acidic environment, which limits its use in mixtures with pH <6 [99, 100].

In summary, it can be concluded that zeolite A-7 membrane lost its stability, maybe due to the acidic conditions or the high water content of the fresh distilled fermentation broth. Possibly, the zeolite A crystals suffered dealumination due to the pH conditions of the distilled fermentation broth, which decrease the hydrophilicity typical of the zeolite A membranes and increased the permeate alcohol composition in the pervaporation experiments with the standard composition of ≈ 90 wt % EtOH.

Zeolite A membranes can be used to dehydrate bioethanol from distilled fermentation broth by neutralizing with NaOH the organic acids dissolved in the fermentation broth. Even though, the zeolite A membranes show short-term stability in solutions with high content of water, which is the case of distilled fermentation broths with intermediate concentration. Also, the fermentation broth neutralization process will add complexity and operational costs to the bioethanol production process.

4.2.3.2 X-ray Diffraction

The zeolite A-7 membrane was analyzed by X-ray diffraction after being immersed in the distilled fermentation broth for 13.5h. Figure 4.18 shows the XRD patterns of the zeolite A-7 membrane, after being immersed in the distilled fermentation broth

(figure 4.18a), and the zeolite A powder and the mullite support (figure 4.18b).

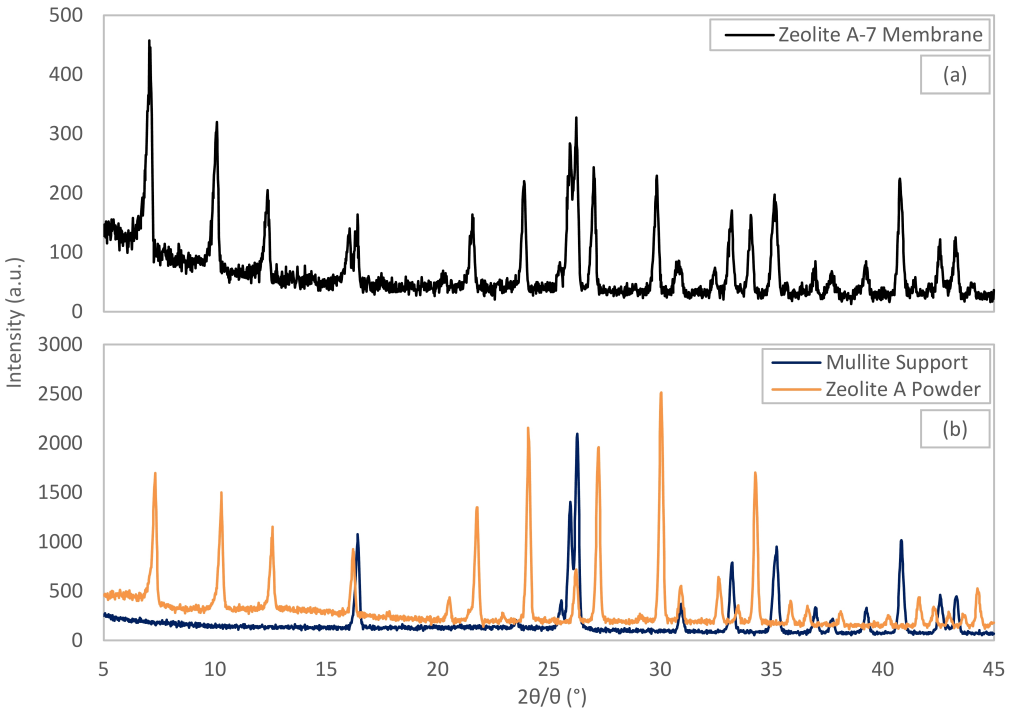

Figure 4.18: XRD patterns of (a) zeolite A-7 membrane after being immersed in the distilled fermentation broth for 13.5h, (b) zeolite A powder and mullite support [101].

As depicted in figure 4.18, all the diffraction peaks in figure 4.18a well corresponding to the zeolite A structure and the mullite support (figure 4.18b), which indicates that the zeolite A-7 membrane did not show structure changes. Although, in the pervaporation experiments with the standard composition of ≈ 90 wt % EtOH, after being immersed in the fresh distilled fermentation broth, the zeolite A-7 membrane showed a reduction in the pervaporation performance, which indicate low stability in fermentation broth conditions.

4.3 Membrane Unit Size Estimation

In order to understand the current feasibility of the scale-up of pervaporation with zeolite membranes, the surface area of the mordenite membranes was modeled considering the continuous dehydration of an ethanolic distilled fermentation broth. The main objective of this section is to estimate the size of a mordenite membrane unit for bioethanol dehydration. For a better understanding of the modeling problem, a simplified scheme of the surface area modeling is represented in figure 4.19.

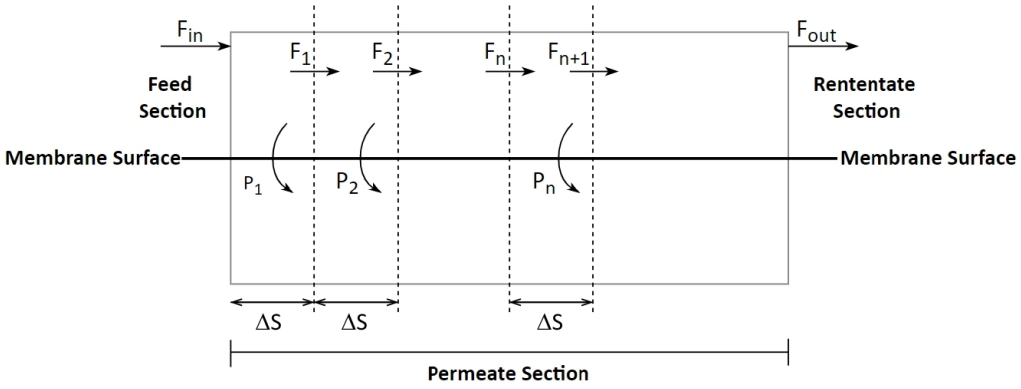

Figure 4.19: Scheme of the surface area modeling.

where F is the flow rate outside the membrane, P is the permeation flow rate through the membrane and S is the membrane surface area.

To solve this modeling problem, it was assumed a F_{in} of 1000 kg/h with a composition of 41 wt % EtOH. Using the Modified Raoult's Law (equation 3.8) and the Wilson's Equation (equation 3.10) it is possible to calculate the driving forces for permeation of ethanol and water for a mixture with certain composition ($\Delta P_{n,i}$). However, the driving force of permeation is not constant, because, in the course of the continuous dehydration, the ethanol feed composition increases due to the water permeation. For this reason, it was considered small fractions of membrane surface area (ΔS) where it was assumed that the driving force is practically constant.

In addition, it was considered that ethanol and water permeances (P_i/δ) are constant with the increase of feed ethanol composition, which was found and discussed in the results of pervaporation experiments with synthetic ethanol-water mixtures. Furthermore, it was used the permeances of the first steady state pervaporation experiment with the distilled fermentation broth (run no. 56).

To calculate the component permeation flow rate ($P_{n,i}$) through the membrane was used the equation 4.1, however, it was necessary to assume a value of ΔS. Thus, it was considered a ΔS of 5 m^2. In addition, it was previously studied that even using a smaller value of ΔS the modeling problem would converge to the same result.

$$P_{n,i} = \left(\frac{P_i}{\delta}\right) \Delta P_{n,i} \Delta S \tag{4.1}$$

Moreover, the flow rate F_{n+1} is calculated using the mass balance equation (equation 4.2).

$$F_{n+1,i} = F_{n,i} - P_{n,i} \tag{4.2}$$

The modeling problem was iteratively solved until it reaches a rententate composition previously defined. In this study, the model was solved until it reaches a rententate composition of ≈ 100 wt % EtOH.

The permeation area required is the sum of all small fractions of membrane surface area iterated (equation 4.3). It is important to highlight that the permeation area depends on the retentate composition required.

$$S = \sum \Delta S \tag{4.3}$$

Table 4.16 summarizes the fixed variables used to solve the modeling problem.

Table 4.16: Fixed variables used in the modeling.

Temperature	75°C
Feed flow rate (F_{in})	1000 kg h^{-1}
Feed composition	41 wt % EtOH
Ethanol permeance	1.4×10^{-10} mol m^{-2} s^{-1} Pa^{-1}
Water permeance	6.6×10^{-7} mol m^{-2} s^{-1} Pa^{-1}
Module area	20 m^2

Recently, Rangnekar et al. reported that the *Dalian Institute of Chemical Physics* (DICP) installed at *Jiangsu Xinhua Chemical Co. Ltd* a zeolite A membrane unit for isopropanol dehydration with a capacity of 50,000 tons per year. This separation unit is considered the largest zeolite membrane facility in the world, and consists of 35 modules with a total permeation area of about 350 m^2 (10 m^2/module) [64]. One of the big advantages of membrane modules is that each individual membrane can be exchanged for a new membrane. For a better understanding, in figure 4.20 is presented a typical tubular membrane module with 20 m^2 of permeation area.

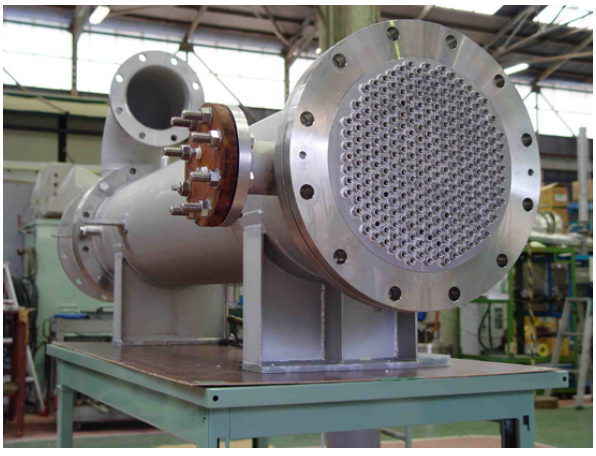

Figure 4.20: Tubular membrane module after zeolite membrane tube insertion [102].

As a result of the modeling problem, in figure 4.21 is presented the membrane surface area in function of the rententate ethanol composition for the base case and two different cases. In case 1 it was considered a water permeance two times higher than the value used in the base case (table 4.16), and in case 2 it was considered a water permeance five times higher.

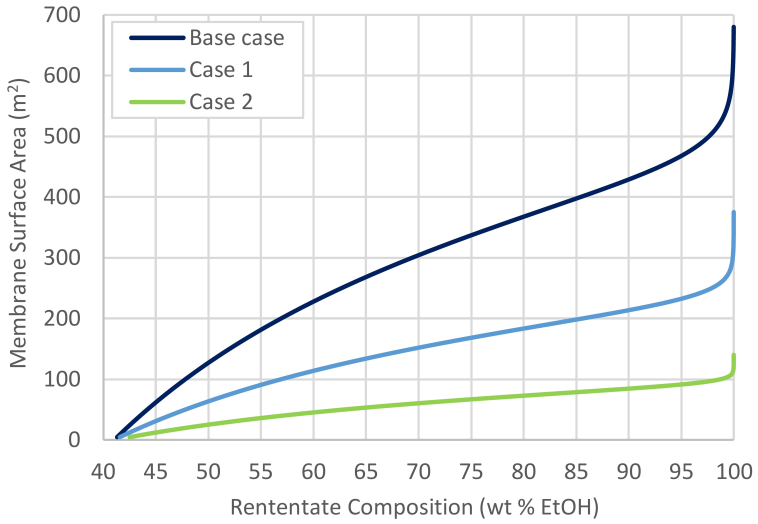

Figure 4.21: Membrane surface area in function of the rententate ethanol composition. Case 1: water permeance x2; Case 2: water permeance x5.

Looking to the base case in figure 4.21, it is easy to observe that the membrane surface area required for a certain separation increase with increase of rententate ethanol composition. Therefore, it can be observed that at high ethanol content in the rententate side, the required surface area increases drastically, because the continuous water extraction has a limit value, mainly due to the continues decrease in the driving force for water permeation.

It is worth to note that the separation limit increase to high rententate ethanol composition, and, also, the membrane surface area required decreased by increasing the water permeance. In summary, enhancing the water permeance it is possible to concentrate the distilled fermentation broth until higher retentate ethanol concentrations, without requiring extremely high membrane permeation area.

Table 4.17 shows the permeation area and the number of modules required to concentrate a distilled fermentation broth from 41.0 to 99.9 wt % EtOH.

Table 4.17: Permeation area and number of modules required to concentrate a distilled fermentation broth from 41,0 wt % to 99,9 wt % EtOH.

Case	Ethanol Permeance (mol m^{-2} s^{-1})	Water Permeance (mol m^{-2} s^{-1})	Permeation Area (m^2)	Number of modules
Base	1.4×10^{-10}	6.6×10^{-7}	600	30
1		1.3×10^{-6}	295	15
2		3.3×10^{-6}	110	6

As shown in table 4.17, for the base case the permeation area required is too high compared to the current industrial situation of zeolite membrane units. However, just doubling the water permeance the number of modules required becomes viable. Hence, the membrane performance can be enhanced by optimizing the synthesis parameters, until it reaches an optimum combination of selectivity and permeation properties. It is important to highlight that these calculations are based on a pervaporation process at 75°C, but usually the industrial membrane units work at higher temperatures, such as 130°C [59].

The ethanol recovery rate is 100 % when no ethanol is found in the permeate section. In order to understand the impact of membrane selectivity in the ethanol losses, figure 4.22 shows the ethanol recovery rate, in percentage, as function of the rententate ethanol composition for the base case and three different cases. In case 3 it was considered an ethanol permeance two times higher than the value used in the base case (table 4.17), in case 4 it was considered an ethanol permeance five times higher, and, finally, in case 5 it was considered an ethanol permeance ten times higher.

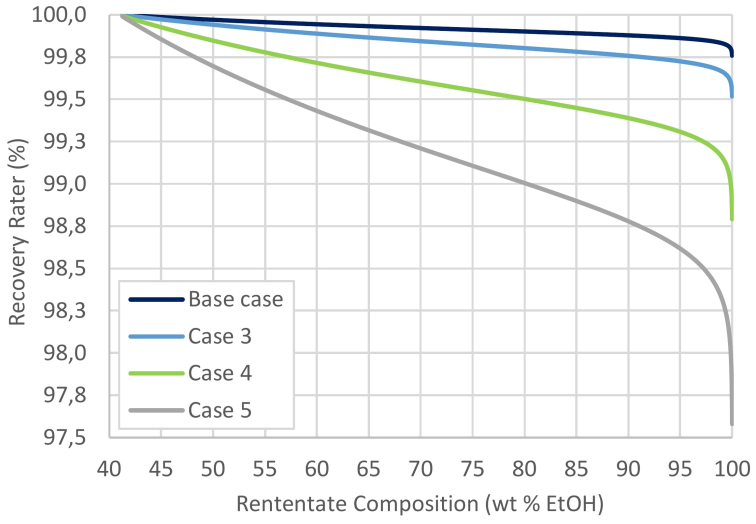

Figure 4.22: Recovery rate in function of the rententate ethanol composition. Case 3: ethanol permeance x2; Case 4: ethanol permeance x5; Case 5: ethanol permeance x10.

As shown in figure 4.22, the ethanol recovery rate decreased with the increase of rententate ethanol composition, which indicates that higher ethanol concentration in the final product leads to greater ethanol losses. In the base case, it can be observed that the ethanol recovery rate is above 99.8% for all the range of rententate ethanol composition, which indicates that the mordenite membranes studied are very hydrophilic. As expected, decreasing the membrane selectivity by increasing the ethanol permeance leads to higher ethanol losses for the permeate side, which is reflected in lower ethanol recovery rates.

In summary, it can be concluded that the mordenite membranes studied are selective enough to perform dehydration processes without wasting large amounts of bioethanol. However, the permeation properties need to be enhanced in order to decrease the membrane surface area required for bioethanol dehydration to fuel-grade specifications. As mentioned previously, the pervaporation performance can be enhanced by optimizing the synthesis parameters. However, it is worth to highlight that a decrease in zeolite layer thickness leads to an increase in permeation properties, but also leads to an increase in structure defects, which negatively affects the membrane selectivity and lead to higher ethanol losses. In conclusion, mordenite membranes synthesis needs to be improved in order to produce membranes with an ultrathin mordenite layer and low defects concentration. Furthermore, the development of supports that offer low resistance to permeation is required.

Chapter 5

Conclusions and Future Work

The main focus of this study was to understand the potential of zeolite membranes to dehydrate aqueous mixtures of organic compounds from fermentation processes. Initially, it was evaluated the pervaporation performance and the stability of mordenite membranes in synthetic aqueous alcohol mixtures. Moreover, it was studied the influence of operating conditions on the pervaporation performance of mordenite membranes. Regarding biofuels production, it was evaluated the pervaporation performance and the stability of mordenite membranes in the dehydration of an ethanolic fermentation broth. Finally, it was also studied the stability of zeolite A membranes in ethanolic fermentation broth conditions.

The mordenite membrane morphology was evaluated, and highly intergrown and aggregated spherical mordenite crystals were found. The mullite support was fully covered by mordenite crystals and it was observed a clear boundary between the mordenite layer and the mullite support.

Mordenite membrane MOR-73 showed water perm-selectivity, with a permeate water composition above 98.82 and 99.83 wt % H_2O for synthetic methanol-water and ethanol-water systems, respectively. Also, mordenite membrane MOR-72 showed water perm-selectivity, with a permeate water composition above 99.87 wt % H_2O for synthetic ethanol-water systems. Both mordenite membranes studied were very selective to water due to their hydrophilic nature, which is caused by their medium Si/Al ratio of 5.

The feed composition influenced the pervaporation performance of mordenite membranes. In methanol-water systems, the total flux decreased linearly and the permeate

composition increased with the increase of feed methanol composition. In ethanol-water systems, also the total flux decreased and the permeate composition increased with the increase of feed ethanol composition, however in the range of 20 to 50 wt % EtOH the pervaporation performance of the mordenite membrane MOR-73 remained almost stable. This behavior is due to the hydrophilic nature and the high affinity of mordenite membranes for water. Thus, the mordenite layer selectively sorbs water over ethanol and as result, the pervaporation performance remains stable over a wide range of ethanol concentrations.

The influence of feed composition on the membrane permeance showed that the water permeance linearly decreased with the increase of methanol concentration in the feed side. On the contrary, water permeance remained almost stable in ethanol-water separations, which indicates that the presence of methanol molecules in the feed side affected the water adsorption, yet the presence of ethanol molecules did not affect significantly the water adsorption. Therefore, it can be concluded that the competitive adsorption between methanol and water molecules needs to be taken into account when separating methanol solutions, but it can be negligible for the separation of ethanol solutions.

In summary, the mordenite membrane MOR-73 showed better pervaporation performance for ethanol-water systems due to the adsorption differences and the molecular size of methanol and ethanol molecules.

The feed temperature influenced the pervaporation performance of mordenite membranes. In general, in both methanol-water and ethanol-water systems, the water permeation flux increased with the increase of feed temperature. Thus, it can be concluded that the pervaporation performance of mordenite membranes can be easily improved by increasing the operating temperature.

Due to the influence of the order of experiments, it was found that pervaporation with distilled water can regenerate the performance of the mordenite membranes studied.

Mordenite membrane MOR-73 kept its stability and performance during 22 pervaporation experiments with binary aqueous alcohol mixtures. However, mordenite membrane MOR-72 showed loss of stability despite continuing to exhibit high performance, with a permeate composition mostly composed by water and a high water permeation flux. In general, it can be concluded that mordenite membranes are stable in synthetic aqueous alcohol solutions.

In the first pervaporation experiment with the distilled fermentation broth (run no.

56), the mordenite membrane MOR-72 reached a well defined steady state, with a total flux, a permeate composition and a separation factor of 1.43 kg m^2 h^{-1}, 0.07 wt % EtOH and 1127, respectively. The presence of the unknown impurity in the broth did not affect the pervaporation performance of the mordenite membrane MOR-72, which indicates that the first pervaporation experiment with the distilled fermentation broth was successful.

In the batch concentration process (run no.62), the mordenite membrane MOR-72 showed similar steady state pervaporation performance to the run no. 56. After reaching the steady state, this membrane was able to concentrate the distilled fermentation broth from ≈ 44 to 49 wt % EtOH in 5h, keeping practically the same steady state pervaporation performance and confirming the potential of these membranes to selective remove water from a fermentation broth with intermediate concentration.

In summary, the mordenite membrane MOR-72 kept a similar pervaporation performance during 53.4h of soaking and pervaporation experiments with the distilled ethanolic fermentation broth, which indicates the high stability and potential of mordenite membranes in the dehydration of ethanolic fermentation broths.

On the contrary, zeolite A-7 membrane lost its pervaporation performance during the soaking experiments in the distilled ethanolic fermentation broth. Despite the fact that the XRD analysis did not indicate structure changes, the results of the pervaporation experiments with the standard composition showed a great loss of selectivity after the first soaking experiment (13.5h). This lost of stability possibly is related to the acidic conditions or the high water content of the distilled fermentation broth.

Based on the membrane unit size estimate, it can be concluded that doubling the water permeance of the mordenite membranes, the number of membrane modules required to concentrate an ethanolic fermentation broth from 41.0 wt % to 99.9 wt % EtOH become viable, with a ethanol recovery rate above 99.8%. The permeation properties can be enhanced by optimizing the synthesis parameters, until it reaches an optimum combination of selectivity and permeation.

After this study, it is possible to conclude that the mordenite membranes prepared on porous mullite supports by secondary hydrothermal synthesis [24] with a Si/Al ratio of 5 can be considered a promising membrane for the production of bioethanol by continuous dehydration of distilled fermentation broth.

For future work, would be interesting to perform sorption studies with pure compounds and binary mixtures at different temperatures to confirm the results discussion about mass transport mechanism in mordenite membranes.

A deep study on synthesis parameters optimization, with resource to SEM, XRD and EPMA analysis, probably would lead to the necessary improvements on the pervaporation performance of the mordenite membranes.

In order to understand the effect of concentration polarization on mordenite membranes performance, it would be interesting to perform a study of fluid dynamics on the feed side, by varying the cross-flow velocity of the feed liquid in the annular space between the housing and the membrane.

A complete characterization of the impurities present in the fermentation broths would lead to a better understanding of the pervaporation experiments results with real fermentation broths.

Further pervaporation experiments with synthetic aqueous mixtures of butanol and isopropanol would be an interesting study, because these molecules have a bigger molecular size than ethanol, and, probably, mordenite membranes pervaporation performance would be similar or even better than in ethanol-water systems.

In addition, pervaporation studies with biobutanolic fermentation broths possibly would lead to a promising industrial application for mordenite membranes, because biobutanol has higher energy content than bioethanol, and it can be easily blended with conventional gasoline at higher concentrations than ethanol for use in unmodified engines [103].

References

[1] IER. (2016). Fossil fuels. Institute for Energy Research (IER). Retrieved 7 April 2017. URL: http://instituteforenergyresearch.org/topics/encyclopedia/fossil-fuels/.

[2] International Energy Agency. (2016). Key World Energy Statistics (1st ed., pp. 1-80). France: IEA. URL: https://www.iea.org/publications/freepublications/publication/KeyWorld2016.pdf.

[3] Nguyen, Q., Bowyer, J., Howe, J., Bratkovich, S., Groot, H., Pepke, E., & Fernholz, K. (2017). Global Production of Second Generation Biofuels: Trends and Influences (1st ed., pp. 1-16). Minneapolis: Dovetail Partners, Inc.

[4] Guo, M., Song, W., & Buhain, J. (2015). Bioenergy and biofuels: History, status, and perspective. *Renewable And Sustainable Energy Reviews*, 42, 712-725. DOI: http://dx.doi.org/10.1016/j.rser.2014.10.013.

[5] Renewables 2017 Global Status Report (1st ed., p. 21). Paris: REN21 Secretariat. URL: http://www.ren21.net.

[6] Agarwal, A.K., Agarwal, R.A., Gupta, T., & Gurjar, B.R. (2017). Introduction to Biofuels - Biofuels, Green Energy and Technology (1st ed.). Singapore: Springer Nature Singapore Pte Ltd.

[7] Types Of Renewable Energy: Bioproducts. Renewable Energy Work. Retrieved 7 April 2017. URL: http://www.renewableenergyworld.com/bioenergy/tech/bioproducts.html.

[8] Speight, J. G. (2017). Rules of Thumb for Petroleum Engineers (2nd ed., pp. 79-80). John Wiley & Sons, Inc.

[9] REW. (2016). Types Of Renewable Energy: Bioenergy. Renewable Energy Work. Retrieved 7 April 2017. URL: http://www.renewableenergyworld.com/bioenergy/tech.html.

[10] Gaurav, N., Sivasankari, S., Kiran, G., Ninawe, A., & Selvin, J. (2017). Utilization of bioresources for sustainable biofuels: A Review. *Renewable And Sustainable Energy Reviews*, 73, 205-214. DOI: http://dx.doi.org/10.1016/j.rser.2017.01.070.

[11] Nigam, P., & Singh, A. (2011). Production of liquid biofuels from renewable resources. *Progress In Energy And Combustion Science*, 37(1), 52-68. DOI: http://dx.doi.org/10.1016/j.pecs.2010.01.003.

[12] World Energy Council. (2017). Biomass in southeast Asia and Pacific. World Energy Council. Retrieved 2 April 2017. URL: https://www.worldenergy.org/data/resources/region/southeast-asia-pacific/biomass/.

[13] Klimowicz, G. (2013). Southeast Asia set for biomass boom. *Eco-Business*. Retrieved 17 April 2017. URL: http://www.eco-business.com/news/southeast-asia-set-biomass-boom/.

[14] Zhou, A., & Thomson, E. (2009). The development of biofuels in Asia. *Applied Energy*, 86, S11-S20. DOI: http://dx.doi.org/10.1016/j.apenergy.2009.04.028.

[15] Yan, J., & Lin, T. (2009). Biofuels in Asia. *Applied Energy*, 86, S1-S10. DOI: http://dx.doi.org/10.1016/j.apenergy.2009.07.004.

[16] Chanthawong, A., & Dhakal, S. (2015). Liquid Biofuels Development in Southeast Asian Countries: An Analysis of Market, Policies and Challenges. *Waste And Biomass Valorization*, 7(1), 157-173. DOI: http://dx.doi.org/10.1007/s12649-015-9433-9.

[17] Murata, M., Nitiyon, S., Lertwattanasakul, N., Sootsuwan, K., Kosaka, T., & Thanonkeo, P. et al. (2015). High-temperature Fermentation Technology for Low-cost Bioethanol. *Journal Of The Japan Institute Of Energy*, 94(10), 1154-1162. DOI: http://dx.doi.org/10.3775/jie.94.1154.

[18] Nonklang, S., Abdel-Banat, B., Cha-aim, K., Moonjai, N., Hoshida, H., & Limtong, S. et al. (2008). High-Temperature Ethanol Fermentation and Transformation with Linear DNA in the Thermotolerant Yeast Kluyveromyces marxianus DMKU3-1042. *Applied And Environmental Microbiology*, 74(24), 7514-7521. DOI: http://dx.doi.org/10.1128/aem.01854-08.

[19] Choudhary, J., Singh, S., & Nain, L. (2016). Thermotolerant fermenting yeasts for simultaneous saccharification fermentation of lignocellulosic biomass. *Electronic Journal Of Biotechnology*, 21, 82-92. DOI: http://dx.doi.org/10.1016/j.ejbt.2016.02.007.

[20] Vane, L. (2008). Separation technologies for the recovery and dehydration of alcohols from fermentation broths. *Biofuels, Bioproducts And Biorefining*, 2(6), 553-588. DOI: http://dx.doi.org/10.1002/bbb.108.

[21] Matsukata, M., Sawamura, K., Sekine, Y., & Kikuchi, E. (2011). Review on Prospects for Energy Savings in Distillation Process with Microporous Membranes. Oyama, S. and Stagg-Williams, S. (2011). Inorganic, polymeric and composite membranes - Structure, Function and Other Correlations (1st ed., pp. 175-193). Amsterdam: Elsevier.

[22] EMIS. (2010). Pervaporation. Energie - en milieu-informatiesysteem voor het Vlaamse Gewest. Retrieved 7 April 2017. URL: https://emis.vito.be/nl/node/19386.

[23] Khan, S., Usman, M., Gull, N., Butt, M., & Jamil, T. (2013). An overview on Pervaporation (An Advanced Separation Technique). *Journal Of Quality And Technology Management*, 4(1), 155-161.

[24] Zhu, M., Hua, X., Liu, Y., Hu, H., Li, Y., & Hu, N. et al. (2016). Influences of Synthesis Parameters on Preparation of Acid-Stable and Reproducible Mordenite Membrane. *Industrial & Engineering Chemistry Research*, 55(47), 12268-12275. DOI: http://dx.doi.org/10.1021/acs.iecr.6b02125.

[25] Zhu, M., Xia, S., Hua, X., Feng, Z., Hu, N., & Zhang, F. et al. (2014). Rapid Preparation of Acid-Stable and High Dehydration Performance Mordenite Membranes. *Industrial & Engineering Chemistry Research*, 53(49), 19168-19174. DOI: http://dx.doi.org/10.1021/ie501248y.

[26] Sillanpaa, M., & Ncibi, C. (2017). A sustainable Bioeconomy: The Green Industrial Revolution (1st ed., pp. 108-111). Springer International.

[27] Huang, H., Ramaswamy, S., Tschirner, U., & Ramarao, B. (2008). A review of separation technologies in current and future biorefineries. *Separation And Purification Technology*, 62(1), 1-21. DOI: http://dx.doi.org/10.1016/j.seppur.2007.12.011.

[28] Nguyen, H., DeJaco, R., Mittal, N., Siepmann, J., Tsapatsis, M., & Snyder, M. et al. (2017). A Review of Biorefinery Separations for Bioproduct Production via Thermocatalytic Processing. *Annual Review Of Chemical And Biomolecular Engineering*, 12(8), 6.1-6.23. DOI: http://dx.doi.org/https://doi.org/10.1146/annurev-chembioeng-060816-101303.

[29] Singh, A., & Rangaiah, G. (2017). Review of Technological Advances in Bioethanol Recovery and Dehydration. *Industrial & Engineering Chemistry Research*, 56(18), 5147-5163. DOI: http://dx.doi.org/10.1021/acs.iecr.7b00273.

[30] Loy, Y. Y., Lee, X. L., & Rangaiah, G. P. (2015). Bioethanol recovery and purification using extractive dividing-wall column and pressure swing adsorption: An economic comparison after heat integration and optimization. *Separation And Purification Technology*, 149, 413-427. DOI: http://dx.doi.org/10.1016/j.seppur.2015.06.007.

[31] Batista, F., Follegatti-Romero, L., Bessa, L., & Meirelles, A. (2012). Computational simulation applied to the investigation of industrial plants for bioethanol distillation. *Computers & Chemical Engineering*, 46, 1-16. DOI: http://dx.doi.org/10.1016/j.compchemeng.2012.06.004.

[32] CSN EN 15376. (2014). CSN EN 15376 - Automotive fuels - Ethanol as a blending component for petrol - Requirements and test methods. Chemical Industry Standards. Retrieved 7 June 2017. URL: https://www.chemicalindustrystandards.com.

[33] ASTM D4806 - 16a. (2016). ASTM D4806 - 16a Standard Specification for Denatured Fuel Ethanol for Blending with Gasolines for Use as Automotive Spark-Ignition Engine Fuel. ASTM International. Retrieved 7 June 2017. URL: https://www.astm.org.

[34] Ramírez-Márquez, C., Segovia-Hernández, J., Hernández, S., Errico, M., & Rong, B. (2013). Dynamic Behavior of Alternative Separation Processes for Ethanol Dehydration by Extractive Distillation. *Industrial & Engineering Chemistry Research*, 52(49), 17554-17561. DOI: http://dx.doi.org/10.1021/ie402834p.

[35] Kiss, A., & Suszwalak, D. (2012). Enhanced bioethanol dehydration by extractive and azeotropic distillation in dividing-wall columns. *Separation And Purification Technology*, 86, 70-78. DOI: http://dx.doi.org/10.1016/j.seppur.2011.10.022.

[36] Pla-Franco, J., Lladosa, E., Loras, S., & Montón, J. (2014). Thermodynamic Analysis and Process Simulation of Ethanol Dehydration via Heterogeneous Azeotropic Distillation. *Industrial & Engineering Chemistry Research*, 53(14), 6084-6093. DOI: http://dx.doi.org/10.1021/ie403988c.

[37] Avilés Martínez, A., Saucedo-Luna, J., Segovia-Hernandez, J., Hernandez, S., Gomez-Castro, F., & Castro-Montoya, A. (2012). Dehydration of Bioethanol by Hybrid Process Liquid–Liquid Extraction/Extractive Distillation. *Industrial & Engineering Chemistry Research*, 51(17), 5847-5855. DOI: http://dx.doi.org/10.1021/ie200932g.

[38] Kiss, A., & Ignat, R. (2012). Innovative single step bioethanol dehydration in an extractive dividing-wall column. *Separation And Purification Technology*, 98, 290-297. DOI: http://dx.doi.org/10.1016/j.seppur.2012.06.029.

[39] Kumar, S., Singh, N., & Prasad, R. (2010). Anhydrous ethanol: A renewable source of energy. *Renewable And Sustainable Energy Reviews*, 14(7), 1830-1844. DOI: http://dx.doi.org/10.1016/j.rser.2010.03.015.

[40] Gyamerah, M., & Glover, J. (1996). Production of Ethanol by Continuous Fermentation and Liquid-Liquid Extraction. *Journal Of Chemical Technology & Biotechnology*, 66(2), 145-152. DOI: http://dx.doi.org/10.1002/(sici)1097-4660(199606)66:2<145::aid-jctb484>3.0.co;2-2.

[41] Graaf, J. (1999). Permeation and separation properties of supported silicalite-1 membranes. (1st ed., pp. 1-5). Delft, Netherlands: EburonP&L.

[42] Takht Ravanchi, M., Kaghazchi, T., & Kargari, A. (2009). Application of membrane separation processes in petrochemical industry: a review. *Desalination*, 235(1-3), 199-244. DOI: http://dx.doi.org/10.1016/j.desal.2007.10.042.

[43] Ladewig, B., & Al-Shaeli, M. (2017). Fundamentals of Membrane Bioreactors (1st ed., pp. 13-37). Singapore: Springer Singapore.

[44] Peinemann, K., & Nunes, S. (2017). Membrane Technology in the Chemical Industry (2nd ed., pp. 151-155). Weinheim, Germany: 6 Wiley-Vch Verlag GmbH & Co. KGaA.

[45] Bowen, T., Noble, R., & Falconer, J. (2004). Fundamentals and applications of pervaporation through zeolite membranes. *Journal Of Membrane Science*, 245(1-2), 1-33. DOI: http://dx.doi.org/10.1016/j.memsci.2004.06.059.

[46] Baker, R. (2004). Membrane Technology and Applications (2nd ed., pp. 354-388). John Wiley & Sons Ltd.

[47] Wei, P., Cheng, L., Zhang, L., Xu, X., Chen, H., & Gao, C. (2014). A review of membrane technology for bioethanol production. *Renewable And Sustainable Energy Reviews*, 30, 388-400. DOI: http://dx.doi.org/10.1016/j.rser.2013.10.017.

[48] Vane, L. (2005). A review of pervaporation for product recovery from biomass fermentation processes. *Journal Of Chemical Technology & Biotechnology*, 80(6), 603-629. DOI: http://dx.doi.org/10.1002/jctb.1265.

[49] Tusel, G., & Ballweg, A. (1983). Method and apparatus for dehydrating mixtures of organic liquids and water. US Patent 4405409 A.

[50] Ikeda, S. (2009). Method for concentrating water-soluble organic material. US 7594981 B2.

[51] Côté, P., Roy, C., Bernier, N., Schwartz, M., Kazmir, M., & Shamash, R. (2007). Field demonstration of the Siftek™ membrane for ethanol production. Presentation at International Fuel Ethanol Workshop, St-Louis.

[52] Cejka J., Bekkum, H., Corma, A., & Schuth, F. (2007). Introduction to zeolite science and practice (3rd ed., pp. 7-18). Amsterdam: Elsevier.

[53] Ferraz, E., Andrejkovicová, S., Velosa, A., Silva, A., & Rocha, F. (2014). Synthetic zeolite pellets incorporated to air lime–metakaolin mortars: Mechanical properties. *Construction And Building Materials*, 69, 243-252. DOI: http://dx.doi.org/10.1016/j.conbuildmat.2014.07.030.

[54] Auerbach, S., Carrado, K., & Dutta, P. (2003). Handbook of zeolite science and technology (1st ed.). New York: Dekker.

[55] Ye, P. (2016). Zeolite Membrane Separation at Low Temperature (Doctoral Thesis). Lulea University of Technology.

[56] Graaf, J. (1999). Permeation and separation properties of supported silicalite-1 membranes. (1st ed., pp. 5-7). Delft, Netherlands: EburonP&L.

[57] Baerlocher, Ch., McCusker, L. B., Olson, D. H. (2007). Atlas of zeolite framework types (1st ed., pp. 194-219). Amsterdam: Elsevier.

[58] Baerlocher, Ch., & McCusker, L. B. (2017). Database of Zeolite Structures. IZA Structure Commission. Retrieved 17 May 2017. URL: http://www.iza-structure.org/databases/.

[59] Gascon, J., Kapteijn, F., Zornoza, B., Sebastián, V., Casado, C., & Coronas, J. (2012). Practical Approach to Zeolitic Membranes and Coatings: State of the Art, Opportunities, Barriers, and Future Perspectives. *Chemistry Of Materials*, 24(15), 2829-2844. DOI: http://dx.doi.org/10.1021/cm301435j.

[60] Mittal, N., Bai, P., Kelloway, A., Siepmann, J., Daoutidis, P., & Tsapatsis, M. (2016). A mathematical model for zeolite membrane module performance and its use for techno-economic evaluation of improved energy efficiency hybrid membrane-distillation processes for butane isomer separations. *Journal Of Membrane Science*, 520, 434-449. DOI: http://dx.doi.org/10.1016/j.memsci.2016.06.041.

[61] Yu, M., Noble, R., & Falconer, J. (2011). Zeolite Membranes: Microstructure Characterization and Permeation Mechanisms. *Accounts Of Chemical Research*, 44(11), 1196-1206. DOI: http://dx.doi.org/10.1021/ar200083e.

[62] Suzuki, H.(1987). Composite membrane having a surface layer of an ultrathin film of cage-shaped zeolite and processes for production thereof, U.S. Patent 4,699,892.

[63] Julbe, A. (2007). Zeolite membranes - synthesis, characterization and application. Cejka J., Bekkum, H., Corma, A., and Schuth, F. (2007). Introduction to zeolite science and practice (3rd ed., pp. 182-219). Amsterdam: Elsevier.

[64] Rangnekar, N., Mittal, N., Elyassi, B., Caro, J., & Tsapatsis, M. (2015). Zeolite membranes - a review and comparison with MOFs. *Chemical Society Reviews*, 44(20), 7128-7154. DOI: http://dx.doi.org/10.1039/c5cs00292c.

[65] Wee, S., Tye, C., & Bhatia, S. (2008). Membrane separation process—Pervaporation through zeolite membrane. *Separation And Purification Technology*, 63(3), 500-516. DOI: http://dx.doi.org/10.1016/j.seppur.2008.07.010.

[66] McLeary, E., Jansen, J., & Kapteijn, F. (2006). Zeolite based films, membranes and membrane reactors: Progress and prospects. *Microporous And Mesoporous Materials*, 90(1-3), 198-220. DOI: http://dx.doi.org/10.1016/j.micromeso.2005.10.050.

[67] Morigami, Y., Kondo, M., Abe, J., Kita, H., & Okamoto, K. (2001). The first large-scale pervaporation plant using tubular-type module with zeolite NaA membrane. *Separation And Purification Technology*, 25(1-3), 251-260. DOI: http://dx.doi.org/10.1016/s1383-5866(01)00109-5.

[68] Sato, K., Aoki, K., Sugimoto, K., Izumi, K., Inoue, S., & Saito, J. et al. (2008). Dehydrating performance of commercial LTA zeolite membranes and application to fuel grade bio-ethanol production by hybrid distillation/vapor permeation process. *Microporous And Mesoporous Materials*, 115(1-2), 184-188. DOI: http://dx.doi.org/10.1016/j.micromeso.2007.10.053.

[69] Zhu, M., Kumakiri, I., Tanaka, K., & Kita, H. (2013). Dehydration of acetic acid and esterification product by acid-stable ZSM-5 membrane. *Microporous And Mesoporous Materials*, 181, 47-53. DOI: http://dx.doi.org/10.1016/j.micromeso.2012.12.044.

[70] Li, L., Yang, J., Li, J., Han, P., Wang, J., & Zhao, Y. et al. (2016). Synthesis of high performance mordenite membranes from fluoride-containing dilute solution under microwave-assisted heating. *Journal Of Membrane Science*, 512, 83-92. DOI: http://dx.doi.org/10.1016/j.memsci.2016.03.056.

[71] Zhu, M., Feng, Z., Hua, X., Hu, H., Xia, S., & Hu, N. et al. (2016). Application of a mordenite membrane to the esterification of acetic acid and alcohol using sulfuric acid catalyst. *Microporous And Mesoporous Materials*, 233, 171-176. DOI: http://dx.doi.org/10.1016/j.micromeso.2016.01.038.

[72] Zhang, Y., Nakasaka, Y., Tago, T., Hirata, A., Sato, Y., & Masuda, T. (2015). Preparation and optimization of mordenite nanocrystal-layered membrane for dehydration by pervaporation. *Microporous And Mesoporous Materials*, 207, 39-45. DOI: http://dx.doi.org/10.1016/j.micromeso.2014.12.032.

[73] Zhou, R., Hu, Z., Hu, N., Duan, L., Chen, X., & Kita, H. (2012). Preparation and microstructural analysis of high-performance mordenite membranes in fluoride media. *Microporous And Mesoporous Materials*, 156, 166-170. DOI: http://dx.doi.org/10.1016/j.micromeso.2012.02.023.

[74] Navajas, A., Mallada, R., Téllez, C., Coronas, J., Menéndez, M., & Santamaría, J. (2002). Preparation of mordenite membranes for pervaporation of water-ethanol mixtures. *Desalination*, 148(1-3), 25-29. DOI: http://dx.doi.org/10.1016/s0011-9164(02)00648-3.

[75] Navajas, A., Mallada, R., Téllez, C., Coronas, J., Menéndez, M., & Santamaría, J. (2006). The use of post-synthetic treatments to improve the pervaporation performance of mordenite membranes. *Journal Of Membrane Science*, 270(1-2), 32-41. DOI: http://dx.doi.org/10.1016/j.memsci.2005.06.038.

[76] Li, G., Su, X., & Lin, R. (2007). Preparation of highly water-selective mordenite membranes via post-synthetic treatment with oxalic acid. *Materials Letters*, 61(23-24), 4576-4578. DOI: http://dx.doi.org/https://doi.org/10.1016/j.matlet.2007.02.054.

[77] Li, X., Kita, H., Zhu, H., Zhang, Z., & Tanaka, K. (2009). Synthesis of long-term acid-stable zeolite membranes and their potential application to esterification reactions. *Journal Of Membrane Science*, 339(1-2), 224-232. DOI: http://dx.doi.org/10.1016/j.memsci.2009.04.054.

[78] Ethanol. (2017). Ethanol (Ethyl Alcohol) | Products | Mitsubishi Chemical Corporation. Mitsubishi Chemical Corporation. Retrieved 24 July 2017. URL: https://www.m-chemical.co.jp/en/products/departments/mcc/c2/product/1200982_7910.html.

[79] Methanol 137-01823. (2017). Methanol [JIS K 8891] - Product Specification. Siyaku. Retrieved 12 July 2017. URL: http://www.siyaku.com/uh/Shs.do?dspCode=W01W0113-0182.

[80] Shimadzu. (2017). GC-8A Basic Gas Chromatograph Model. Shimadzu - Global Analytical and Measuring Instruments. Retrieved 16 July 2017. URL: http://www.shimadzu.com/an/gc/gc8a.html.

[81] Baker, R., Wijmans, J., & Huang, Y. (2010). Permeability, permeance and selectivity: A preferred way of reporting pervaporation performance data. *Journal Of Membrane Science*, 348(1-2), 346-352. DOI: http://dx.doi.org/10.1016/j.memsci.2009.11.022.

[82] Green, D., & Perry, R. (2008). Perry's Chemical Engineers' Handbook (8th ed., p. 671). New York: The McGraw-Hill Companies, Inc.

[83] Kagaku Kogaku benran-Handbook of Chemical Engineering. (1995). Ed.5. pg 18.

[84] Kagaku Kogaku benran-Handbook of Chemical Engineering. (1995). Ed.5. pg 44-47.

[85] Haynes, W. M., Lide, D. R., & Bruno, T. J. (2017). CRC Handbook of Chemistry and Physics (97th ed.), pp. Section 6 (7-8). Taylor & Francis Group.

[86] Haynes, W. M., Lide, D. R., & Bruno, T. J. (2017). CRC Handbook of Chemistry and Physics (97th ed.), pp. Section 15 (23-42). Taylor & Francis Group.

[87] Feng, X., & Huang, R. (1996). Estimation of activation energy for permeation in pervaporation processes. *Journal of Membrane Science*, 118, 127-131. DOI: https://doi.org/10.1016/0376-7388(96)00096-8.

[88] Casado, L., Mallada, R., Tellez, C., Coronas, J., Menendez, M., & Santamaria, J. (2003). Preparation, characterization and pervaporation performance of mordenite membranes. *Journal Of Membrane Science*, 216(1-2), 135-147. DOI: http://dx.doi.org/10.1016/s0376-7388(03)00065-6.

[89] Zhang, Y., Xu, Z., & Chen, Q. (2002). Synthesis of small crystal polycrystalline mordenite membrane. *Journal Of Membrane Science*, 210(2), 361-368. DOI: http://dx.doi.org/10.1016/s0376-7388(02)00414-3.

[90] Shah, D., Kissick, K., Ghorpade, A., Hannah, R., & Bhattacharyya, D. (2000). Pervaporation of alcohol–water and dimethylformamide-water mixtures using hydrophilic zeolite NaA membranes: mechanisms and experimental results. *Journal Of Membrane Science*, 179(1-2), 185-205. DOI: http://dx.doi.org/10.1016/s0376-7388(00)00515-9.

[91] Baker, R., Wijmans, J., & Huang, Y. (2010). Permeability, permeance and selectivity: A preferred way of reporting pervaporation performance data. *Journal Of Membrane Science*, 348(1-2), 346-352. DOI: http://dx.doi.org/10.1016/j.memsci.2009.11.022.

[92] Borjigin, T., Sun, F., Zhang, J., Cai, K., Ren, H., & Zhu, G. (2012). A microporous metal–organic framework with high stability for GC separation of alcohols from water. *Chemical Communications*, 48(61), 7613. DOI: http://dx.doi.org/10.1039/c2cc33023g.

[93] Asghari, M., Hassanvand, A., & Mohammadi, T. (2013). Fabrication and characterization of highly crystalline mordenite membranes on α-alumina disks via a seeded in situ template-free hydrothermal treatment. *Adsorption*, 19(5), 903-908. DOI: http://dx.doi.org/10.1007/s10450-013-9505-8.

[94] Nomura, M., Bin, T., & Nakao, S. (2002). Selective ethanol extraction from fermentation broth using a silicalite membrane. *Separation And Purification Technology*, 27(1), 59-66. DOI: http://dx.doi.org/10.1016/s1383-5866(01)00195-2.

[95] Ikegami, T., Yanagishita, H., Kitamoto, D., Negishi, H., Haraya, K., & Sano, T. (2002). Concentration of fermented ethanol by pervaporation using silicalite membranes coated with silicone rubber. *Desalination*, 149(1-3), 49-54. DOI: http://dx.doi.org/10.1016/s0011-9164(02)00690-2.

[96] Ikegami, T., Yanagishita, H., Kitamoto, D., Haraya, K., Nakane, T., Matsuda, H., Koura, N., & Sano, T. (1999). Highly concentrated aqueous ethanol solutions by pervaporation using silicalite membrane-improvement of ethanol selectivity by addition of sugars to ethanol solution. *Biotechnology letters*, 21(12), 1037-1041.

[97] Ikegami, T., Yanagishita, H., Kitamoto, D., Haraya, K., Nakane, T., Matsuda, H., & Sano, T. (1997). Production of highly concentrated ethanol in a coupled fermentation/pervaporation process using silicalite membranes. *Biotechnology techniques*, 11(12), 921-924.

[98] Richter, H., Voigt, I., & Kuhnert, J. (2006). Dewatering of ethanol by pervaporation and vapour permeation with industrial scale NaA-membranes. *Desalination*, 199(1-3), 92-93. DOI: http://dx.doi.org/10.1016/j.desal.2006.03.150.

[99] Cannilla, C., Bonura, G., & Frusteri, F. (2017). Potential of Pervaporation and Vapor Separation with Water Selective Membranes for an Optimized Production of Biofuels-A Review. *Catalysts*, 7(6), 187. DOI: http://dx.doi.org/10.3390/cata7060187.

[100] Pera-Titus, M., Llorens, J., & Cunill, F. (2009). Technical and economical feasibility of zeolite NaA membrane-based reactors in liquid-phase etherification reactions. *Chemical Engineering And Processing: Process Intensification*, 48(5), 1072-1079. DOI: http://dx.doi.org/10.1016/j.cep.2009.02.006.

[101] Saeda, T. (2017). Zeolite A powder and mullite support: X-ray Diffraction data. Rigaku Smartlab X-ray diffractometer.

[102] MZM. (2017). Zeolite membrane module. Mitsui Zosen Machinery & Service Inc. Retrieved 2 September 2017, from. URL: https://www.mzm.co.jp/products/industrial/film/module.html.

[103] ThoughtCo. (2017). The Process, Pros, and Cons of Biobutanol. ThoughtCo. Retrieved 4 September 2017, from. URL: https://www.thoughtco.com/pros-cons-biobutanol-85645.

Appendix A

Pervaporation Experiments

A.1 Mordenite Membrane MOR-73

Table A.1: PV experiments with mordenite membrane MOR-73 in terms of permeate composition, total flux and separation factor.

					Composition ≈		Average in Steady State			
Run No.	Date	Type	T (°C)	System	wt %	mol %	Feed (ln) (EtOH wt %)	Permeate (EtOH wt %)	J (total) (kg m^{-2} h^{-1})	Separation factor, $\alpha_{w/o}$
0.1.	19/04/2017	short	75	EtOH/H_2O	90/10	78/22	87.85 ± 0.77	0.156 ± 0.125	0.719 ± 0.010	8028 ± 4206
0.2.	20/04/2017	short	75	EtOH/H_2O	90/10	78/22	89.80 ± 0.36	0.250 ± 0.113	0.780 ± 0.007	5166 ± 3637
0.3.	21/04/2017	short	75	EtOH/H_2O	90/10	78/22	89.26 ± 0.07	0.106 ± 0.029	0.780 ± 0.007	8472 ± 2278
0.4.	22/04/2017	short	75	EtOH/H_2O	90/10	78/22	89.67 ± 0.02	0.114 ± 0.046	0.787 ± 0.002	8676 ± 2712
1	26/04/2017	short	75	EtOH/H_2O	72/28	50/50	71.59 ± 0.16	0.045 ± 0.003	1.182 ± 0.001	5548 ± 380
2	27/04/2017	short	75	EtOH/H_2O	72/28	50/50	72.49 ± 0.02	0.039 ± 0.001	1.206 ± 0.003	6813 ± 93
3	28/04/2017	short	75	EtOH/H_2O	90/10	78/22	90.86 ± 0.09	0.071 ± 0.000	0.762 ± 0.011	14011 ± 217
4	29/04/2017	short	75	EtOH/H_2O	50/50	28/72	48.12 ± 0.04	0.044 ± 0.002	1.242 ± 0.002	2101 ± 204
5	10/05/2017	long	75	EtOH/H_2O	90/10	78/22	91.61 ± 0.03	0.078 ± 0.009	0.673 ± 0.004	14181 ± 1629
6	11/05/2017	long	75	EtOH/H_2O	90/10	78/22	91.70 ± 0.11	0.127 ± 0.002	0.648 ± 0.005	8729 ± 223
7	12/05/2017	long	75	EtOH/H_2O	90/10	78/22	90.99 ± 0.05	0.127 ± 0.005	0.706 ± 0.004	7949 ± 314
8	13/05/2017	short	75	EtOH/H_2O	80/20	61/39	77.84 ± 0.08	0.121 ± 0.007	1.060 ± 0.003	2914 ± 159
9	17/05/2017	short	75	EtOH/H_2O	95/05	88/12	94.65 ± 0.08	0.413 ± 0.024	0.432 ± 0.004	4285 ± 199
10	18/05/2017	short	75	EtOH/H_2O	30/70	14/86	30.54 ± 0.05	0.095 ± 0.004	1.078 ± 0.003	464 ± 18
11	19/05/2017	short	75	EtOH/H_2O	90/10	78/22	90.04 ± 0.36	0.134 ± 0.002	0.704 ± 0.003	6756 ± 392
12	20/05/2017	short	75	EtOH/H_2O	0/100	0/100	0.00 ± 0.00	0.044 ± 0.001	1.435 ± 0.009	-
13	21/05/2017	short	75	EtOH/H_2O	90/10	78/22	90.74 ± 0.03	0.086 ± 0.003	0.709 ± 0.004	11462 ± 491
14	24/05/2017	short	75	EtOH/H_2O	10/90	4/96	8.72 ± 0.01	0.047 ± 0.002	1.521 ± 0.006	204 ± 10
15	25/05/2017	short	75	EtOH/H_2O	90/10	78/22	90.69 ± 0.24	0.099 ± 0.011	0.651 ± 0.010	9978 ± 1238
16	26/05/2017	short	75	EtOH/H_2O	0/100	0/100	0.03 ± 0.00	0.037 ± 0.002	1.511 ± 0.011	-
17	27/05/2017	short	75	MetOH/H_2O	10/90	6/94	10.16 ± 0.02	0.037 ± 0.002	1.194 ± 0.003	310 ± 20
18	28/05/2017	short	75	MetOH/H_2O	20/80	12/88	19.97 ± 0.04	0.076 ± 0.003	1.011 ± 0.004	326 ± 12
19	30/05/2017	short	60	MetOH/H_2O	10/90	6/94	10.12 ± 0.04	0.043 ± 0.002	0.675 ± 0.001	265 ± 14
20	01/06/2017	short	60	MetOH/H_2O	20/80	12/88	19.96 ± 0.05	0.062 ± 0.004	0.578 ± 0.001	401 ± 26
21	02/06/2017	short	60	MetOH/H_2O	50/50	36/64	49.53 ± 0.08	0.194 ± 0.011	0.346 ± 0.002	505 ± 29
22	03/06/2017	short	60	MetOH/H_2O	80/20	69/31	79.96 ± 0.01	0.653 ± 0.016	0.130 ± 0.000	607 ± 15
23	04/06/2017	short	60	MetOH/H_2O	90/10	84/16	89.60 ± 0.03	1.181 ± 0.113	0.057 ± 0.001	728 ± 76
24	06/06/2017	short	60	MetOH/H_2O	10/90	6/94	10.09 ± 0.02	0.061 ± 0.003	0.682 ± 0.006	186 ± 9
25	08/06/2017	short	75	MetOH/H_2O	0/100	0/100	0.00 ± 0.00	0.000 ± 0.000	1.515 ± 0.004	-
26	09/06/2017	short	60	MetOH/H_2O	10/90	6/94	10.16 ± 0.03	0.042 ± 0.001	0.707 ± 0.001	267 ± 5
27	10/06/2017	short	40	MetOH/H_2O	10/90	6/94	10.17 ± 0.01	0.040 ± 0.001	0.299 ± 0.001	282 +5
28	11/06/2017	short	40	MetOH/H_2O	20/80	12/88	19.86 ± 0.02	0.060 ± 0.001	0.242 ± 0.001	415 ± 7
29	14/06/2017	short	60	MetOH/H_2O	0/100	0/100	0.02 ± 0.00	0.000 ± 0.000	0.878 ± 0.006	-
30	15/06/2017	short	40	MetOH/H_2O	0/100	0/100	0.00 ± 0.00	0.000 ± 0.000	0.367 ± 0.002	-
31	16/06/2017	short	60	MetOH/H_2O	10/90	6/94	10.10 ± 0.03	0.043 ± 0.003	0.698 ± 0.002	260 ± 17
32	17/06/2017	short	75	EtOH/H_2O	10/90	4/96	9.93 ± 0.01	0.046 ± 0.002	1.462 ± 0.001	239 ± 11
33	18/06/2017	short	75	EtOH/H_2O	20/80	9/91	20.10 ± 0.03	0.049 ± 0.003	1.156 ± 0.008	515 ± 29
34	19/06/2017	short	75	EtOH/H_2O	50/50	28/72	50.50 ± 0.04	0.059 ± 0.014	1.114 ± 0.001	1830 ± 384
35	20/06/2017	short	75	EtOH/H_2O	80/20	61/39	80.69 ± 0.05	0.140 ± 0.015	0.895 ± 0.005	3012 ± 314
36	22/06/2017	short	75	EtOH/H_2O	90/10	78/22	89.66 ± 0.03	0.172 ± 0.011	0.645 ± 0.005	5051 ± 336
37	23/06/2017	short	75	EtOH/H_2O	0/100	0/100	0.00 ± 0.00	0.056 ± 0.001	1.242 ± 0.006	-
38	24/06/2017	short	75	EtOH/H_2O	20/80	9/91	19.91 ± 0.04	0.053 ± 0.001	1.053 ± 0.005	469 ± 7
39	25/06/2017	short	75	EtOH/H_2O	80/20	61/39	80.67 ± 0.02	0.065 ± 0.001	0.864 ± 0.002	6442 ± 82
40	28/06/2017	short	75	EtOH/H_2O	90/10	78/22	90.28 ± 0.17	0.132 ± 0.009	0.588 ± 0.006	7049 ± 489

Table A.2: PV experiments with mordenite membrane MOR-73 in terms of permeance and selectivity.

					Composition ≈			Permeance (P_i/δ) (mol m^{-2} s^{-1} Pa^{-1})		
Run No.	Date	Type	T (°C)	System	wt %	mol %	Feed (ln) (mol fraction)	EtOH	H_2O	Selectivity $\alpha'_{w/o}$
0.1.	19/04/2017	short	75	EtOH/H_2O	90/10	78/22	0.74	9.74E-11	5.69E-07	5842
0.2.	20/04/2017	short	75	EtOH/H_2O	90/10	78/22	0.77	1.64E-10	6.84E-07	4171
0.3.	21/04/2017	short	75	EtOH/H_2O	90/10	78/22	0.76	7.01E-11	6.64E-07	9472
0.4.	22/04/2017	short	75	EtOH/H_2O	90/10	78/22	0.77	7.59E-11	6.85E-07	9025
1	26/04/2017	short	75	EtOH/H_2O	72/28	50/50	0.50	5.83E-11	6.48E-07	11108
2	27/04/2017	short	75	EtOH/H_2O	72/28	50/50	0.51	4.99E-11	6.68E-07	13377
3	28/04/2017	short	75	EtOH/H_2O	90/10	78/22	0.80	4.47E-11	7.16E-07	16018
4	29/04/2017	short	75	EtOH/H_2O	50/50	28/72	0.27	7.59E-11	5.85E-07	7708
5	10/05/2017	long	75	EtOH/H_2O	90/10	78/22	0.81	4.28E-11	6.69E-07	15631
6	11/05/2017	long	75	EtOH/H_2O	90/10	78/22	0.81	6.67E-11	6.48E-07	9715
7	12/05/2017	long	75	EtOH/H_2O	90/10	78/22	0.80	7.40E-11	6.70E-07	9054
8	13/05/2017	short	75	EtOH/H_2O	80/20	61/39	0.58	1.28E-10	6.32E-07	4938
9	17/05/2017	short	75	EtOH/H_2O	95/05	88/12	0.87	1.37E-10	5.90E-07	4307
10	18/05/2017	short	75	EtOH/H_2O	30/70	14/86	0.15	1.80E-10	4.77E-07	2650
11	19/05/2017	short	75	EtOH/H_2O	90/10	78/22	0.78	7.91E-11	6.27E-07	7927
12	20/05/2017	short	75	EtOH/H_2O	0/100	0/100	0.00	-	5.74E-07	-
13	21/05/2017	short	75	EtOH/H_2O	90/10	78/22	0.79	5.03E-11	6.61E-07	13141
14	24/05/2017	short	75	EtOH/H_2O	10/90	4/96	0.04	3.01E-10	6.28E-07	2086
15	25/05/2017	short	75	EtOH/H_2O	90/10	78/22	0.79	5.35E-11	6.05E-07	11308
16	26/05/2017	short	75	EtOH/H_2O	0/100	0/100	0.00	-	6.04E-07	-
17	27/05/2017	short	75	MetOH/H_2O	10/90	6/94	0.06	2.08E-10	5.05E-07	2428
18	28/05/2017	short	75	MetOH/H_2O	20/80	12/88	0.12	2.06E-10	4.52E-07	2194
19	30/05/2017	short	60	MetOH/H_2O	10/90	6/94	0.06	2.35E-10	5.52E-07	2349
20	01/06/2017	short	60	MetOH/H_2O	20/80	12/88	0.12	1.66E-10	5.00E-07	3012
21	02/06/2017	short	60	MetOH/H_2O	50/50	36/64	0.36	1.51E-10	3.67E-07	2430
22	03/06/2017	short	60	MetOH/H_2O	80/20	69/31	0.69	1.20E-10	2.30E-07	1917
23	04/06/2017	short	60	MetOH/H_2O	90/10	84/16	0.83	8.19E-11	1.64E-07	2002
24	06/06/2017	short	60	MetOH/H_2O	10/90	6/94	0.06	3.39E-10	5.58E-07	1646
25	08/06/2017	short	75	MetOH/H_2O	0/100	0/100	0.00	-	6.06E-07	-
26	09/06/2017	short	60	MetOH/H_2O	10/90	6/94	0.06	2.44E-10	5.78E-07	2369
27	10/06/2017	short	40	MetOH/H_2O	10/90	6/94	0.06	2.22E-10	6.62E-07	2982
28	11/06/2017	short	40	MetOH/H_2O	20/80	12/88	0.12	1.52E-10	5.66E-07	3724
29	14/06/2017	short	60	MetOH/H_2O	0/100	0/100	0.00	-	6.79E-07	-
30	15/06/2017	short	40	MetOH/H_2O	0/100	0/100	0.00	-	7.69E-07	-
31	16/06/2017	short	60	MetOH/H_2O	10/90	6/94	0.06	2.49E-10	5.71E-07	2293
32	17/06/2017	short	75	EtOH/H_2O	10/90	4/96	0.04	2.57E-10	6.06E-07	2358
33	18/06/2017	short	75	EtOH/H_2O	20/80	9/91	0.09	1.29E-10	4.95E-07	3837
34	19/06/2017	short	75	EtOH/H_2O	50/50	28/72	0.29	8.80E-11	5.30E-07	6023
35	20/06/2017	short	75	EtOH/H_2O	80/20	61/39	0.62	1.21E-10	5.64E-07	4661
36	22/06/2017	short	75	EtOH/H_2O	90/10	78/22	0.77	9.37E-11	5.61E-07	5987
37	23/06/2017	short	75	EtOH/H_2O	0/100	0/100	0.00	-	4.96E-07	-
38	24/06/2017	short	75	EtOH/H_2O	20/80	9/91	0.09	1.28E-10	4.51E-07	3523
39	25/06/2017	short	75	EtOH/H_2O	80/20	61/39	0.62	5.41E-11	5.45E-07	10074
40	28/06/2017	short	75	EtOH/H_2O	90/10	78/22	0.78	6.50E-11	5.32E-07	8185

A.2 Mordenite Membrane MOR-72

Table A.3: PV experiments with mordenite membrane MOR-72 in terms of permeate composition, total flux and separation factor.

					Composition ≈		Average in Steady State			
Run No.	Date	Type	T (°C)	System	wt %	mol %	Feed (In) (EtOH wt %)	Permeate (EtOH wt %)	J (total) (kg m^{-2} h^{-1})	Separation factor, $\alpha_{w/o}$
41	29/06/2017	short	75	EtOH/H_2O	10/90	4/96	9.95 ± 0.01	0.010 ± 0.000	2.459 ± 0.028	1105 ± 1
42	30/06/2017	short	75	EtOH/H_2O	20/80	9/91	19.75 ± 0.00	0.023 ± 0.001	1.673 ± 0.017	1067 ± 41
43	01/07/2017	short	60	EtOH/H_2O	20/80	9/91	19.67 ± 0.19	0.028 ± 0.001	1.005 ± 0.006	876 ± 20
44	02/07/2017	short	40	EtOH/H_2O	20/80	9/91	20.25 ± 0.05	0.041 ± 0.001	0.444 ± 0.001	623 ± 16
45	03/07/2017	short	75	EtOH/H_2O	50/50	28/72	50.71 ± 0.03	0.035 ± 0.001	1.709 ± 0.011	2942 ± 61
46	04/07/2017	short	60	EtOH/H_2O	50/50	28/72	50.66 ± 0.00	0.046 ± 0.000	1.007 ± 0.002	2245 ± 17
47	05/07/2017	short	40	EtOH/H_2O	50/50	28/72	50.31 ± 0.10	0.058 ± 0.003	0.441 ± 0.002	1757 ± 85
48	06/07/2017	short	75	EtOH/H_2O	80/20	61/39	80.44 ± 0.03	0.070 ± 0.002	1.424 ± 0.007	5908 ± 149
49	07/07/2017	short	60	EtOH/H_2O	80/20	61/39	80.39 ± 0.10	0.121 ± 0.005	0.835 ± 0.002	3392 ± 158
50	08/07/2017	short	40	EtOH/H_2O	80/20	61/39	80.43 ± 0.04	0.132 ± 0.005	0.355 ± 0.002	3104 ± 120
51	09/07/2017	short	75	EtOH/H_2O	90/10	78/22	90.31 ± 0.08	0.134 ± 0.003	0.993 ± 0.010	6920 ± 74
52	13/07/2017	short	75	EtOH/H_2O	0/100	0/100	0.00 ± 0.00	0.022 ± 0.002	1.893 ± 0.007	-
53	14/07/2017	short	75	EtOH/H_2O	10/90	4/96	9.93 ± 0.06	0.017 ± 0.000	2.012 ± 0.021	667 ± 19
54	15/07/2017	short	75	EtOH/H_2O	90/10	78/22	89.41 ± 0.21	0.100 ± 0.006	0.988 ± 0.027	8439 ± 301
55	20/07/2017	short	75	EtOH/H_2O	0/100	clean	0.00 ± 0.00	0.020 ± 0.002	1.994 ± 0.013	-
56	21/07/2017	long	75	Ferm. Broth	FB	FB	42.51 ± 0.19	0.066 ± 0.006	1.428 ± 0.002	1127 ± 87
57	23/07/2017	short	75	EtOH/H_2O	90/10	78/22	91.59 ± 0.20	0.157 ± 0.015	0.819 ± 0.025	6988 ± 632
58	24/07/2017	short	75	EtOH/H_2O	0/100	clean	0.00 ± 0.00	0.054 ± 0.002	1.717 ± 0.014	-
59	25/07/2017	short	75	EtOH/H_2O	90/10	78/22	90.73 ± 0.32	0.166 ± 0.008	0.861 ± 0.020	5906 ± 479
60	26/07/2017	short	75	EtOH/H_2O	0/100	clean	0.00 ± 0.00	0.050 ± 0.001	1.715 ± 0.028	-
61	26/07/2017	short	75	Ferm. Broth	FB	FB	43.63 ± 0.10	0.070 ± 0.003	1.408 ± 0.010	1110 ± 49
Soaking the membrane in the Ferm. Broth:					44 wt % EtOH; 16h15min; 75°C					
62	27/07/2017	long	75	Ferm. Broth	FB	FB	44.53 ± 0.13	0.078 ± 0.005	1.458 ± 0.000	1034 ± 64
Soaking the membrane in the Ferm. Broth:					49 wt % EtOH; 13h45min; 75°C					
63	28/07/2017	short	75	EtOH/H_2O	90/10	78/22	90.86 ± 0.10	0.160 ± 0.007	0.831 ± 0.030	6203 ± 240
64	29/07/2017	short	75	EtOH/H_2O	0/100	clean	0.00 ± 0.00	0.062 ± 0.003	1.672 ± 0.014	-
65	30/07/2017	short	75	EtOH/H_2O	90/10	78/22	90.86 ± 0.26	0.158 ± 0.011	0.804 ± 0.013	6328 ± 596

Table A.4: PV experiments with mordenite membrane MOR-72 in terms of permeance and selectivity.

					Composition ≈			Permeance (P_i/δ) (mol m^{-2} s^{-1} Pa^{-1})		
Run No.	Date	Type	T (°C)	System	wt %	mol %	Feed (In) (mol fraction)	EtOH	H_2O	Selectivity $\alpha'_{w/o}$
41	29/06/2017	short	75	EtOH/H_2O	10/90	4/96	0.04	9.35E-11	1.02E-06	10900
42	30/06/2017	short	75	EtOH/H_2O	20/80	9/91	0.09	8.90E-11	7.17E-07	8054
43	01/07/2017	short	60	EtOH/H_2O	20/80	9/91	0.09	1.23E-10	8.33E-07	6794
44	02/07/2017	short	40	EtOH/H_2O	20/80	9/91	0.09	2.02E-10	9.99E-07	4940
45	03/07/2017	short	75	EtOH/H_2O	50/50	28/72	0.29	8.03E-11	8.13E-07	10133
46	04/07/2017	short	60	EtOH/H_2O	50/50	28/72	0.29	1.17E-10	9.28E-07	7947
47	05/07/2017	short	40	EtOH/H_2O	50/50	28/72	0.28	1.69E-10	1.10E-06	6511
48	06/07/2017	short	75	EtOH/H_2O	80/20	61/39	0.62	9.62E-11	8.93E-07	9287
49	07/07/2017	short	60	EtOH/H_2O	80/20	61/39	0.62	1.85E-10	1.01E-06	5450
50	08/07/2017	short	40	EtOH/H_2O	80/20	61/39	0.62	2.25E-10	1.16E-06	5160
51	09/07/2017	short	75	EtOH/H_2O	90/10	78/22	0.78	1.12E-10	8.99E-07	8064
52	13/07/2017	short	75	EtOH/H_2O	0/100	0/100	0.00	-	7.57E-07	-
53	14/07/2017	short	75	EtOH/H_2O	10/90	4/96	0.04	1.27E-10	8.34E-07	6580
54	15/07/2017	short	75	EtOH/H_2O	90/10	78/22	0.77	8.39E-11	8.48E-07	10098
55	20/07/2017	short	75	EtOH/H_2O	0/100	clean	0.00	-	7.97E-07	-
56	21/07/2017	long	75	Ferm. Broth	FB	FB	0.22	1.39E-10	6.58E-07	4734
57	23/07/2017	short	75	EtOH/H_2O	90/10	78/22	0.81	1.05E-10	8.12E-07	7743
58	24/07/2017	short	75	EtOH/H_2O	0/100	clean	0.00	-	6.86E-07	-
59	25/07/2017	short	75	EtOH/H_2O	90/10	78/22	0.79	1.19E-10	8.02E-07	6757
60	26/07/2017	short	75	EtOH/H_2O	0/100	clean	0.00	-	6.85E-07	-
61	26/07/2017	short	75	Ferm. Broth	FB	FB	0.23	1.43E-10	6.52E-07	4554
Soaking the membrane in the Ferm. Broth:					44 wt % EtOH; 16h15min; 75°C					
62	27/07/2017	long	75	Ferm. Broth	FB	FB	0.24	1.63E-10	6.77E-07	4141
Soaking the membrane in the Ferm. Broth:					49 wt % EtOH; 13h45min; 75°C					
63	28/07/2017	short	75	EtOH/H_2O	90/10	78/22	0.80	1.10E-10	7.81E-07	7090
64	29/07/2017	short	75	EtOH/H_2O	0/100	clean	0.00	-	6.68E-07	-
65	30/07/2017	short	75	EtOH/H_2O	90/10	78/22	0.80	1.05E-10	7.56E-07	7192

A.3 Zeolite A-7 Membrane

Table A.5: PV experiments with zeolite A-7 membrane in terms of permeate composition, total flux and separation factor.

					Composition ≈		Average in Steady State			
Run No.	Date	Type	T (°C)	System	wt %	mol %	Feed (ln) (EtOH wt %)	Permeate (EtOH wt %)	J (total) (kg m^{-2} h^{-1})	Separation factor, $\alpha_{w/o}$
66	01/08/2017	short	75	EtOH/H_2O	90/10	78/22	92.06 ± 0.05	0.119 ± 0.003	2.118 ± 0.049	9767 ± 254
Soaking the membrane in distilled water:				100 wt % H_2O; 5min; 25°C						
Soaking the membrane in the Ferm. Broth:				41 wt % EtOH; 13h30min; 75°C						
67	02/08/2017	short	75	EtOH/H_2O	90/10	78/22	91.07 ± 0.28	2.205 ± 0.044	1.980 ± 0.016	454 ± 24
X-ray diffraction analysis										
Soaking the membrane in the Ferm. Broth:				41 wt % EtOH; 44h55min; 75°C						
68	04/08/2017	short	75	EtOH/H_2O	90/10	78/22	90.43 ± 0.39	2.388 ± 0.039	1.996 ± 0.007	387 ± 23
Soaking the membrane in the Ferm. Broth:				41 wt % EtOH; 63h45min; 75°C						
69	07/08/2017	short	75	EtOH/H_2O	90/10	78/22	92.08 ± 0.07	1.002 ± 0.088	1.684 ± 0.021	1158 ± 99
70	08/08/2017	short	75	EtOH/H_2O	90/10	78/22	0.00 ± 0.00	0.023 ± 0.001	3.793 ± 0.010	-
71	08/08/2017	short	75	EtOH/H_2O	90/10	78/22	91.75 ± 0.05	1.353 ± 0.150	1.639 ± 0.014	820 ± 87

Table A.6: PV experiments with zeolite A-7 membrane in terms of permeance and selectivity.

					Composition ≈			Permeance (P_i/δ) (mol m^{-2} s^{-1} Pa^{-1})		
Run No.	Date	Type	T (°C)	System	wt %	mol %	Feed (ln) (mol fraction)	EtOH	H_2O	Selectivity $\alpha'_{w/o}$
66	01/08/2017	short	75	EtOH/H_2O	90/10	78/22	0.82	2.03E-10	2.18E-06	10747
Soaking the membrane in distilled water:				100 wt % H_2O; 5min; 25°C						
Soaking the membrane in the Ferm. Broth:				41 wt % EtOH; 13h30min; 75°C						
67	02/08/2017	short	75	EtOH/H_2O	90/10	78/22	0.80	3.59E-09	1.85E-06	515
X-ray diffraction analysis										
Soaking the membrane in the Ferm. Broth:				41 wt % EtOH; 44h55min; 75°C						
68	04/08/2017	short	75	EtOH/H_2O	90/10	78/22	0.79	3.97E-09	1.78E-06	448
Soaking the membrane in the Ferm. Broth:				41 wt % EtOH; 63h45min; 75°C						
69	07/08/2017	short	75	EtOH/H_2O	90/10	78/22	0.82	1.36E-09	1.72E-06	1264
70	08/08/2017	short	75	EtOH/H_2O	90/10	78/22	0.00	-	1.52E-06	-
71	08/08/2017	short	75	EtOH/H_2O	90/10	78/22	0.81	1.80E-09	1.63E-06	902

Appendix B

Gas chromatograms - Fermentation Broth

B.1 Run No. 56

Date: 21/07/2017

Operating Conditions: Distilled fermentation broth; MOR-72; 75 °C; 8h.

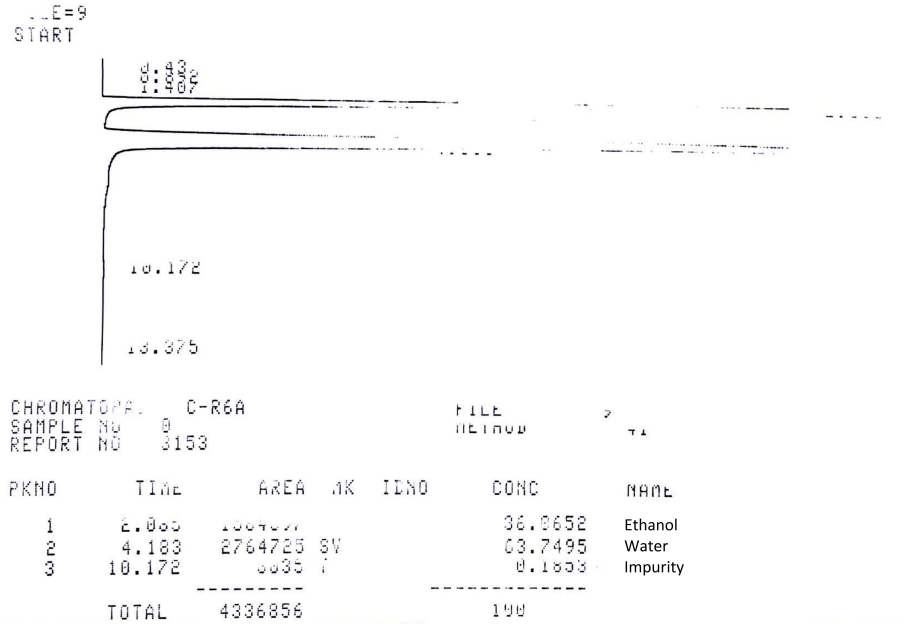

Figure B.1: Gas chromatogram of the 1st feed sample; 41.05 wt % EtOH.

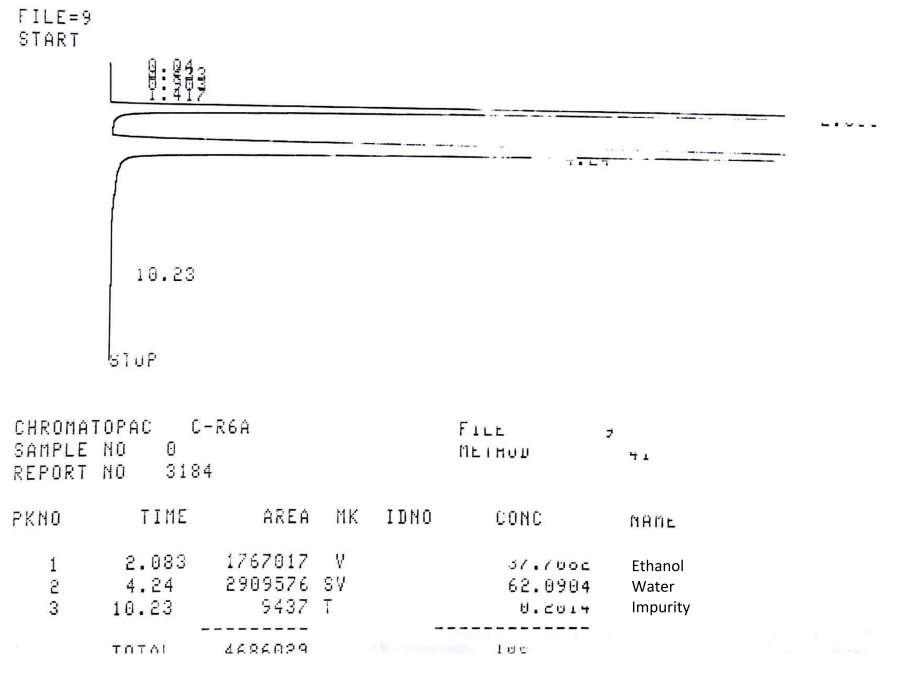

Figure B.2: Gas chromatogram of the 9th feed sample; 42.75 wt % EtOH.

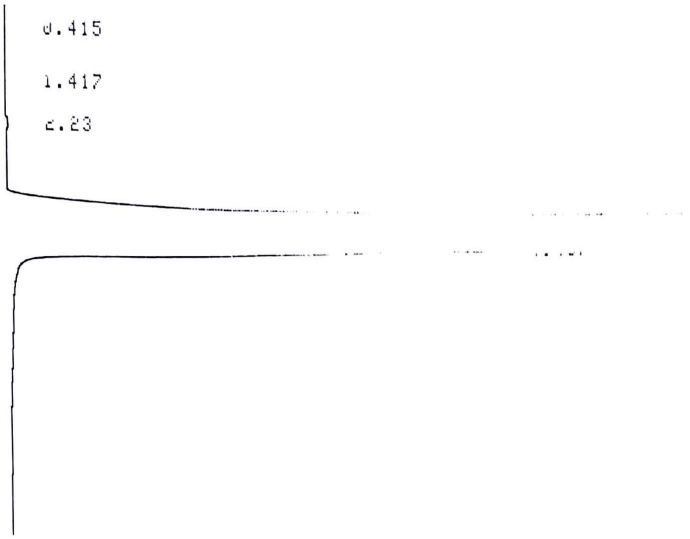

CHROMATOPAC C-R6A FILE 6
SAMPLE NO 0 Method 41
REPORT NO 3156

PKNO	TIME	AREA	MK	IDNO	CONC	NAME
1	0.415	196			0.0038	undefined
2	1.417	149			0.0029	Acetone
3	2.23	4271			0.0839	Ethanol
4	4.467	5087170			99.9093	Water
	TOTAL	5091786			100	

FILE=8
START

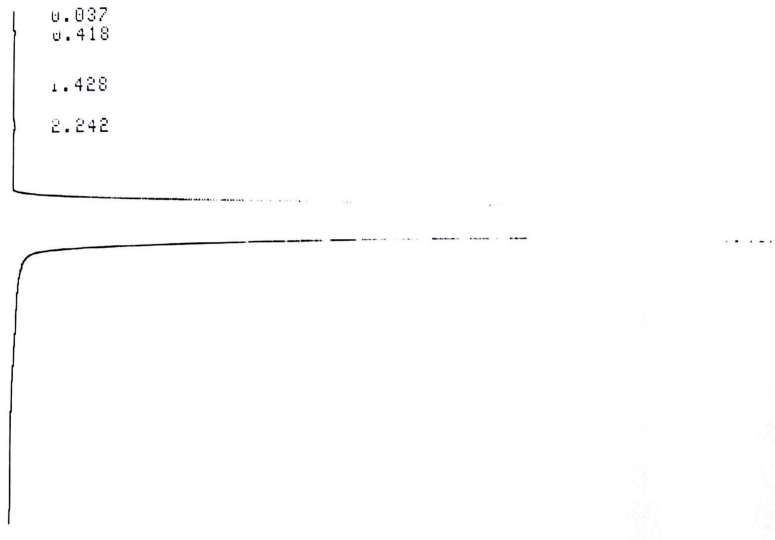

CHROMATOPAC C-R6A FILE 6
SAMPLE NO 0 Method 41
REPORT NO 3157

PKNO	TIME	AREA	MK	IDNO	CONC	NAME
1	0.037	36			0.0007	undefined
2	0.418	1061	V		0.0222	undefined
3	1.428	877			0.0183	Acetone
4	2.242	3244			0.0678	Ethanol
5	4.457	4778164			99.8909	Water

Figure B.3: Gas chromatograms of the 1st permeate sample; 0.10 wt % EtOH (average value).

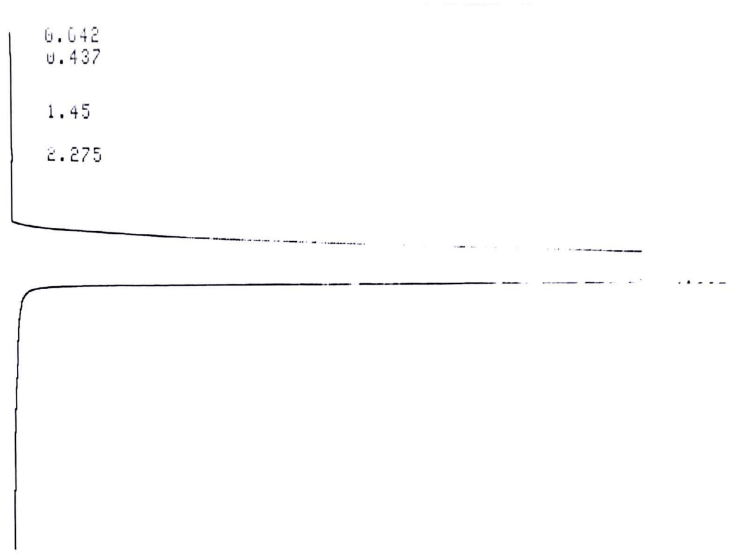

CHROMATOPAC C-R6A FILE 8
SAMPLE NO 0 METHOD 41
REPORT NO 3189

PKNO	TIME	AREA	MK	IDNO	CONC	NAME
1	0.042	24			0.0005	undefined
2	0.437	466			0.0092	undefined
3	1.45	235			0.0046	Acetone
4	2.275	3245			0.0643	Ethanol
5	4.532	5046000			99.9214	Water
	TOTAL	5049969			100	

FILE=8
START

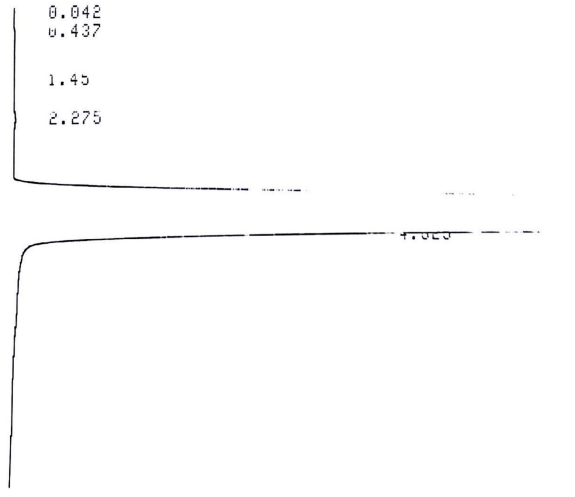

CHROMATOPAC C-R6A FILE 8
SAMPLE NO 0 METHOD 41
REPORT NO 3190

PKNO	TIME	AREA	MK	IDNO	CONC	NAME
1	0.042	20			0.0004	undefined
2	0.437	298			0.0059	undefined
3	1.45	408			0.0080	Acetone
4	2.275	3058			0.0606	Ethanol
5	4.625	6015746			99.9251	Water

Figure B.4: Gas chromatograms of the 9th permeate sample; 0.08 wt % EtOH (average value).

B.2 Run No. 62

Date: 27/07/2017

Operating Conditions: Distilled fermentation broth; MOR-72; 75 °C; 10.35h.

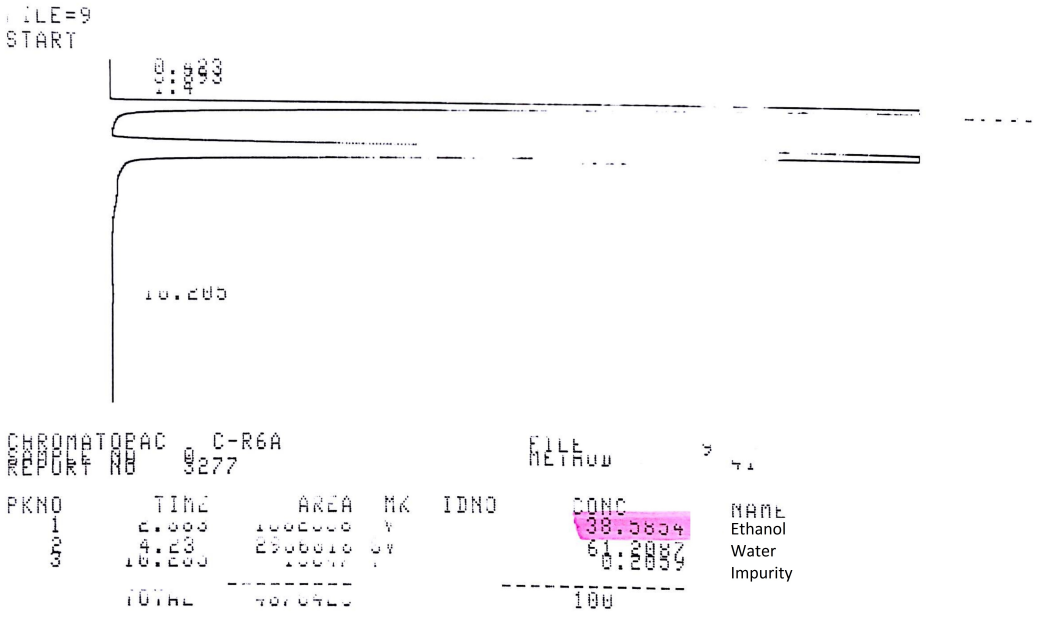

Figure B.5: Gas chromatogram of the 1st feed sample; 43.65 wt % EtOH.

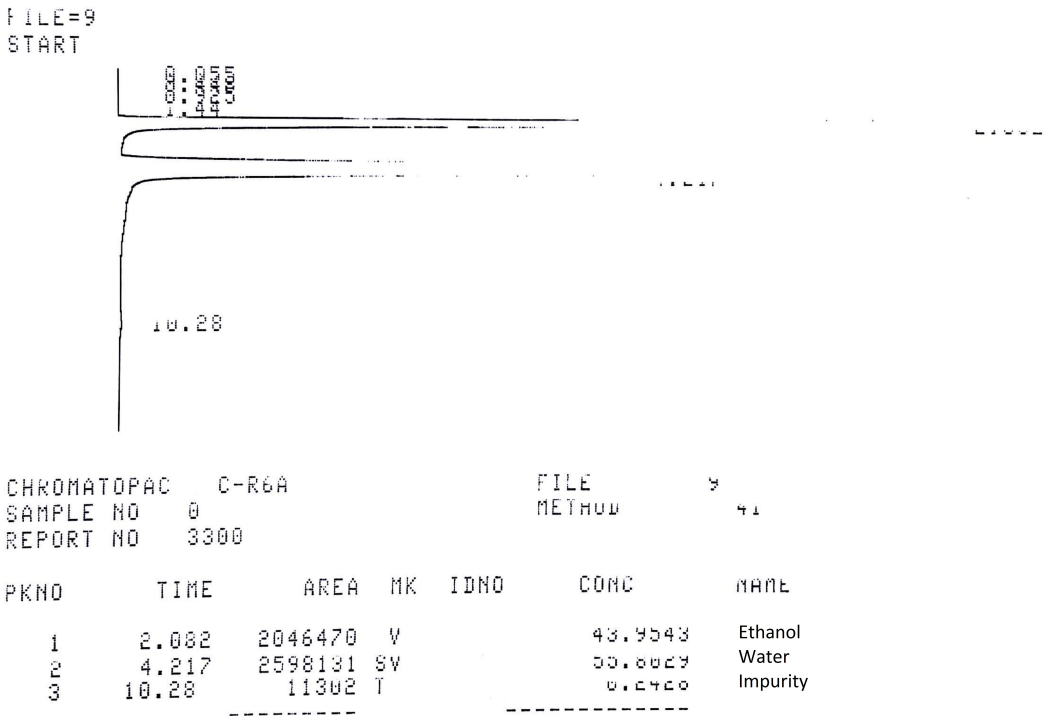

Figure B.6: Gas chromatogram of the 13th feed sample; 49.10 wt % EtOH.

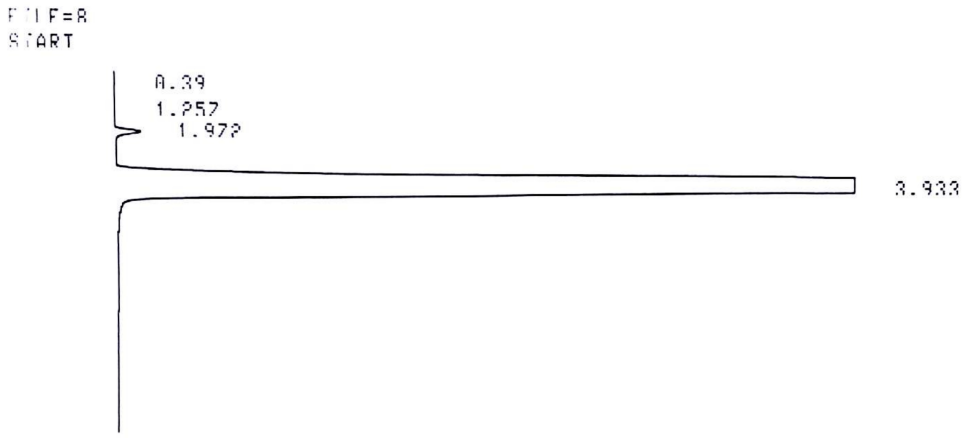

CHROMATOPAC C-R6A FILE 8
SAMPLE NO 0 METHOD 41
REPORT NO 00045

PKNO	TIME	AREA	MK	TYPE	CONC	NAME
1	1.972	22077			0.5396	Ethanol
2	3.933	4069116			99.4604	Water
	TOTAL	4091193			100	

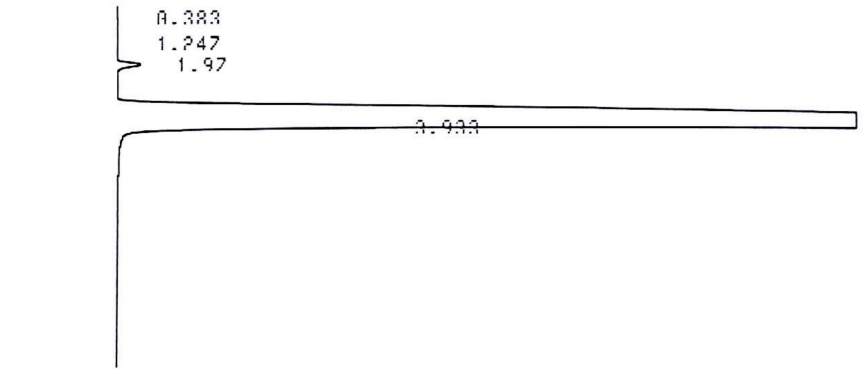

CHROMATOPAC C-R6A FILE 8
SAMPLE NO 0 METHOD 41
REPORT NO 00046

PKNO	TIME	AREA	MK	TYPE	CONC	NAME
1	1.97	21357			0.5284	Ethanol
2	3.933	4020572			99.4716	Water
	TOTAL	4041929			100	

Figure B.7: Gas chromatograms of the 1st permeate sample; 0.67 wt % EtOH (average value).

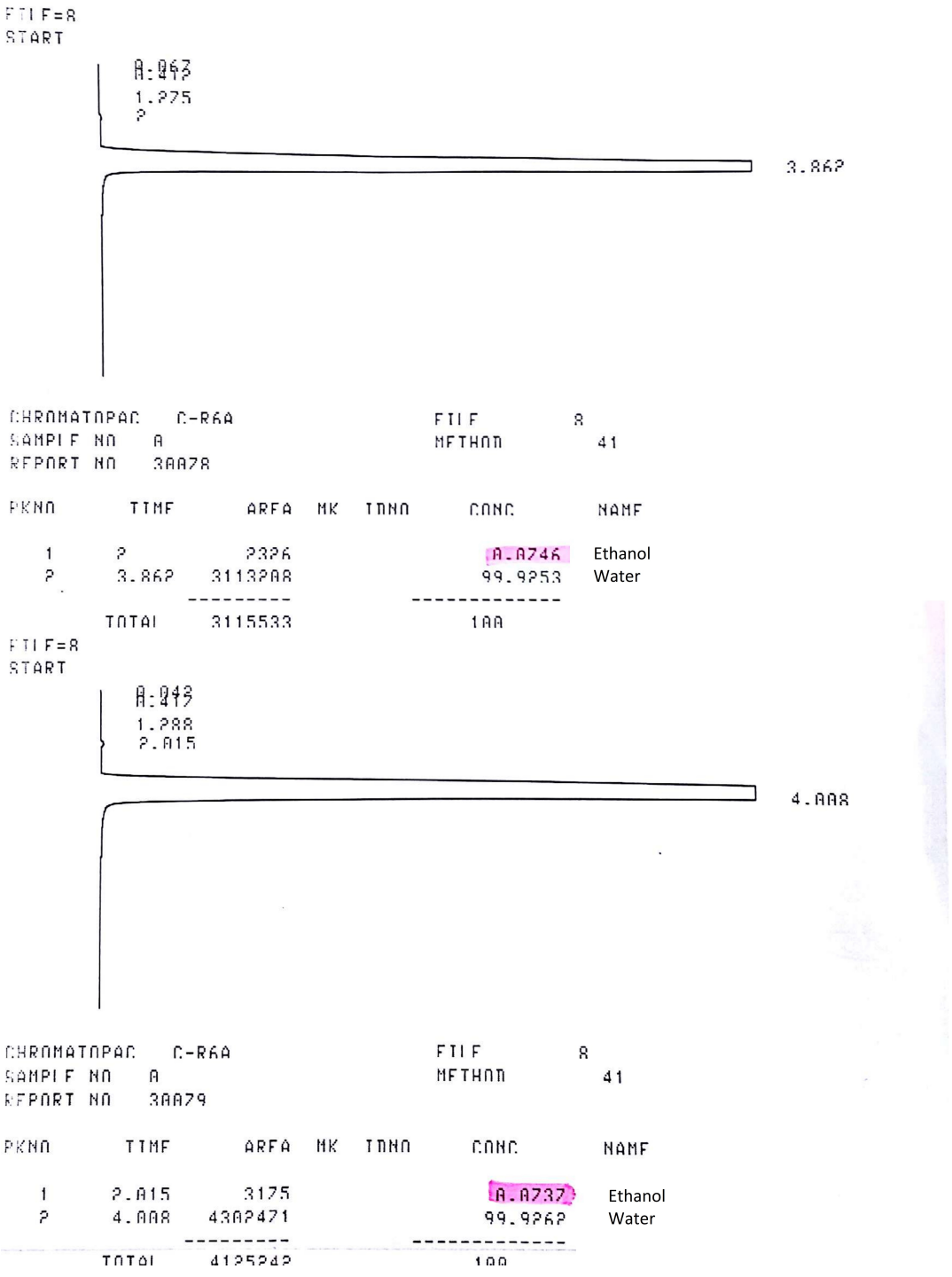

Figure B.8: Gas chromatograms of the 12th permeate sample; 0.09 wt % EtOH (average value).